SOME HYPERFINE INTERACTIONS IN SOLIDS

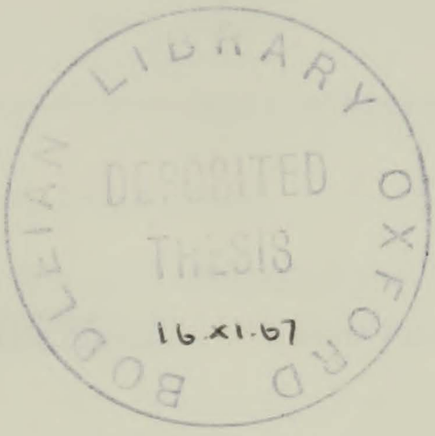

G. M. Copland

Merton College

A thesis submitted for the degree of Doctor of Philosophy in the University of Oxford.

Trinity Term, 1967.

C O N T E N T S

Page

Page

APPENDICES

ABSTRACT

This thesis describes electron nuclear double resonance (ENDOR) measurements of hyperfine interactions in various rare-earth systems. A Q-band (8 mm.) ENDOR spectrometer was built to perform experiments on Yb^{171} and Yb^{173} in CaF_2 and Gd^{155} and Gd^{157} in ThO_2 and CeO_2. Two other spectrometers are described which were built to perform experiments on Tb^{3+} in $CaWO_4$ and yttrium ethylsulphate (YES). All the spectrometers operated basically on the principles described by Baker and Williams (1962), using 115 kc/s magnetic field modulation. The nuclear r.f. frequencies were introduced by a single loop for the Yb and Gd experiments, but for the Tb experiments a tuned resonant line was used for a Q-band spectrometer, and a microwave helix for a J-band (2 cm.) spectrometer.

The measurements on Yb^{3+} in the cubic site of CaF_2 have provided some very interesting results. Firstly no reliable determination of the crystal field splitting of Yb^{3+} in cubic CaF_2 has been made (Kirton and McLaughlan 1967). The nuclear moments for Yb^{171} and Yb^{173} in diamagnetic Yb^{2+} ions and in the free atom have been measured by Gossard et. al.

(1964) and Olschewski and Otten (1967). A measurement of the effective nuclear g-factor for these isotopes in the paramagnetic Yb^{3+} ion by ENDOR showed that the effective nuclear g-factor was 64% larger than the true g-factor. This enabled the Γ_8 quartet excited state of Yb^{3+} in CaF_2 to be determined to have an energy of 597 ± 6 cm^{-1} relative to the Γ_7 doublet which is the ground state. Using a value for the spin orbit coupling and the value of the one optical transition positively identified by Kirton and McLaughlan to arise from an excited state to the ground state of Yb^{3+} in cubic sites in CaF_2, the crystal field parameters were deduced to be :

$$b_4 = 60\ B_4 = 37.8 \text{ cm}^{-1} \quad \text{and} \quad b_6 = 180\ B_6 = 9.9 \pm 2 \text{ cm}^{-1}.$$

These values were deduced without accounting for the crystal field admixtures discussed by Bleaney (1964) for isoelectronic Tm^{2+}.

The ENDOR measurements on Yb^{171} ($I = \frac{1}{2}$) were fitted to a simple spin Hamiltonian, from which A^{171} and g_N^{171} were found. Yb^{173} has $I = \frac{5}{2}$, and to fit the spectrum higher order interactions of the type suggested by Ray (1964) had to be included in the spin Hamiltonian. As Yb^{3+} consists

essentially of a single hole in an otherwise complete 4f shell it should be possible to account for these higher order terms by perturbation theory. This was attempted, using combinations of the Zeeman interaction, the magnetic hyperfine interaction and the quadrupole interaction coupling Γ_6 and Γ_8 levels within the ground manifold to the Γ_7 ground doublet. The predicted interactions agreed reasonably well with the observed spin Hamiltonian terms, assuming a quadrupole interaction for the free ion of - 4.7 ± 1.2 Mc/s. No such interaction can be observed directly in the ground state of Yb^{3+} in cubic CaF_2, as the effective electronic spin is ½. These higher order perturbations also produce correction terms which appear in the spin Hamiltonian as $\underline{S}.\underline{I}$, thus having the same form as the magnetic hyperfine interaction. It is essential for this work that these terms be correctly evaluated. For Yb^{171} a correction of - 130 ± 5 kc/s has to be applied by A^{171} derived from the spin Hamiltonian, whilst for Yb^{173} the correction is + 121 ± kc/s.

The corrected hyperfine interaction values are $A^{171} = 2638.53 \pm 0.04$ Mc/s, $A^{173} = -727.123 \pm 0.06$ Mc/s. The ratio of these is $\frac{A^{171}}{A^{173}} = -3.6288 \pm 0.0004$, leading to a hyperfine structure anomaly of - 0.03 ± 0.03%. From the

value for the anomaly deduced by Budick and Snir (1967) for the 6s6p state of the Yb atom of - 0.376 ± 0.020%, a value for the core polarisation in the ion can be deduced. This gives $\frac{A(s)}{A(f)}$ = + 8 ± 8%, whilst Bleaney (1963) predicts this ratio to be -1%. The disagreement in sign suggests that further experimental work should be performed, preferably ENDOR at a different EPR frequency.

The ENDOR measurements on Gd^{3+} in ThO_2 were a continuation of the work reported by Hurrell (1965). His measurements were made at X-band and the comparison with the results reported here at Q-band showed interesting differences in the A value and in the term A $\underline{S}^3.\underline{I}$. To obtain agreement between these experiments more higher order terms had to be invoked, having the form SIH^2 and S^3IH^2. ENDOR measurements were also performed on Gd^{157} and Gd^{155} in CeO_2. These crystals appeared to be internally strained and the hyperfine structure EPR lines were unresolved. This resulted in reliable ENDOR measurements being made only on $\Delta I_z = \frac{1}{2} \rightarrow -\frac{1}{2}$ transitions, as the energies of the $I_z = \frac{3}{2}$ levels were smeared out by the crystal field strains. The results for the Gd isotopes gave the following values for the hyperfine interactions :

	A^{157}	A^{155}
CeO_2	15817.2 ± 0.7 Mc/s	12059.8 ± 0.5 Mc/s
ThO_2	15796.1 ± 0.5 Mc/s	

No hyperfine structure anomaly was detected. Application of the Sandars and Beck (1965) relativistic theory of hyperfine structure to this system gave reasonable values for the quadrupole interaction. When combined with Bleaney's core polarisation formula the relativistic theory gave values for the hyperfine interactions that were 17% too large.

Considerable time was spent searching for the ENDOR of Tb^{3+} in $CaWO_4$ and YES, using the two spectrometers designed for these experiments. The hyperfine interaction for Tb^{159} in these crystals is ~6200 Mc/s and thus the design of the nuclear frequency side of the apparatus required care and is discussed at length. No ENDOR was seen in either host using either apparatus. When using the 2 cm. spectrometer one is likely to encounter ENDOR linewidths of several Mc/s, as in this case the Zeeman interaction is not large compared with the zero field splitting. Tb^{3+} is a non-Kramers ion and thus has no spin Hamiltonian terms of the form S_+I_-. This has a serious effect upon the techniques required for the ENDOR experiment.

To determine the saturation conditions for Tb^{3+} in $CaWO_4$, a study of the electronic spin-lattice relaxation time as a function of temperature in the range 1 - 9°K was made using a pulse saturation recovery technique. This was found to

be :

$$T_1^{-1} = 2.67\,T + 7.7 \times 10^{-4}\,T^7 + 6.65 \times 10^{8} \exp\left(-\frac{78.7}{T}\right)$$

This indicated that the first excited state was at 55 cm^{-1} which agreed well with a spectroscopic measurement. These results were compared with the published crystal field parameters for this system (Shekun 1965, 1967).

The computer programs, experimental data and computed results used throughout this thesis are contained in the appendices.

REFERENCES

Baker, J.M. and Williams, F.I.B., 1962. Proc. Roy. Soc. A267, 283.

Bleaney, B., 1963. Proc. 3rd Int. Conf. on Quantum Electronics, Dunod, Paris. p. 595.

Bleaney, B., 1964. Proc. Roy. Soc. A277, 289.

Budick, B. and Snir, J., 1967. Phys. Letts. 24B, 276.

Hurrell, J.P., 1965. Brit. J. Appl. Phys. 16, 755.

Kirton J. and McLaughlan, S.D., 1967. Phys. Rev. 155, 279.

Olschewski, L. and Otten, E.W., Zeits. für Phys. 200, 224.

Ray, T., 1964. Proc. Roy. Soc., A277, 76.

Sandars, P.G.H. and Beck, J., 1965. Proc. Roy. Soc. A289, 97.

Shekun, L. Ya., 1965. JETP Letts. 2, 437.

Shekun, L. Ya., 1967. Sov. Phys. Solid State, 8, 2340.

ACKNOWLEDGEMENTS

I should like to express my thanks to :

Professor B. Bleaney for providing the facilities of the Clarendon Laboratory, and for supervision of this work 1963-1964.

Dr. J.M. Baker who supervised this work from 1964 onwards, and for the many helpful discussions, valuable advice and encouragement through the work.

Professor L. Fox for providing the facilities of the Oxford University Computing Laboratory.

Dr. J.P. Hurrell for his help and interest in the earlier stages of this work.

Dr. D.P. Breen for his assistance with the relaxation time measurements.

Messrs. W.B.J. Blake, P.J. King and K. Maxwell for performing peripheral experiments for this work.

Mr. E.J. Jenkinson for his advice and his workshop staff for their skill in building much of the apparatus.

Mr. A.A.F. Sussums for help in assembling and maintaining the equipment.

To all members of the laboratory, particularly in the

paramagnetic resonance groups for loan of equipment at crucial times, advice and discussions.

To my wife for her help in the preparation of the draft and to Mrs. E. Browne for accurate and efficient typing of the manuscript.

To the Science Research Council for the award of a Research Studentship and to Merton College for the award of a Harmsworth Senior Scholarship.

CHAPTER 1

INTRODUCTION

The work described in this thesis consists principally of the determination of hyperfine interactions of various rare-earth ions in solids by means of electron-nuclear double resonance. This will be abbreviated to ENDOR throughout the thesis. The primary interest in this work was in the hyperfine interactions rather than in the ENDOR technique. However a considerable portion of the experimental time was spent in finding satisfactory ENDOR systems. This will be considered briefly here.

The ENDOR technique which was first suggested and demonstrated by Feher (1956, 1959), essentially consists of performing electron paramagnetic resonance (EPR) under conditions of partial saturation, whilst inducing nuclear resonance in the same system. The level of the EPR signal varies when the nuclear resonance is induced, and ENDOR consists of monitoring this change. ENDOR transitions are characterised by $\Delta m_I = \pm 1$, $\Delta M_s = 0$, as in nuclear magnetic resonance (NMR).

ENDOR is mainly used to observe resonance in nuclei

which are strongly coupled to paramagnetic centres, either paramagnetic ions of the 4f or 3d groups or defect centres. These systems are not normally amenable to study by conventional NMR techniques, although to a large extent the information derived from ENDOR measurements is similar to that from NMR. NMR experiments in paramagnetic materials are usually hampered by the large electronic moment. There are two factors which prevent the use of NMR in these systems. Firstly the surrounding paramagnetic centres produce random static magnetic fields at the nucleus, the order of magnitude for 1% Eu^{2+} in CaF_2 being 100 gauss. However more serious, is that for the concentrations required for conventional NMR $\backsim 10^{20}$ centres per c.c. there is a strong interaction between the paramagnetic electrons. This produces a fast spin-spin relaxation between these centres. As the nuclei are strongly coupled to these centres, the nuclei also experience a short T_2. If one had a 10 gauss homogeneous EPR linewidth, this may produce a width $\gamma_e H_e \backsim$ 28 Mc/s in the nuclear resonance, corresponding to a Δ H of $\backsim$ 28 K gauss for a typical nuclear magnetic moment. If however the spin-spin relaxation is sufficiently fast to satisfy the condition $A\tau << 1$, where A is the electron-nucleus hyperfine interaction and τ is the mean lifetime of an electronic state,

the nucleus sees only an average field. This field is non-zero because of the different populations for the electronic states $S_z = \pm \frac{1}{2}$. The NMR is then observable with a line width $\Delta\nu \sim A^2\tau$. If this is $\ll$ the nuclear Zeeman Larmor frequency, NMR would be observable, but at a frequency shifted by a few per cent from the value observed in diamagnetic compounds (Abragam 1961). It is difficult to extract any accurate measurements of hyperfine interactions from such a resonance.

Thus to observe NMR in paramagnetic materials, one needs to work with much lower concentrations of nuclei than is usual for conventional NMR. Williams (1967) shows that in $^{151}Eu^{2+}$ in CaF_2, the concentration required to overcome these problems should be not greater than 0.005% Eu^{2+}, which would render NMR unobservable. However ENDOR experiments are possible in these materials. Here one makes use of the strong EPR signal in such material and the strong coupling between the electrons and nuclei. When a nuclear resonance is excited the relative populations of the appropriate pair of hyperfine levels are changed. If one is performing EPR from one of these hyperfine levels to a different electron state in the system, this will change the EPR signal. Essentially the NMR radio frequency photon is detected by

the resulting exchange of a much higher energy microwave photon. A detailed qualitative treatment of the ENDOR response of a system with $S_z = \frac{1}{2}$, $I_z = \frac{1}{2}$ is given in Chapter 6.

The mechanism involved in an ENDOR experiment are very complicated in any real physical situation. Various authors, Feher (1959), Lambe et. al (1961), McIrvine et. al. (1964), Williams (1961) and Hurrell (1963) have attempted to explain the behaviour of ENDOR systems with varying degrees of success. However it is to be generally concluded that ENDOR mechanisms are still largely not understood.

There are a few important criteria which it appears should be satisfied for a successful ENDOR system.

(1) The EPR signals should be strong.

(2) The EPR line width should be narrow, the concentration of centres being reduced below the level where the linewidth is limited by T_2 processes.

(3) For ENDOR of the nucleus of the paramagnetic ion, the hyperfine structure should be clearly resolved, reducing cross-relaxation effects to a minimum. (see Chapter 5.)

(4) Spin diffusion within the EPR line should be small to give narrow ENDOR lines. (see Chapter 4.)

(5) The electronic spin-lattice relaxation time should be sufficiently long to enable the EPR to be partially saturated at microwave powers of $\sim$ 10 - 100 mW to reduce the noise introduced in conventional spectrometers by working at high powers.

(6) The Crystal Lattice should be strain-free, to reduce strain broadening of the ENDOR line (Stoneham 1966).

(7) There should be no overlapping EPR spectra from ions in different site symmetries in the crystal or from other paramagnetic impurities to prevent cross-relaxation of the EPR line.

In the idealised case of an inhomogeneously broadened EPR line with small spin diffusion the ENDOR linewidth should be close to the width of a single spin packet in the EPR line. This appears to be the case for Eu^{2+} in CaF_2, where Williams observed line widths of 8 kc/s. In Yb^{3+} in CaF_2, discussed in Chapter 4 of this thesis, the ENDOR linewidth is typically of the order of 400 kc/s, suggesting that spin diffusion transfers the saturation of the EPR spin packet throughout the EPR line.

Of the specimens studied during the experimental work described in this thesis, that of Gd^{157} in ThO_2 best satisfies

the criteria shown above, and it is satisfactory that in this system the ENDOR response was largest, with the narrowest lines of those systems studied. A comparison was made between the specimen of Eu^{2+} in CaF_2 used by both Hurrell and Williams with a similar specimen of slightly larger concentration of Eu^{2+}. It was found that whilst the ENDOR spectra could be seen easily in the original specimen, no ENDOR was observed at all in the second specimen. This perhaps illustrates that to observe ENDOR in a specimen the relaxation conditions have to be carefully balanced, and with our present lack of knowledge of the optimum conditions required, the choice of a specimen which will produce good ENDOR responses is to a certain extent a matter of luck.

The information that was extracted from the ENDOR measurements in this thesis were the hyperfine interaction spin Hamiltonian parameters for Gd^{157} and Gd^{155} in CeO_2 and ThO_2, and Yb^{171} and Yb^{173} in CaF_2. The magnetic dipole interactions and nuclear magnetic moments had all been previously reported for these systems from EPR measurements. The narrowness of the ENDOR lines gave much more accurate measurement of these parameters, and also enabled higher order interactions to be measured. The theory underlying the hyperfine interactions is reviewed in Chapter 2.

REFERENCES

Abragam, A., 1961. The Principles of Nuclear Magnetism. Clarendon Press, Oxford.

Feher, G., 1956. Phys. Rev. 103, 500.

Feher, G., 1959. Phys. Rev. 114, 1219.

Hurrell, J.P., 1963. D. Phil. Thesis, Oxford University.

Lambe, J., Laurence N., McIrvine, E.C. and Terhune, R.W., 1961. Phys. Rev. 122, 1161.

McIrvine, E.C., Lambe, J. and Laurence, N., 1964. Phys. Rev. 136, A467.

Stoneham, A.M. 1966. Proc. Phys. Soc. 89, 909.

Williams, F.I.B., 1961. D. Phil. Thesis, Oxford University.

CHAPTER 2

HYPERFINE INTERACTIONS

The theory of hyperfine interactions of paramagnetic ions in solids has been reviewed extensively by Freeman and Watson (1965). I shall review those aspects of the theory that are relevant to the experiments described in this thesis.

The interaction between electrons and nuclei of paramagnetic ions arises from electric and magnetic interactions with the nuclear electric and magnetic multipole moments. From the fact that wavefunctions have a definite parity it is readily deduced that the only allowed electric multipole moments are of even parity, being monopole, quadrupole, etc., whilst the magnetic multipoles have odd parity. The electric monopole moment is essentially the Coulombic electron-nucleus interaction, which affects all electrons in a given shell in the ion equally, and is not measurable by EPR experiments in the ground state of the ion. The quadrupole interaction can only arise for nuclei with spin $I > \frac{1}{2}$. The magnetic dipole moment occurs in all nuclei with non-zero spin.

The next magnetic interaction is a magnetic octupole interaction, which can only arise for nuclei of spin $\geq 3/2$.

Such an interaction was observed in I^{127} in an atomic beam experiment by Jaccarino et.al. (1954). The theory of octupole interactions is derived in a semi-classical manner by Casimir and Karreman (1942), where they show that the order of magnitude of the magnetic octupole interaction is $\beta\beta_N R^2 \langle r^{-5} \rangle$ where R is the nuclear radius. The chief contribution to this interaction occurs when the electron is close to the nucleus, where its orbit is only slightly affected by the shielding of the other electrons. This suggests that the effective electronic radius is the unshielded Bohr radius, $\frac{a_o}{Z}$, whence it can be shown easily that the ratio of octupole to dipole magnetic interactions is approximately

$$\frac{W_{oct}}{W_{dip}} = \frac{Z^2 R^2}{a_o^2} \approx 10^{-5} \quad \text{for large Z.}$$

Baker and Williams (1962) have shown that this ratio is reasonable in Eu^{151} ($I = \frac{5}{2}$), when they fit a spin Hamiltonian including the diagonal terms of the octupole interaction to their observed ENDOR data. They arrived at a value for the interaction which was 0.2 ± 0.3 kc/s. In the experiments described in this thesis, an octupole interaction might arise for both Gd^{155} and Gd^{157}, also Yb^{173}. However assuming the ratio given above, one expects the effect to be negligible in the Gd isotopes, where the magnetic dipole interaction is

$\sim$ 8 times smaller than in Eu^{151}. In Yb^{173}, the dipole interaction is larger by a factor of 7, but the observed ENDOR linewidths are $\sim$ 40 times wider than those of Eu^{151} in CaF_2, thus making the observation of an octupole interaction exceedingly unlikely. Hence, the results of the ENDOR experiments were fitted to spin Hamiltonians neglecting the octupole interaction, which will not be considered further in this thesis.

1. Magnetic Hyperfine Interaction

This interaction may be considered as consisting of three components. Firstly the interaction between the magnetic dipole moment of the nucleus and the magnetic field produced by the electron orbital motion around the nucleus, which has the form:

$$W_{orb} = -\mu_N \cdot \int \left(\frac{\underline{r} \wedge \underline{v}}{r^3} \right) \, dr$$

for the interaction with a single electron. Summing over all electrons in unclosed shells, and assuming L-S coupling this has the form:

$$W_{orb} = g g_N \beta \beta_N \, \underline{L} \cdot \underline{I} \, \left\langle r^{-3} \right\rangle_{orb}$$

where $\langle r^{-3} \rangle_{orb}$ is assumed to be constant for all electrons in the unclosed shell, $\langle r^{-3} \rangle_{orb} = -\frac{1}{e} \int \frac{dq}{r^3}$ over the electron charge density.

The second component arises from the magnetic dipole-dipole interaction energy between the electron spin moment and the nuclear magnetic moment. This can be expressed as :

$$W_{dip} = - \sum_i g g_N \beta \beta_N I.(\underline{s}_i - 3\underline{r}_o(\underline{s}_i \cdot \underline{r}_o)) \langle r^{-3} \rangle_{dip}$$

where $\langle r^{-3} \rangle_{dip}$ is averaged over the spin density. To a first order approximation one may assume that this integral is zero over closed electron shells, and arises only from electrons in incompleted shells, in which case $\langle r^{-3} \rangle_{dip}$ is closely equal to $\langle r^{-3} \rangle_{orb}$. However there is considerable evidence for the assumption of zero contribution from closed shells to be incorrect. Freeman and Watson (1961) discuss the case of Gd^{3+}, showing a considerable unpairing of the electron spins. This is a consequence of core polarisation which will be discussed briefly later.

The third contribution to the magnetic hyperfine interaction is the Fermi contact interaction, arising from the non-vanishing of the wave function for s electrons at the nucleus. This may be expressed as $W_c = g g_N \beta \beta_N \sum_i 2 (\underline{s}_i \cdot \underline{I}) \langle r^{-3} \rangle_c$. Thus in the case of spin-orbit coupling the

overall magnetic hyperfine interaction has the form:

$$\mathcal{H}_D = gg_N \underline{S}.\underline{I} \left\langle r^{-3} \right\rangle_c + \underline{L}.\underline{I} \left\langle r^{-3} \right\rangle_{orb} - (\underline{S}.\underline{I} - \frac{3(\underline{S}.\underline{r})(\underline{I}.\underline{r})}{r^2}) \left\langle r^{-3} \right\rangle_{dip}$$

This is often written in the form $A\underline{S}.\underline{I} = 2\beta\beta_N g_N \left\langle r^{-3} \right\rangle \underline{N}.\underline{I}$

where $\underline{N} = (\underline{L} - \underline{S} + \frac{3(\underline{r}.\underline{S})\underline{r}}{r^2}) = \underline{L} + \sqrt{10}\,(SC^{(2)})^{(1)}$ (Judd 1963).

This takes no account of possible differences between the effective $\left\langle r^{-3} \right\rangle$ values for the different types of interaction. Recently Harvey (1965) and Woodgate (1966) have shown that this approximation is not valid, and different values for the particular $\left\langle r^{-3} \right\rangle_i$ can be measured. The importance of this description of the interaction has been emphasised by the relativistic theory of hyperfine structure of Sandars and Beck (1965). To determine the values for these parameters measurements of the hyperfine interaction have to be made in different spectroscopic states, being therefore best determined by atomic beam experiments as in Woodgate's work on Samarium. ENDOR has only been performed in the ground state, and thus $\left\langle r^{-3} \right\rangle_i$ cannot be distinguished, the hyperfine interaction giving some sort of average $\left\langle r^{-3} \right\rangle$.

2. Electric Quadrupole Interaction

Quadrupole effects have been reviewed extensively by Das and Hahn (1958), Cohen and Reif (1957), and Abragam (1961). If the nucleus is considered to be of finite size, then the electrostatic interaction between the charged nucleons and electrons may be written as :

$$\mathcal{H}_{elec} = e^2 \int_{\tau_e} \int_{\tau_n} \frac{\rho(r_e)\rho(r_n)}{|r_e - r_n|} \, d\tau_e \, d\tau_n$$

where $e\rho(r_e)$ and $e\rho(r_n)$ are the electronic and nuclear charge densities and $\underline{r}_e$ and $\underline{r}_n$ are measured relative to the centre of the nucleus. This may be treated most conveniently in terms of tensor operators, as using the usual multipole expansion for $\frac{1}{r}$, this may be written as :

$$\mathcal{H}_{elec} = -e^2 \int_{\tau_e} \int_{\tau_n} \rho(r_e)\rho(r_n) \frac{r_n^k}{r_e^{k+1}} (C_e^{(k)} \cdot C_n^{(k)}) d\tau_e \, d\tau_n$$

assuming that $r_e > r_n$. Parity arguments limit k to even values only. $k = 0$ is the monopole term, $k = 2$ is the quadrupole term. Higher orders are neglected as insignificant in our work. Thus the quadrupole interaction Hamiltonian takes the form :

$$\mathcal{H}_Q = -e^2 \int_{\tau_e} \int_{\tau_n} \rho(r_e)\rho(r_n) \frac{r_n^2}{r_e^3} (C_e^{(2)} \cdot C_n^{(2)}) d\tau_e \, d\tau_n .$$

In a magnetic field the angular momenta J,I are effectively uncoupled and we can express the quadrupole interaction in the form:

$$W_Q = -e^2 \left\langle aJJ_z II_z \left| \frac{C_e^{(2)}}{r_e^3} \cdot C_n^{(2)} r_n^2 \right| a'JJ'_z II'_z \right\rangle$$

$$= -e^2 \sum_{q=0,1,2} \left\langle aJJ_z II_z \left| \frac{C_{eq}^{(2)}}{r_e^3} \cdot C_{n(-q)}^{(2)} r_n^2 \right| aJJ'_z II'_z \right\rangle$$

$$= -e^2 \sum_{q=0,1,2} (-1)^{J-J_z} \begin{pmatrix} J & 2 & J \\ -J_z & q & J \end{pmatrix} (-1)^{I-I_z}$$

$$\times \begin{pmatrix} I & 2 & I \\ -I_z & -q & I_z \end{pmatrix} \left\langle J \left\| \frac{C^{(2)}}{r^3} \right\| J \right\rangle \times \left\langle I \left\| C^{(2)} r^2 \right\| I \right\rangle$$

But the nuclear quadrupole moment is conventionally defined by evaluating the stretched case matrix elements $\left\langle II \left| C^{(2)} r^2 \right| II \right\rangle$

$$\text{Therefore } Q = \begin{pmatrix} I & 2 & I \\ -I & 0 & I \end{pmatrix} \left\langle I \left\| C^{(2)} r^2 \right\| I \right\rangle$$

$$W_Q = \frac{-e^2Q}{\begin{pmatrix} I & 2 & I \\ -I & 0 & I \end{pmatrix}} \sum_{q=0,1,2} (-1)^{J+J-I_z-J_z}$$

$$\begin{pmatrix} J & 2 & J \\ -J_z & q & J_z \end{pmatrix} \begin{pmatrix} I & 2 & I \\ -I_z & -q & I'_z \end{pmatrix} \left\langle J \left\| \frac{C^{(2)}}{r^3} \right\| J \right\rangle$$

This has three sets of non-zero matrix elements, for the three possible values of q. For q = 0 we have the diagonal elements in the form: $a(3J_z^2 - J(J+1))(3I_z^2 - I(I+1))$. For $q = \pm 1$ we have terms of the form : $a \frac{3}{2} ((S_zS_+ + S_+S_z)$ $(I_zI_- + I_-I_z) + (S_zS_- + S_-S_z)(I_zI_+ + I_+I_z))$ and for q = 2 $\frac{3a}{2} (S_+^2I_-^2 + S_-^2I_+^2)$.

The coefficient a is of the form $\left\langle J \left\| \frac{C^2}{r^3} \right\| J \right\rangle$ x e^2Q x function (I,J). It is usual to extract $\langle r^{-3} \rangle$ as a parameter assumed to be constant for all electrons of a particular ion. The term $\langle J \| C^2 \| J \rangle$ can be computed in the approximation of pure Russell-Saunders coupling, but in general this approximation is not a good one and an intermediate coupling approach is required to evaluate the constant. Thus the determination of a nuclear quadrupole moment from a measured quadrupole interaction is unreliable in view of the approximations that

have to be made in evaluating this coefficient.

3. Core Polarisation

A further difficulty always present arises due to anti-shielding corrections of the type discussed extensively by Sternheimer (1966). These arise from distortions of the otherwise spherical closed electronic shells. Electric field gradients can induce distortions in these electron shells which produce additional field gradients which are sometimes several orders of magnitude greater than the source gradients. There are two such sources, the field gradient arising from the aspherical valence electron distribution (q_v) and the crystalline electric field gradient (q_c). The values for the field gradient q are replaced by $q_v (1 - R_q)$ and $q_c (1 - \gamma_\infty)$ where $|R_q| < 1.0$ but γ_∞ as appears to have a roughly constant value of - 80 for the rare earth trivalent ions (Blok and Shirley (1966)). The term $\langle J \| C^{(2)}/r^3 \| J \rangle$ may be interpreted as the electric field gradient at the nucleus, and thus is greatly modified by the distortions just mentioned. This causes further difficulty in the evaluation of nuclear quadrupole moments.

Similar distortion effects from non-spherically symmetric valence electron shells can be significant in

magnetic hyperfine interactions, modifying $\langle r^{-3} \rangle_{orb}$ and $\langle r^{-3} \rangle_{dip}$ terms. Unlike the case of quadrupole interactions, Coulomb interactions between closed and open shells alone will not affect $\langle r^{-3} \rangle$ parameters. For the spin dipolar term not only must the closed shells be aspherically distorted by either or both of Coulomb and exchange interactions, but orbital differing in m_s value must have differing spatial behaviour in order that the spin term be non-zero for closed shells. This requires an imbalance in the distorting open shell exchange terms for $\pm m_s$. For the orbital term, Coulomb interactions have identical effects upon the $\pm m_l$ orbitals, thus giving no contribution. However, exchange interactions can treat these orbitals differently yielding a non-zero $\underline{L}.\underline{I}$ type interaction from the closed shells. These effects may be interpreted as the origins of the differing values of $\langle r^{-3} \rangle_{dip}$ and $\langle r^{-3} \rangle_{orb}$ measured by Harvey. Freeman and Watson (1963a,b) attempt to deal quantitatively with these effects using spin polarised Hartree-Fock wavefunctions. Experimental evidence for the existence of core polarisation effects of the type discussed above comes most directly from the observation of hyperfine interactions in nominally S-state ions. This has been extensively discussed by Heine (1957) for Mn^{2+}, Baker and Williams (1962) and Evans, Sanders and Woodgate (1965) for Eu. Similar considerations apply to

Gd^{3+} described in Chapter 5 of this thesis.

On the simple model discussed earlier for magnetic and electric hyperfine interactions, an ion with electronic configuration $4f^7\ {}^8S_{\frac{7}{2}}$ should show zero hyperfine interaction. However such interactions are observed which may be attributed to core polarisation and relativistic effects (Sanders and Beck 1965). In the 3d group it is found empirically that the magnetic field at the nucleus per unit of electron spin is constant to about 10% for similar salts, although it decreases with increasing covalent bonding. It has been assumed by Bleaney (1964) and Freeman and Watson (1963b) that a similar empirical rule governs the much weaker core polarisation in the 4f group. Bleaney suggests an empirical formula $A_{core} = -(63 \pm 10)(\Lambda_{JJ} - 1)g_N$ Mc/s for tripositive 4f ions, basing his formula upon estimates of core-polarisation in Eu^{2+} by Baker and Williams.

Sanders and Beck (1965) show that the magnetic hyperfine interaction should be expressed as the sum of three components which can be represented by double tensor operators $(U^{k_s k_l})^1$ where k_s operates in spin space, k_l in orbit space. The combinations of k_s, k_l that are possible are (10), (01), (12). These correspond to the terms $\underline{S}.\underline{I}$, $\underline{L}.\underline{I}$, $\underline{s}C^2$ in the non-

relativistic approach. The most interesting feature of this is the term $U^{(10)1}$ which gives a contribution to the hyperfine structure of exactly the same form as the contact term $\underline{S}.\underline{I}$. This implies that the detection of a term of this sort in the hyperfine structure of a configuration containing no unpaired s electrons is not a definite test for configuration interaction or core polarisation. In light elements the configuration interaction is likely to be considerably larger than the relativistic effects, but for the rare earths these are likely to be comparable in magnitude. A distinction between these contributions could be made if a hyperfine structure anomaly is detected, due to unpaired electrons at the nucleus, in which case the hyperfine structure must partly arise from an s electron (see Section 5). If no measurable anomaly can be seen where one might be expected from nuclear structure then this may be taken as strong evidence for relativistic rather than core polarisation interaction contribution. This is exemplified by Europium as discussed by Evans et. al. (1965).

Relativistic treatment of the quadrupole interaction gives an effective operator consisting of three components $U^{(02)2}$, $U^{(13)2}$, and $U^{(11)2}$. Even in the presence of configuration interaction, the quadrupole interaction can be written in the form of a tensor $U^{(02)2}$, which means that the

relativistic effects are directly separable from configuration interaction effects, as the coefficients of $U^{(13)2}$ and $U^{(11)2}$ are identically zero in the non-relativistic limit taken to any order. This has been illustrated by experiment. The term $U^{(02)2}$ vanishes for S state ions as the expectation value of a spherical tensor operator of rank 2 in orbital space is zero for an S state. Thus the observed quadrupole interaction for S state ions must arise from relativistic effects.

For Europium relativistic results give a reasonable explanation of the hyperfine interactions in the atom, but for the divalent ion, where a hyperfine structure anomaly is observed, configuration interaction has to be invoked to explain the dipolar interaction. Gd^{3+} investigated in this thesis is isoelectronic with Eu^{2+} and thus the theory developed by Sanders and Beck is directly applicable to this system. In non S state ions in the 4f group, relativistic effects are generally negligible compared with the hyperfine interactions arising from the nonrelativistic behaviour.

4. Higher Order Effects

The theory of hyperfine interactions outlined in the previous sections may be expressed, for a rare earth ion in a crystal field with effective ground state spin S as a spin H

$$\mathcal{H} = A\underline{S}\cdot\underline{I} + \frac{B}{2I(2I-1)2S(2S-1)}\Big([3S_z^2 - S(S+1)][3I_z^2 - I(I+1)]$$

$$+ \frac{3}{2}[(S_zS_+ + S_+S_z)(I_zI_- + I_-I_z)$$

$$+ (S_zS_- + S_-S_z)(I_zI_+ + I_+I_z)]$$

$$+ \frac{3}{2}(S_+^2I_-^2 + S_-^2I_+^2)\Big) - g_n\beta_N\underline{H}\cdot\underline{I}.$$

This Hamiltonian generally is sufficient to describe the hyperfine structure observable with EPR, but the higher sensitivity of ENDOR techniques has shown that higher order interactions must be considered. The theory of these higher order effects is based upon the group theoretical treatment of spin Hamiltonians given by Koster and Statz (1959), and extended specifically to hyperfine interactions by Ray (1964). The spin Hamiltonian will consist of tensors for the effective electron spin, the nuclear spin, and the magnetic field coupled up to give tensors of the form $(S_{l_1}I_{l_2}H_{l_3})_1^m$. The physical basis on which the use spin Hamiltonians rests is that the spin Hamiltonian must be invariant under any symmetry operation of the crystal point group at the ion site. But we know from group theory that Γ_1 is the only irreducible representation of a particular group which remains invariant

under all the operations of all the elements of the group. Thus the spin Hamiltonian must belong to the Γ_1 representation of the group describing the ion site symmetry, showing that it is the sum of all independent operators which belong to the Γ_1 representation of the particular symmetry. Ray shows that the tensors developed in this way can be reduced to the summation:

$$= \sum_{n_1=1}^{2S} \sum_{n_2=1}^{2I} \sum_{n_3} A(n_1 n_2 n_3)\, S^{n_1}.\, I^{n_2}.\, H^{n_3}.$$

The values that the integers n_1, n_2 and n_3 can take are restricted by the conditions

1) the spin wavefunctions S and I have definite parity and thus any operator acting between them must have even parity. This restricts the sum of integers to be even.

2) from the triangular rule for the addition of angular momenta n_1 and n_2 cannot connect angular momentum states differing by more than 2S and 2I respectively, thus imposing maximum values of 2S and 2I on these integers. In principle n_3 is unlimited except by condition (1) but in practice terms of higher powers of n_3 than quadratic will be insignificant.

Ray has considered in detail the case for an ion in a

cubic site where she writes the spin Hamiltonian explicitly in three parts, Zeeman field independent, linearly field dependent and quadratically field dependent. Higher powers of H are neglected. The resulting spin Hamiltonian is extremely long, but fortunately it can be condensed in any real physical case. The order of magnitude of any particular parameter in this spin Hamiltonian may be estimated by a perturbation theory calculation, taking into account the mechanisms which could contribute to a particular term. These will be considered together with the experimental data for each ion in this thesis where these parameters are measured, in the relevant chapters.

Baker and Bleaney (1958) considered two correction factors to be applied to the nuclear g factors and hyperfine interactions measured by EPR. These corrections are essentially the same as those introduced by the higher order effects discussed above, being those terms which are indistinguishable from first order hyperfine interaction parameters in the spin Hamiltonian. It is worth considering these in detail as they provide a good example of the method of calculating other higher order terms. Firstly, consider the term

$$\sum_j \frac{\langle \phi_i | A\underline{J}.\underline{I} | \phi_j \rangle \langle \phi_j | A\underline{J}.\underline{I} | \phi_i \rangle}{(E_i - E_j)}$$

This may be written as:

$$\sum_j \frac{A^2}{E_i - E_j} \left[I_z^2 \left| \langle \phi_i | J_z | \phi_j \rangle \right|^2 + \frac{I(I+1) - I_z(I_z+1)}{4} \left| \langle \phi_i | J_{\pm} | \phi_j \rangle \right|^2 \right]$$

The first term in this expression is proportional to I_z^2 and thus behaves like a quadrupole interaction, giving rise to a pseudo-quadrupole interaction. The second term is the sum of a constant term which shifts all levels equally and thus has no effect on measurements in the ground state, a term proportional to I_z^2 which adds to the pseudo-quadrupole term above, and a term proportional to I_z which is indistinguishable from the magnetic hyperfine interaction, thus adding a correction term to A.

A second correction term arises from the combination $A\underline{J}.\underline{I}, \Lambda\beta H.J$

$$\sum_j \frac{\langle \phi_i | A\underline{J}.\underline{I} | \phi_j \rangle \langle \phi_j | \Lambda\beta H.J | \phi_i \rangle}{E_i - E_j}$$

which gives a pseudo-nuclear g factor

$g'_n = g_n - 2A\Lambda \sum_j \frac{\left| \langle \phi_j | J_z | \phi_i \rangle \right|^2}{(E_i - E_j)}$. This term is of particular importance in the discussion of the Yb^{3+} ENDOR measurements.

5. Hyperfine Structure Anomaly

In the preceding sections no account has been taken of the possible distribution of magnetic moment within the nucleus. It has been assumed that the nucleus could be represented as a point magnetic dipole for magnetic interactions. Whilst this approximation is good for interactions between the nucleus and electrons with orbital angular momentum quantum number > 1, it is reasonable that for s, and to a much smaller extent for p, electrons it should break down. The presence of the contact term discussed in section 1 shows that the s electron wave function does not vanish at the nucleus. Also if the nucleus is of finite extent it is expected that there will be a small overlap with p electron wavefunctions.

The original quantitative theory of the effects of finite nuclear size on hyperfine interactions was developed by Bohr and Weisskopf (1950) and subsequently refined by several authors, for example, Eisinger and Jaccarino (1958). Bohr and Weisskopf showed that the effect of the finite size on an s electron was two-fold. Firstly, the electric potential within the nuclear volume becomes non-Coulombic, and secondly, the nuclear charge is distributed throughout the volume of the nucleus. Since the magnitude of the hyperfine interaction, depends upon the electron distribution, the change in electric

potential within the nuclear volume changes the hyperfine interaction, the change being shown to be negative. One of the problems inherent in a calculation of this effect is that of finding a description of the electronic potential within the nucleus. Bohr and Weisskopf assumed a uniform charge distribution throughout the nucleus, and calculated the reduction in contact interaction relative to a point nucleus. If one compares the interactions for two isotopes of the same atomic number Z, it is clear that the nuclei will be different, and should show different changes in hyperfine interaction. Further the distribution of magnetic moments in the nucleus has to be considered. The nucleons, analogously with electrons, show orbital and spin magnetic moments, and it is easy to see that these will give markedly different contributions to the interaction with an s electron. On a classical picture, a rotating uniformly charged sphere corresponds to an inwardly increasing magnetisation leading to the orbital contribution to the nuclear magnetisation being small near to surface of the nucleus and increasing towards the centre, whilst the spin magnetisation is assumed to be uniformly distributed throughout the nuclear volume. Bohr and Weisskopf calculated the interaction of a Dirac electron with the magnetic potentials associated with the spin and orbital currents. Thus if one has two isotopes

of the same nucleus, the hyperfine interaction due to the contact term may be expressed as

$$A_1 = g g_{1n} \beta \beta_n \langle r^{-3} \rangle - \varepsilon_1 \qquad A_2 = g g_{2n} \beta \beta_N \langle r^{-3} \rangle - \varepsilon_2$$

$\varepsilon_1, \varepsilon_2$ represent the reduction in A_c due to the finite nuclear size.

giving $$\frac{A_1 \, g_{2n}}{A_2 \, g_{1n}} = 1 + \Delta$$

where Δ is a small quantity typically of the order of 0.5% determined by the values of ε_1 and ε_2. This is termed the hyperfine structure anomaly for isotopes 1 and 2. $\Delta = 0$ for a point nucleus.

Δ has been determined experimentally for a number of isotopes recently, of particular interest in this thesis are the measurements on Eu by Baker and Williams (1962) and Evans, Sanders and Woodgate (1965), and on Yb by Budick and Snir (1967) and Unna (1967). The determination of Δ is useful for both hyperfine structure theory as it provides information about the s electron density of a system, and for nuclear structure theory, providing a test of nuclear models.

Let us consider the information provided about hyperfine

structure first, with particular reference to the experiments on Europium mentioned above. In Eu^{2+} Baker and Williams found a hyperfine structure anomaly of -0.63% for the isotopes Eu^{151} and Eu^{153}, but in the Eu atom Evans et. al. found zero anomaly. Thus in the atom there must be no s electron contribution to the hyperfine interaction, which can only originate therefore from relativistic effects. In the divalent ion however the existence of a hyperfine structure anomaly shows that there must be core polarisation producing unpaired s electrons at the nucleus. This will give a contribution to the hyperfine structure in addition to the relativistic effects. It can thus be seen that if an anomaly can be measured in different valence states and environments useful information relating to core polarisation and relativistic electron effects can be obtained.

The nuclear information that may be obtained from a measurement of the hyperfine structure anomaly will be mentioned very briefly. The method of calculation of Δ outlined above from Bohr and Weisskopf requires a knowledge of the electron configuration, the electric potential within the nucleus and the distribution of nuclear magnetic moment within the nucleus. The crude picture by Bohr and Weisskopf has been refined by several authors, particularly Eisinger and Jaccarino (1958) who make better approximations for the

electron wavefunctions, and Stroke, Blin-Stoyle and Jaccarino (1961) who show that the form of the potential inside the nucleus is important. They use a trapezoidal charge distribution in the place of the earlier spherically symmetric distribution, this type of distribution being based on results of high energy electron scattering experiments.

The distribution of nuclear magnetism also affects the theoretical anomaly strongly. In the strongly deformed rare earth nuclei, the multipole moments are best predicted using Nilsson wavefunctions (1955) and it would appear reasonable to use these states to calculate the anomalies. This has been done by Unna for Yb^{171} and Yb^{173} who shows reasonable agreement between his calculation using Nilsson states and the experimental value of Δ obtained by Budick and Snir (1967) for the excited $^3P_1$ state of the Yb atom.

REFERENCES

Abragam, A., 1961. The Principles of Nuclear Magnetism, Clarendon Press, Oxford.

Baker, J.M. and Bleaney, B., 1958. Proc. Roy. Soc. A245, 156.

Baker, J.M. and Williams, F.I.B., 1962. Proc. Roy. Soc. A267, 283.

Bleaney, B., 1964. Proc. Conf. on Quantum Electronics, Vol. 3, 595, Columbia Univ. Press.

Blok, J., and Shirley, D.A., 1966. Phys. Rev. 143, 278.

Bohr, A. and Weisskopf, V.F., 1950. Phys. Rev. 77, 94.

Budick, B. and Snir, J 1967. Phys. Letts. 24B, 276.

Casimir, H.B.G. and Karreman, G., 1942. Physica, 9, 494.

Cohen, M.H. and Reif, F., 1957. Solid State Physics, 5, 321.

Das, T.P. and Hahn, E.L., 1958. Solid State Physics Supplement 1.

Eisinger, J. and Jaccarino, V., 1958. Rev. Mod. Phys. 30, 528.

Evans, L., Sandars, P.G.H. and Woodgate, G.K., 1965. Proc. Roy. Soc. A289, 114.

Freeman, A.J. and Watson, R.E., 1961. Phys. Rev. Letts. 6, 277, 388.

Freeman, A.J. and Watson, R.E., 1963a. Phys. Rev. 131, 250.

Freeman, A.J. and Watson, R.E., 1963b. Phys. Rev. 131, 2566.

Freeman, A.J. and Watson, R.E., 1965. Magnetism IIA, 167. Ed. Rado and Suhl.

Harvey, J.S.M., 1965. Proc. Roy. Soc., A285, 581.

Heine, V., 1957. Phys. Rev. 107, 1002.

Jaccarino, V., King, J.G., Satten, R.A. and Stroke, H.H., 1954. Phys. Rev. 94, 1798.

Judd, B.R., 1963. "Operator Techniques in Atomic Spectroscopy", McGraw-Hill.

Koster, G.F. and Statz, H., 1959. Phys. Rev. 113, 445.

Nilsson, S.G., 1955. Mat. Fys. Medd. Dan. Vid. Selsk, 28, No.16.

Ray, T., 1964. Proc. Roy. Soc. A277, 76.

Sandars, P.G.H. and Beck, J., 1965. Proc. Roy. Soc. A289. 97.

Sternheimer, R.M., 1966. Phys. Rev. 146, 140.

Stroke, H.H., Blin-Stoyle, R.J., Jaccarino, V., 1961. Phys. Rev. 123, 1326.

Unna, I., 1967. Phys. Letts. 24B, 499.

Woodgate, G.K., 1966. Proc. Roy. Soc. A293, 117.

CHAPTER 3

EXPERIMENTAL APPARATUS

Three separate ENDOR spectrometers were constructed to perform the experiments described in this thesis. However, the basic principles of operation were identical and will be considered before detailed descriptions of each is given.

The principle of operation was similar to that of the apparatus described by Baker and Williams (1962). A microwave source feeds into a resonant cavity via a magic tee. The EPR signals are detected by 115 kc/s modulation of the magnetic field, the amplitude modulated reflected microwaves being detected by a crystal rectifier and 115 kc/s phase sensitive detector. A second r.f. field is fed into the resonant cavity from some frequency or amplitude modulated oscillator to induce the nuclear transitions. The orientations of the fields in the cavity depend upon the experiment in question and will be discussed in that context. The output of the 115 kc/s detector is phase sensitively detected at the nuclear modulation frequency, the output from this detector being recorded on a chart recorder. When an ENDOR transition is induced, an amplitude modulated change in the EPR signal occurs, which gives a signal on the output of the second

detector. The modulation frequency of the nuclear frequency is determined by the nuclear relaxation rate, which leads typically to frequencies in the low audio range of a few tens of cycles. If the nuclear frequency is amplitude modulated, the output of the second phase sensitive detector will be the direct ENDOR line shape, whilst if the frequency is frequency modulated the output will be a first derivative of the ENDOR line shape. For the work described in this thesis both types of modulation were used depending on the oscillator and frequency range in use. This will be discussed specifically in each case.

In all cases the experimental procedure was the same. The EPR signals were observed on an oscilloscope using 115 kc/s modulation and 50 c/s field sweep. The EPR spectrometer was adjusted to give the best signal/noise ratio on a fast passage line, the microwave power being adjusted to the level at which the signal/noise ratio began to decrease with increasing power. It was found that this crude measure of the onset of saturation was close to the power level required for maximum ENDOR signals. The 50 c/s sweep was removed and the magnetic field adjusted to the centre of the EPR line. The nuclear frequency appropriately modulated was swept mechanically with a Venner clock motor coupled to the oscillator dial. The rate of sweep could be varied by driving the synchronous

motor with the output from a variable frequency audio frequency oscillator, in the range 25 to 200 c/s. By removing the governors from the motor the direction of rotation could be reversed. The ENDOR frequencies were measured with either a Rohde and Schwartz WIK or JAC 331 frequency meter.

The particular configuration for applying, modulating and measuring the frequencies is described for each experiment. The magnetic field was provided by a Varian 12 inch fieldial regulated electromagnet, the field being measured with a transistorised proton resonance probe built to the design given by Robinson (1965), with a small pair of Helmholtz coils wound around the NMR coil to provide a 5 gauss 50 c/s field sweep to enable the proton resonance signal to be displayed on an oscilloscope. The frequency was measured by locking the probe to the JAC frequency meter. A block diagram of the general aspects of the apparatus is shown in Figure 3.1.

Q Band Spectrometer

The Q band spectrometer which was used for measurements on the Gd and Yb isotopes consisted of a TE011 cylindrical cavity used in a reflection mode with a simple microwave magic tee balanced bridge detection system. The cavity shown in Figure 3.2 was mounted with its axis horizontal coupling to

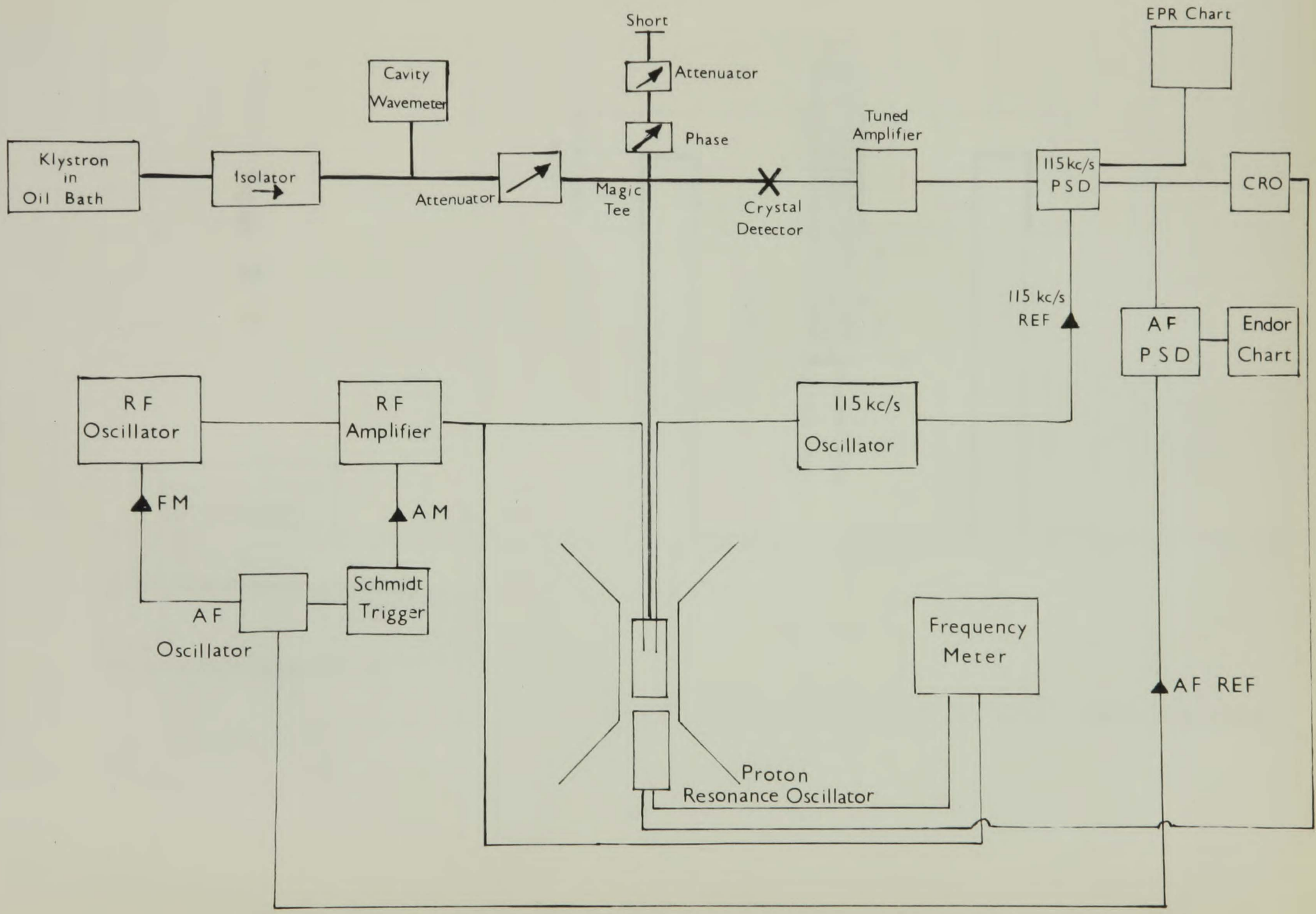
Short
EPR Chart
Cavity
Wavemeter
Attenuator
Phase
Tuned
Amplifier
Klystron
in
Oil Bath
Isolator
Attenuator
Magic
Tee
Crystal
Detector
115kc/s
PSD
CRO
115 kc/s
REF
AF
PSD
Endor
Chart
RF
Oscillator
RF
Amplifier
115kc/s
Oscillator
FM
AM
Schmidt
Trigger
AF
Oscillator
Frequency
Meter
AF REF
Proton
Resonance Oscillator

Figure 3. 1

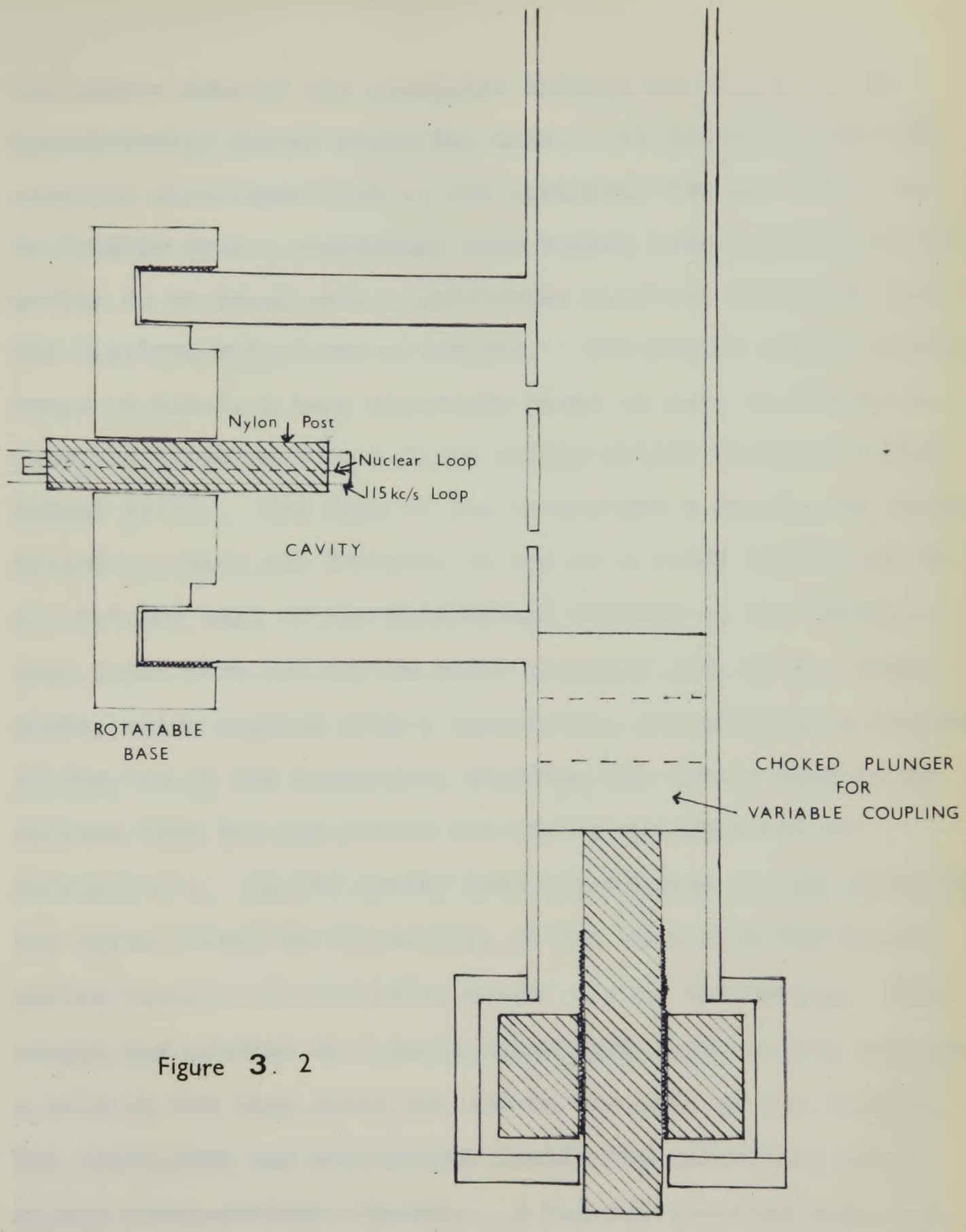

Figure 3. 2

Q BAND ENDOR SPECTROMETER

Four times actual size

the narrow face of the waveguide through two small holes symmetrically placed about the axis. It had been found by previous experience that it was desirable for the cavity to be tunable over a reasonably wide tuning range, to enable the cavity to be tuned onto a particular klystron frequency where the klystron output was a maximum. The rather narrow tuning range of E.M.I. Q band klystrons makes it more difficult to tune the klystron onto a fixed cavity whilst ensuring a high output level. The base of the cavity was a re-entrant brass cylinder, which was threaded to run on a screw thread cut on the outside wall of the cylindrical section of the cavity. Gear teeth were cut on the outer circular wall of the base plate, which engaged with a worm-drive, connected to a control at the top of the apparatus, enabling the cavity base to be rotated from the top whilst the cavity was immersed in refrigerant. As the cavity base was rotated it was driven on the screw thread on the cavity, giving it a slow horizontal motion parallel to the iris, hence tuning the cavity. The sample was mounted on a small nylon post which passed through a hole in the base plate centred on the axis of the cavity. The nylon post was cylindrical inside the cavity and of square cross-section outside. A 0.5 mm. diameter hole was drilled along its axis, and three narrow slots cut parallel to this hole along the outside of the dielectric. A fine

insulated wire was passed up one slot, over the sample and returned outside the cavity in the second slot. This wire carried the 115 kc/s current to provide the high frequency field modulation and with care could be inserted in the cavity without lowering the cavity Q. A second wire ran through the central hole, over the crystal and returned along the third slot. This was connected to the source of nuclear signal, the central wire being connected to the centre conductor of a coaxial line, the wire in the slot being earthed to the cavity base. This arrangement allowed the production of 115 kc/s, microwave field and nuclear field, to be mutually orthogonal to the first order, but a small coupling was used between the nuclear and 115 kc/s loops to detect when the nuclear field was a maximum in the cavity by measuring the r.f. voltage picked up by the 115 kc/s loop, which was greatest when the nuclear field was greatest, and so maximise the nuclear field in the cavity. The whole crystal mount assembly could be rotated about its central axis independently of rotation of the cavity base through which it passed by connecting the square cross-section of the post to a pivoted lever, controlled by a micrometer screw head at the top of the apparatus. This arrangement enabled the sample to be rotated through 90° in a plane perpendicular to the plane of

rotation of the magnet. This greatly facilitated the orientation of specimens which is essential for ENDOR.

The coupling of the cavity to the waveguide could be varied, by moving a shorting plunger inside the waveguide, again driven through a gearing mechanism from the top of the apparatus. The Q of the system, with a crystal in the cavity and both wire loops correctly installed was about 3500. The whole cavity assembly was enclosed in a brass can which fitted onto a greased cone-joint.

The Q band microwave power around 36kMc/s was provided by an E.M.I. klystron type R5146 immersed in an oil bath. When surrounded by the large thermal bulk of the oil bath and mounted on rubber pads to reduce mechanical vibration, a very good short term stability of klystron frequency was obtained without use of an electronic Pound type frequency locking system. Such a system had been found to interfere with the low frequency ENDOR measurement in the range 5-10 Mc/s, and hence had been removed from the system, without any marked effect on the klystron stability.

Q Band Apparatus for Tb^{3+} Measurement

The ENDOR transitions for this system were expected to occur at 3135 Mc/s, 3830 Mc/s and 2440 Mc/s as shown in

Chapter 6. Initially the search for ENDOR was concentrated on the $\frac{1}{2} \rightarrow -\frac{1}{2}$ transitions because firstly their positions can be predicted to within about 6 Mc/s and secondly it was expected that these lines would be sharper than the quadrupole lines, which are sensitive to any random crystal field gradients present in the crystal. The zero field splitting of Tb^{3+} in yttrium ethylsulphate is 0.387 cm^{-1} and hence no EPR can be seen at X band. It was originally decided to work at Q band (35 kMc/s) for the EPR as this was the highest frequency that was readily available, with sufficient power to saturate the EPR lines. It is desirable to work at the highest possible frequency with which the EPR can be saturated, as it can easily be shown that a cavity of given Q operating at 35 Mc/s gives an r.f. field roughly 6 times that of an equivalent X band cavity with the same input power. Also it is well known that EPR sensitivity varies as $\omega^{7/2}$ (Feher 1957), and it is desirable to work with the largest EPR signals attainable.

The second important factor governing the design of apparatus is the nuclear frequency and the range over which it is desired to sweep it. For the Tb^{3+} experiment one requires a frequency in the range 2400 - 3800 Mc/s, which lies in the 10 cm. (S band) microwave region. At the time of designing this apparatus the only satisfactory S band source available was an E.M.I. klystron type CV2116 which

gives an output power of 150 - 200 mW over most of the required range. There were no amplifiers available at this frequency and thus to obtain a reasonable nuclear field at the cavity considerable care had to be taken to match the output power of the klystron to the r.f. coil at the cavity. Several types of field coil were investigated, bearing in mind that the system had to be broad band over a wide range or tunable over that range. A single post as described by Baker and Williams (1962) would not fulfil these requirements. In order to obtain the maximum field it was decided to devise a resonant system, and the design finally adopted was a resonant hairpin arrangement. It consisted of a length of 8 mm. waveguide with a narrow slot cut centrally along the broad faces of the guide. The S band frequency was introduced by placing a loop at the end of a coaxial line from the oscillator, across the slot in the waveguide. This magnetic coupling excites a longitudinal mode of propagation along the slot which acts as a transmission line shorted at both ends. The two conductors are the two halves of the guide separated by the slots. When the length of the slot is a half free space wavelength for the S band frequency the system is resonant, producing a maximum r.f. field. The system was found to have a Q of about 50. To tune the resonant line

a pair of phosphor-bronze spring fingers ran along the slots in the guide, shorting the slot and hence changing its effective length. These fingers were driven from a micrometer screw head at the top of the apparatus, enabling the system to be tuned during the experiment. As a check on the performance of this system, the EPR of D.P.P.H. and plasticene was observed at 10 cm. The dependence of the field with position of the tuning fingers was checked and confirmed that the system was acting as a tunable S band resonant transmission line.

The design of the r.f. system determined the design of the 8 mm. (Q band) EPR detection system. The resonant cavity was formed by inserting an iris across the Q band waveguide, and inserting a tightly fitting choked plunger into the bottom of the guide, forming a resonant cavity between the coupling iris and the plunger. The plunger was attached to a worm drive which enabled it to be moved vertically inside the waveguide from a motion at the top of the dewar, thus enabling tuning of the cavity whilst the cavity is immersed in refrigerant. The EPR was detected by the usual 115 kc/s field modulation technique. The 115 kc/s was introduced from a pair of coils wound outside the cavity, adjacent to the r.f. transmission line slot. This cavity gave reasonably

good EPR sensitivity, the relatively poor Q of 1200 being offset by a good filling factor.

The S band klystron output was transformed from a waveguide output to a coaxial line and connected through a tuning stub to the coaxial line feeding the resonant "hairpin". A second loop was attached to the other side of the waveguide and used to monitor the level of r.f. at the hairpin, the power being picked up being maximised by tuning the hairpin and tuning stub. The klystron was either frequency modulated by variation of the reflector voltage, or amplitude modulated, using a waveguide switch, which reduced the power transmitted in the waveguide by about 30 db, when the diode was conducting. The klystron frequency was swept either by variation of the reflector voltage at the power supply, or by mechanically driving the micrometer tuning of the klystron. With the klystron well shielded from draughts and mechanical vibrations the frequency stability of the klystron over short term was better than one part in five thousand, which was adequate for this experiment.

J Band Apparatus

An ENDOR apparatus was constructed working with an EPR frequency of 15 kMc/s and a nuclear frequency in the 3 kMc/s

range. The EPR system consisted of a rectangular cavity operating in a TE 102 mode. The base of the cavity was the top face of a choked plunger which could be moved vertically inside the waveguide, from a geared system. The microwave power was coupled into the cavity through a centrally placed iris of about 2 mm. diameter. Above the cavity the waveguide was tapered from the normal J band german silver guide to a section of guide whose cut-off frequency was above 15 kMc/s. A piece of dielectric filled the cut off guide and taper. To vary the coupling of the microwaves to the cavity, the dielectric could be moved vertically in the waveguide with a tongued bush which protruded through a slot machined in the broad face of the guide.

The nuclear frequency was introduced by a helix wound across the centre of the cavity between the broad faces of the guide. The helix was made by winding two parallel 1.2 mm. diameter wires in a tight bifilar manner on a 2.5 mm. diameter former, leaving no spaces between the windings. One of the pieces of wire was then unwound, leaving a helix, with the space between the turns equal to the diameter of the wire. It can be shown that the power attenuated in the helix is a minimum for this condition (Pierce 1951). For a helix wound with the above dimensions, the intrinsic impedance is 140 ohms, and the magnetic field at the centre for 3 Gc/s microwaves

with an input power of 0.1 watt should be about 5 gauss. The helix was also used to carry the 115 kc/s current to produce the magnetic field modulation. The experimental arrangement is shown in Figure 3.3. The crystal was mounted inside the helix with its symmetry axis lying in a horizontal plane at 45° to the axis of the helix. It was held in place by glueing it to a cylinder of styrofoam, which fitted inside the helix.

The cavity system had a Q factor of 1500 when fully assembled at 15 kMc/s and was shown to work adequately as an ENDOR cavity, by observing the ENDOR of Co^{2+} in MgO. This enabled the electronic detection system to be tuned up for maximum sensitivity. These experiments showed the system to be highly susceptible to microphonics. Several unsuccessful attempts were made to reduce the effect of the microphonics by potting the helix in various araldites and perspex cement. When the cavity was used for the Tb^{3+} investigations, it was essential to match the 3 Gc/s power into the helix. This was done by making the german silver coaxial lines feeding the helix with an impedance roughly equal to that of the helix and by using a matching stub at the junction between the 50Ω coaxial lines from the klystron output to the 140Ω coaxial line.

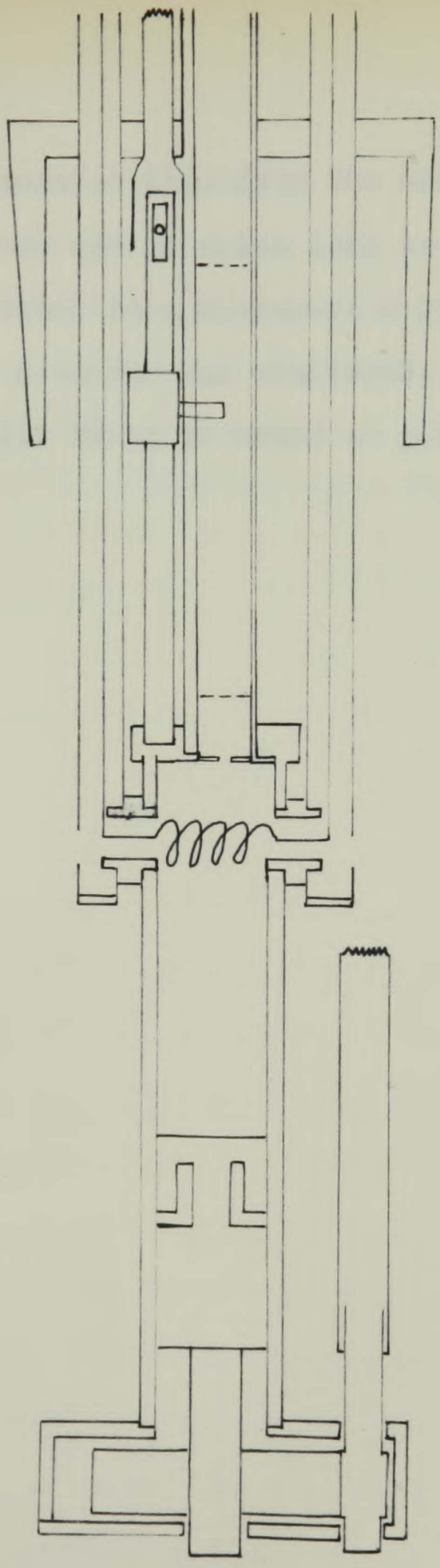

Figure 3. 3

J BAND ENDOR SPECTROMETER

The second coaxial line from the helix was connected to a T-section, one arm of which lead to the 115 kc/s oscillator, the other to a microwave crystal detector. Power output from this detector was monitored, the tuning stub preceding the helix being adjusted to give a maximum crystal current.

REFERENCES

Baker, J.M. and Williams, F.I.B., 1962. Proc. Roy. Soc. A267, 283.

Feher, G., (1957). Bell.Syst. Tech. J. Vol. 36. p. 449.

Pierce, J.R., (1950). Travelling Wave Tubes. Van Nostrand.

C H A P T E R 4

ENDOR OF TRIVALENT YTTERBIUM IN CALCIUM FLUORIDE

1. Introduction

Trivalent ytterbium has a number of properties which make it an interesting system to study by ENDOR techniques. The free ion ground state electronic configuration is $4f^{8}$, $^{2}F_{7/2}$, and can thus be visualised as a single hole in an otherwise completed 4f shell. This results in an electronic configuration which is simple and relatively straightforward to treat theoretically. It is isoelectronic with Tm^{2+}, which when substituted into CaF_2, has been studied in detail by EPR, ENDOR and optical techniques, as discussed by Bleaney (1964) and Bessant and Hayes (1965). Ytterbium has two isotopes with non zero nuclear spin, Yb^{171} ($I = \frac{1}{2}$) and Yb^{173} ($I = 5/2$) which are 14% and 16% abundant respectively. There are a number of zero spin isotopes, which comprise 70% of naturally occurring Yb. Recently several authors have studied the nuclear magnetic properties of Yb^{171} and Yb^{173}. Gossard et. al. (1964) measured the nuclear magnetic moments of Yb^{171} in the diamagnetic

divalent ytterbium ion by observing NMR in Yb Cl_2 and Yb S. They were unable to detect the NMR of Yb^{173}, which was probably broadened by quadrupolar effects. Olschewski and Otten (1967) measured the nuclear magnetic moments of Yb^{171} and Yb^{173} very accurately using an optical pumping technique, and Budick and Snir (1967) used level-crossing spectroscopy to measure the hyperfine interactions of these isotopes in the $^3P_1$ excited state of the Yb atom. From these measurements they deduced a hyperfine structure anomaly of -0.376% for the two isotopes from the $^3P_1$ atomic state, which was the subject of a theoretical paper by Unna (1967).

The optical spectrum of Yb^{3+} in CaF_2 has been studied by several authors, whose work is reviewed by Kirton and McLaughlan (1967). They show by correlation of EPR spectra and optical spectra arising from Yb^{3+} in sites of different symmetries, that the positions of the excited states in Yb^{3+} at the cubic site of CaF_2 are unknown.

ENDOR experiments on Yb^{171} and Yb^{173} in CaF_2 complement the results mentioned above in several ways. An accurate measurement of the magnetic hyperfine interaction for these isotopes, combined with the ratio of nuclear moments obtained by Olschewski and Otten would give an accurate value for the hyperfine structure anomaly in the trivalent

ion. Using the value of this anomaly obtained by Budick and Snir for the atom a value for the core polarisation contribution to the hyperfine structure may be deduced. This is discussed in Section 6 of this chapter where it is compared with the value predicted by Bleaney (1963). A comparison between the nuclear g-factor measured by ENDOR in the paramagnetic ion and by NMR in the atom or diamagnetic ion enables the position of the first excited crystal field state to be determined to be 600 cm^{-1}. Further, the accuracy of the ENDOR measurements of the hyperfine interactions shows that the spectrum requires higher order interactions to be included in the spin-Hamiltonian as discussed in Chapter 2.

2. Crystal Field Behaviour

The crystal structure of CaF_2 can be visualised as a simple cubic array of F^- ions with Ca^{2+} ions at the body centres of alternate cubes. The symmetry at the Ca^{2+} site can be represented by the point group O_h. CaF_2 has the very useful property that it will accept all the rare-earths as substitutional impurities at the Ca^{2+} sites. The rare-earth ions are often trivalent and compensation for the excess positive charge occurs in several ways, giving rise to local symmetries of the crystal field at the rare-earth

ion sites which are non-cubic. The general properties of rare-earth ions in CaF_2 have been reviewed by Weber and Bierig (1964), Bierig, Weber and Warshaw (1964), and Kirton and McLaughlan (1967). All the work to be reported here has been performed on Yb^{3+} in cubic sites, where the charge compensation is sufficiently far removed from the rare-earth site for the symmetry not to be lowered from O_h.

The crystal field may be represented in terms of operator equivalents as $B_4(O_4^0 + 5O_4^4) + B_6(O_6^0 - 21O_6^4)$. The electronic configuration $4f^{13}$ has only two J manifolds. Hund's rules predict $J = 7/2$ for the lowest manifold, the $J = 5/2$ manifold being at $7/2\,\zeta$ where ζ is the spin-orbit coupling parameter. This level is roughly 10,000 cm^{-1} above the ground manifold. In a cubic crystal field the $J = 7/2$ manifold splits into two doublets Γ_6 and Γ_7, and a quartet Γ_8. The $J = 5/2$ manifold splits into a Γ_7 doublet and Γ_8 quartet. Lea, Leask and Wolf (1962) have shown that for Yb^{3+} in a cubic crystal field, the ground level is either Γ_6 or Γ_7 depending upon the relative values for the crystal field terms B_4 and B_6. The EPR spectrum for this system is isotropic with $g = 3.443 \pm 0.002$ which indicates that the Γ_7 doublet is lowest as this should show a g-factor of $\frac{24}{7} = 3.428$, if no other states are admixed

into it. Using the crystal field potential given above in terms of operator equivalents, the eigenfunctions of the crystal field states may be calculated. These are shown in Table (4.1), expressed in terms of $|J, J_z\rangle$ quantisation. No account is taken of crystal field admixtures between the two manifolds. A difficulty arises in expressing the eigenvalues of these states directly in terms of the crystal field parameters, as these have different values in the two different J manifolds (Bleaney 1964). It is convenient in this respect to work in $|L,S\ (L,S)\rangle$ quantisation as we are dealing with a single hole in an otherwise complete 4-f shell. Using the notation given by Bleaney (1964) we define $b_4 = 60\ B_4$, and $b_6 = 180\ B_6$, where B_4 and B_6 are applicable to $|LS\rangle$ quantisation. The eigenvalues of these levels expressed in this quantisation are shown in Figure (4.1) and Table (4.1).

Bleaney (1964) makes a detailed study of the causes of the deviations of the electronic g-factor of Tm^{2+} in CaF_2 from the theoretical value for a Γ_7 doublet. The principal contribution to the difference arises from the crystal fields admixing Γ_7 and Γ_8 from the $J = 5/2$ manifold into the respective levels in the $J = 7/2$ manifold. However, this admixture, calculated from a knowledge of the positions of

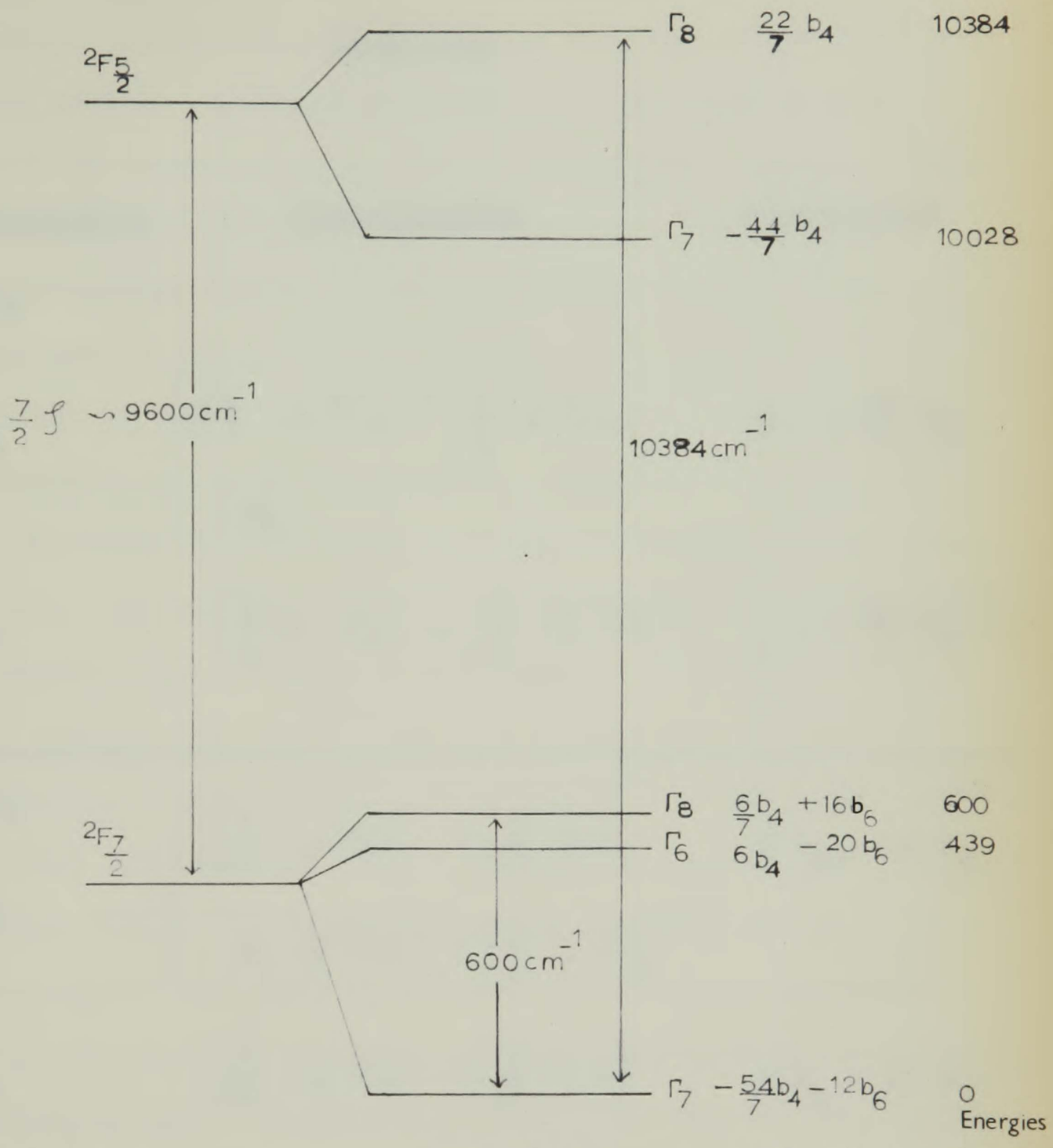

APPROXIMATE ENERGY LEVELS OF Yb^{3+} in CaF_2
SHOWING POSSIBLE CRYSTAL FIELD ENERGIES

Figure 4.1

TABLE 4.1

Representation	Eigenfunction	Eigenvalues
$J = 5/2$		
Γ_8	$\begin{cases} \sqrt{\frac{5}{6}} \lvert \pm 5/2 \rangle + \sqrt{\frac{1}{6}} \lvert \mp 3/2 \rangle \\ \lvert \pm \frac{1}{2} \rangle \end{cases}$	$\frac{7}{2} f + \frac{22}{7} b_4$
Γ_7	$\sqrt{\frac{1}{6}} \lvert \pm 5/2 \rangle - \sqrt{\frac{5}{6}} \lvert \mp 3/2 \rangle$	$\frac{7}{2} f - \frac{44}{7} b_4$
$J = 7/2$		
Γ_8	$\begin{cases} \sqrt{\frac{7}{12}} \lvert \pm 7/2 \rangle - \sqrt{\frac{5}{12}} \lvert \mp \frac{1}{2} \rangle \\ \frac{1}{2} \lvert \pm 5/2 \rangle + \sqrt{\frac{3}{4}} \lvert \mp 3/2 \rangle \end{cases}$	$\frac{6}{7} b_4 + 16 b_6$
Γ_6	$\sqrt{\frac{5}{12}} \lvert \pm 7/2 \rangle + \sqrt{\frac{7}{12}} \lvert \mp \frac{1}{2} \rangle$	$6 b_4 - 20 b_6$
Γ_7	$\sqrt{\frac{3}{4}} \lvert \pm 5/2 \rangle - \frac{1}{2} \lvert \mp 3/2 \rangle$	$-\frac{54}{7} b_4 - 12 b_6$

Crystal field states for Yb^{3+} in cubic sites in CaF_2

the excited states was insufficient to explain fully the g-factor shift. Bleaney accounted for the remainder of the shift by introducing an orbital reduction factor arising from covalent bonding with the F^- ligands. Inoue (1963) however suggests that an orbit-lattice interaction should be important, contributing 30% of the observed shift. Similar considerations should hold for Yb^{3+}, where in principle the same corrections could be applied. However, the problem cannot be solved unambiguously in this case as there is insufficient optical data to enable the crystal field parameters and excited state energies to be found. There have been several conflicting reports in the literature as regards the position of the excited states of Yb^{3+} in CaF_2, Low (1962), Kiss (1962) and Twidell (1963). Recently Kirton and McLaughlan (1967) have re-examined this system and by correlating EPR and optical spectra in specimens prepared under conditions with different charge compensation mechanisms. They conclude that the previous identifications of the optical transitions with allowed transitions in cubic Yb^{3+} were incorrect and that the parameters deduced from these experiments were wrong. They were unable to make any positive measurement for the cubic field splitting but concluded that

it was probably close to that of Tm^{2+} at 410 cm^{-1}, for the separation of Γ_7 and Γ_8 in the $J = 5/2$ manifold.

3. Possible values of the crystal field parameters

The ENDOR data to be discussed later given a value for the pseudo-nuclear g-factor for Yb^{3+} in CaF_2, from which the separation of the Γ_8 quartet from the Γ_7 ground doublet is deduced to be 597 ± 3 cm^{-1}. Using this value, the spin-orbit coupling constant, and the one optical transition positively identified by Kirton and McLaughlan as arising from cubic Yb^{3+}, an estimate of the crystal field parameters can be made. The energy gap between Γ_7 and Γ_8 is given by $\frac{60}{7} b_4 + 28 b_6 = 597 \pm 3$ cm^{-1}. The energy between $^2F_{7/2}$ and $^2F_{5/2}$ in the free ion is $7/2\ \zeta$ where ζ is the spin-orbit coupling parameter. ζ has the value 2882.9 cm^{-1} in the free ion (Dieke and Crosswhite 1963). It is probable that the value of the spin-orbit coupling will not change by more than about 1% from this value when the ion is incorporated in CaF_2. The general behaviour of ζ in rare-earth ions is discussed by Dieke and Crosswhite (1963), Freeman and Watson (1962) and Jorgensen (1956), who conclude that the crystalline environment will only have a small effect on ζ, the effect decreasing as the nuclear charge increases

through the rare-earth series. Indications from measurements of this parameter in various hosts suggest that a deviation of about 1% is usual when the ion in introduced into a crystal.

Kirton and McLaughlan report an optical absorption line at 10384 cm^{-1} which they correlate with a cubic EPR spectrum. As this is greater than $^{7}/_{2}$ f it can only arise from a transition between Γ_8 of $^2F_{5/2}$ and Γ_7 of $^2F_{7/2}$, as shown in diagram (4.1). From this data, assuming that f is accurate to $\pm$ 1%, the values of b_4 and b_6 can be derived to be

$$b_4 = (37.8 \pm 7)\ cm^{-1} \qquad b_6 = (9.9 \pm 2)\ cm^{-1}.$$

4. EPR spectrum

In Figure (4.2) the isotropic EPR spectrum from cubic Yb^{3+} in CaF_2 at 4.2° K is shown. This was measured at 35 Gc/s with the magnetic field aligned parallel to a cube edge of the sample. The spectrum has an electronic g-factor of 3.443 $\pm$ 0.002. The intense central transition arises from the zero spin isotopes, whilst the hyperfine structure from the two non-zero spin isotopes is easily identified, the two larger lines coming from Yb^{171} and the six smaller ones from Yb^{173}. The resolved superhyperfine structure on

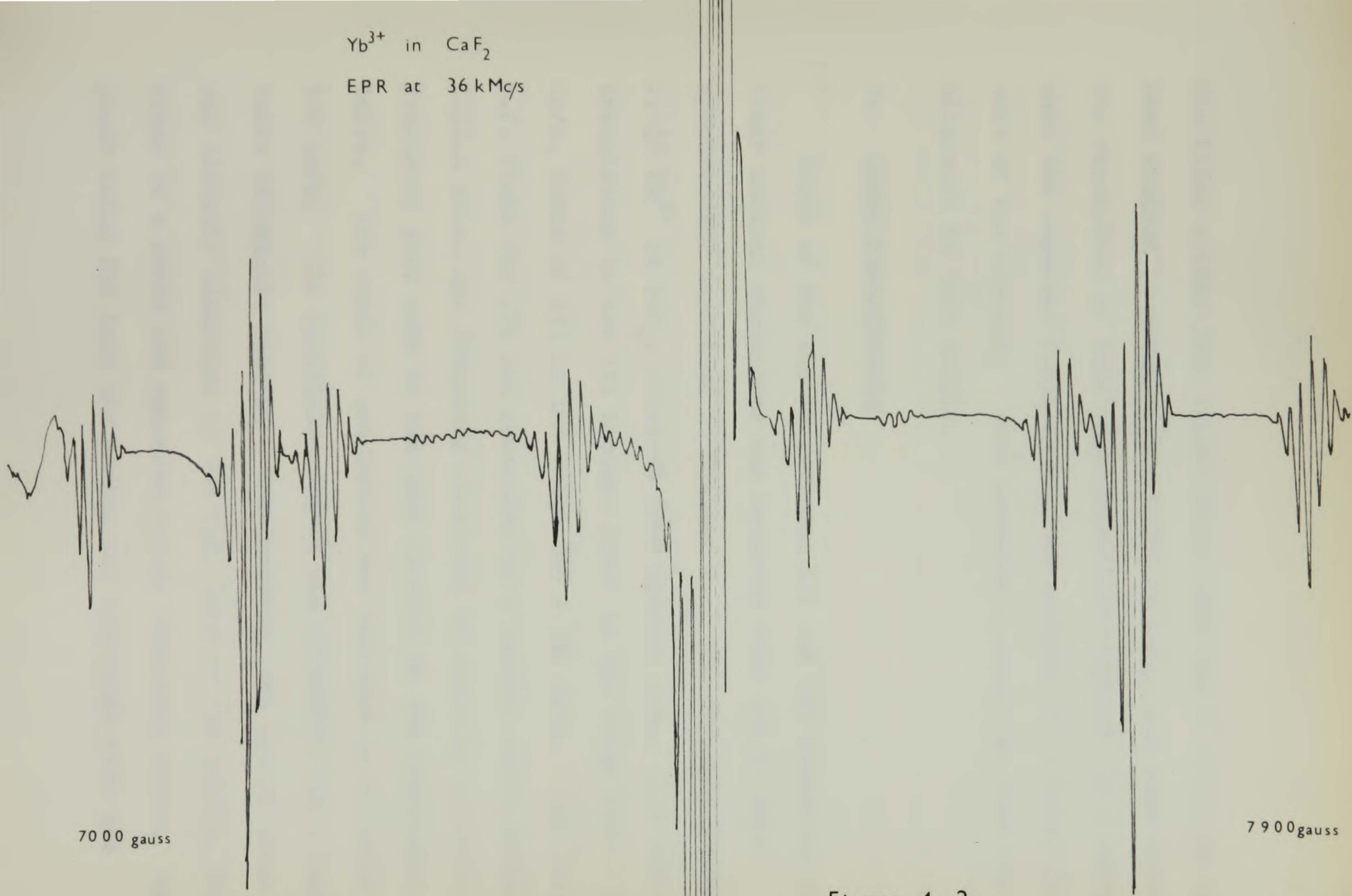

Figure 4. 2

the lines arises from interactions with the F^- ions and has been studied in detail using ENDOR by Ranon and Hyde (1966). The resolution of this superhyperfine structure is a maximum when the magnetic field is aligned parallel to a cubic (100) axis of the crystal. This provided a sensitive test for alignment in this sample.

5. ENDOR measurements

ENDOR of the two Yb isotopes 171 and 173 occurring in their natural abundances was measured with the 35 Gc/s spectrometer described in Chapter 2. The crystals contained 0.05% Yb^{3+} in CaF_2, obtained from Optovac Inc.. The nuclear transitions in the 171 isotope occur in the range 1260 - 1380 Mc/s, those of 173 in the range 340 - 380 Mc/s. The nuclear r.f. field for 171 was generated by a General Radio oscillator 1218-A which was frequency modulated by applying an audio frequency sine wave to the grid circuit of the oscillator valve. The depth of modulation was variable up to about 100 kc/s. The oscillator output was connected via a General Radio adjustable line to a tee-junction, one arm of which was directly connected to the r.f. loop in the cavity, the other to a Rohde and Schwartz W.I.K. frequency meter. The power being fed into the cavity was maximised with the

adjustable line, the level being monitored by r.f. pick up on the nominally orthogonal 115 kc/s loop.

The r.f. field for the 173 isotope was generated with a General Radio 1209-B oscillator. This was adapted for frequency modulation by the insertion of a back-biased variable capacitance diode (Hughes 6002) connected in parallel with the oscillator tuning capacitor, the circuit being essentially that described by Williams (1961). The output from this oscillator was amplified by a Boonton 230-A tuned power amplifier, and then fed to the cavity via a variable line. The operating procedure was very similar to that described earlier, the only additional feature being that the power amplifier had to be tuned as the r.f. frequency was swept.

The ENDOR lines were observed at 4.2° K. The conditions for maximum ENDOR signal were found to arise when the microwave power level was adjusted to the level at which the EPR signal observed on the oscilloscope with a 50 c/s field sweep stopped increasing with increasing power. The 115 kc/s level was adjusted until the amplitude of the EPR signal was a maximum consistent with no broadening of the line and hence no diminution of the resolution of the fluorine superhyperfine structure.

Yb^{171} : As $S = \frac{1}{2}$, $I = \frac{1}{2}$, there are only four possible ENDOR transitions, three of which were observed. The missing line was $I_z = \frac{1}{2} \rightarrow -\frac{1}{2}$ on the $S_z = +\frac{1}{2}$ level of the $I_z = +\frac{1}{2}$ hyperfine EPR line. The lines which were observed are shown in Figures (4.3) and (4.4). Recently Mr. W.B.J. Blake has observed the fourth transition. The ENDOR lines were all about 470 kc/s wide but of markedly different intensities. Using the formula derived by Bessent and Hayes (1965) for ENDOR linewidth it appears that the "spin-packets" from which the ENDOR lines arise are about 26 gauss wide. The EPR lines are of this width, taking the envelope of the fluorine structure. This suggests that there is rapid spin-diffusion through the EPR line, probably due to fast relaxation of the neighbouring fluorines by cross-relaxation between the hyperfine structure lines. This is also the case in Tm^{2+} CaF_2, as discussed by Bessent and Hayes.

Yb^{173} : In this case $I = 5/2$ giving six hyperfine EPR lines separated by about 150 gauss. One expects to observe in all 20 ENDOR lines in this system, of which 18 were observed. Those not observed arose from the transitions

$\Delta I_z = \frac{5}{2} \rightarrow \frac{3}{2}$, $S_z = \frac{1}{2}$ on the $I_z = \frac{3}{2}$ hyperfine line, and

$\Delta I_z = -\frac{5}{2} \rightarrow -\frac{3}{2}$, $S_z = \frac{1}{2}$ on the $I_z = -\frac{5}{2}$ hyperfine line.

Yb^{171} in CaF_2

τ = 2 secs

$S_z = -\frac{1}{2}$

$\Delta I_z = \frac{1}{2} \leftrightarrow -\frac{1}{2}$

τ = 10 secs

$S_z = -\frac{1}{2}$

$\Delta I_z = \frac{1}{2} \leftrightarrow -\frac{1}{2}$

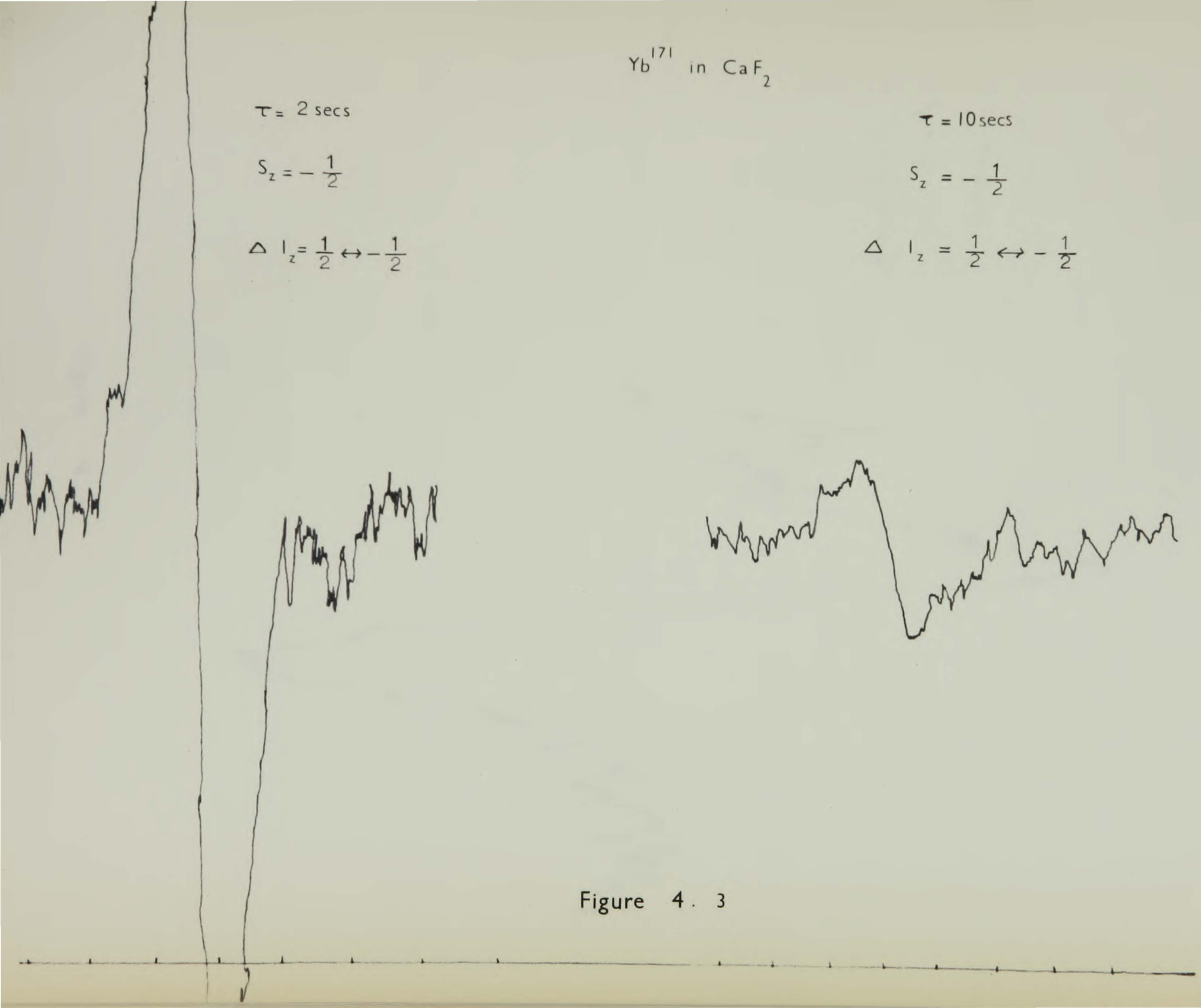

Figure 4.3

Yb^{171} in CaF_2

$\tau = 2$ secs

$S_z = \frac{1}{2}$

$\Delta\ I_z = \frac{1}{2} \leftrightarrow -\frac{1}{2}$

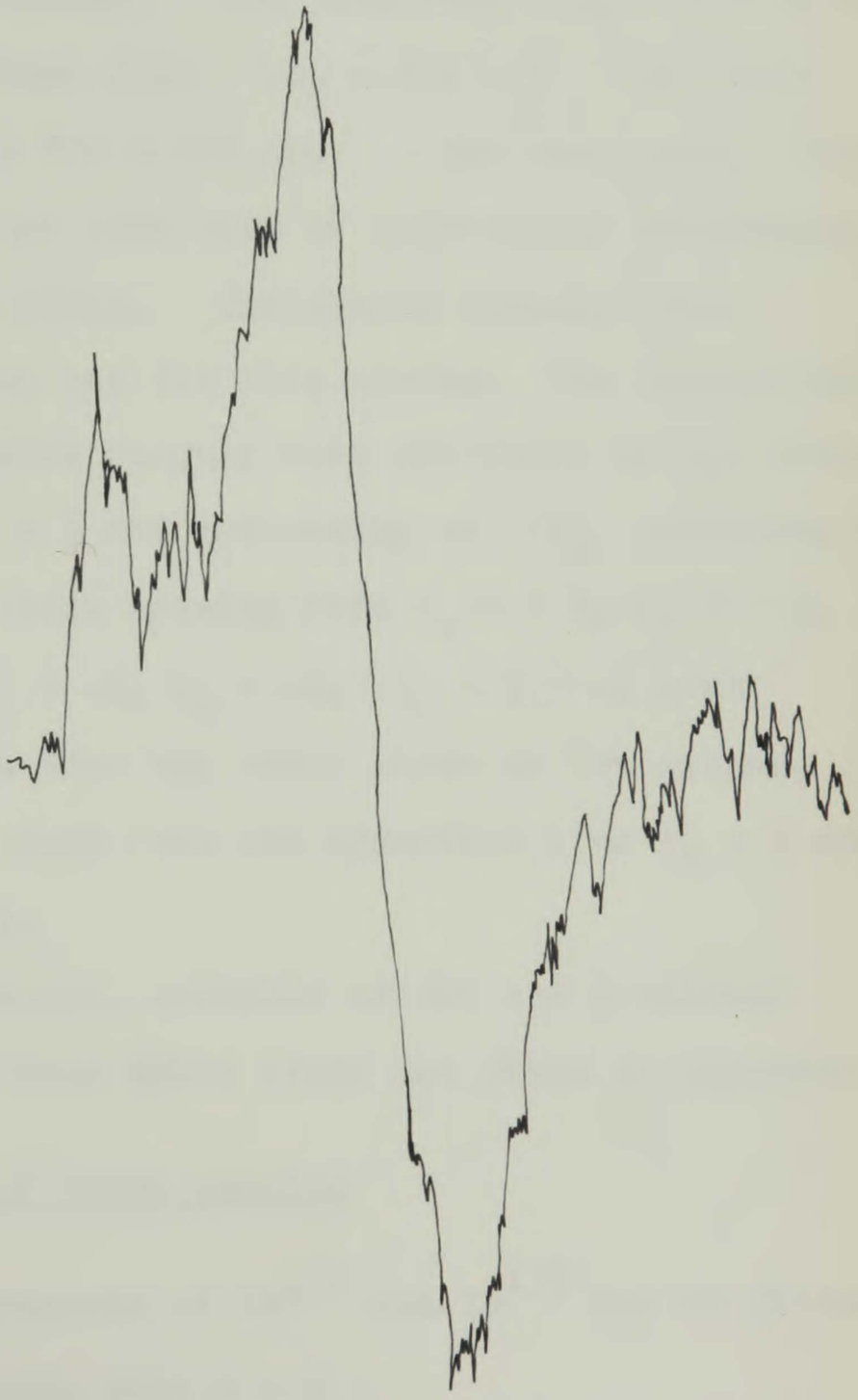

Figure 4. 4

The linewidths of the ENDOR lines varied as a function of the value of I_z describing the hyperfine line from which the ENDOR line was derived. The lines from $\Delta I_z = \frac{1}{2} \rightarrow -\frac{1}{2}$ are $\sim$ 250 kc/s wide, those from $\Delta I_z = 3/2 \rightarrow \frac{1}{2}$ $\sim$ 330 kc/s and those from $\Delta I_z = 5/2 \rightarrow 3/2$ are $\sim$ 500 kc/s wide. This variation suggests that some sort of quadrupolar broadening is occurring in the system. The simple formula from Bessent and Hayes does not fit this system. The intensities of the lines also varied roughly with the value of I_z, being strongest for $|I_z| = \frac{1}{2}$ and decreasing as $|I_z|$ increases to $5/2$. However, the lines arising from $I_z = +\frac{1}{2}$, $S_z = +\frac{1}{2}$, $\Delta I_z = \frac{1}{2} \rightarrow -\frac{1}{2}$, and $I_z = -\frac{1}{2}$, $S_z = -\frac{1}{2}$, $\Delta I_z = \frac{1}{2} \rightarrow -\frac{1}{2}$ were markedly more intense than any other lines in the system. Traces of the ENDOR lines from the hyperfine line $I_z = \frac{1}{2}$ are shown in Figure (4.5).

The mean frequencies, probable errors and predicted frequencies for all these ENDOR lines are given in Appendix 4.

6. Interpretation of ENDOR results

The ENDOR measurements of Yb^{171} and Yb^{173} may be fitted to the spin-Hamiltonian, with $S = \frac{1}{2}$:

$$\mathcal{H} = g\beta \underline{H}.\underline{S} + A\underline{S}.\underline{I} + g_n' \beta \underline{H}.\underline{I} + B\, S_z I_z^2 H_z + C S_z I_z^3 + D[\, 35\, I_z^4 - (30I(I+1)-25) I_z^2 \,].$$

Yb^{173} in CaF_2

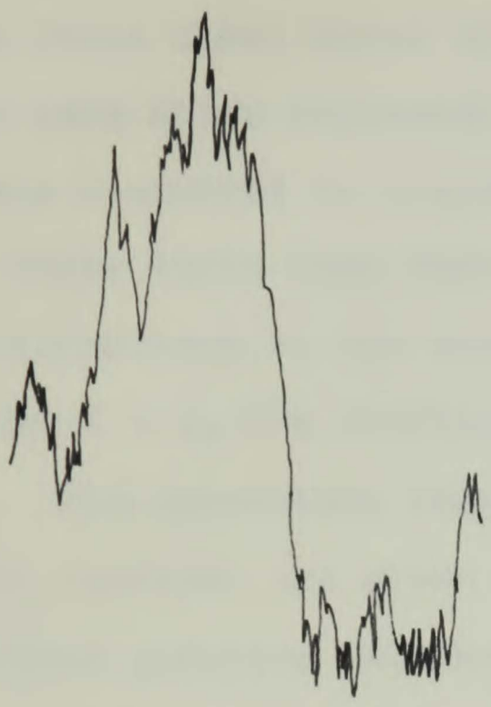

$S_z = \frac{1}{2}$

$\Delta I_z = \frac{3}{2} \leftrightarrow \frac{1}{2}$

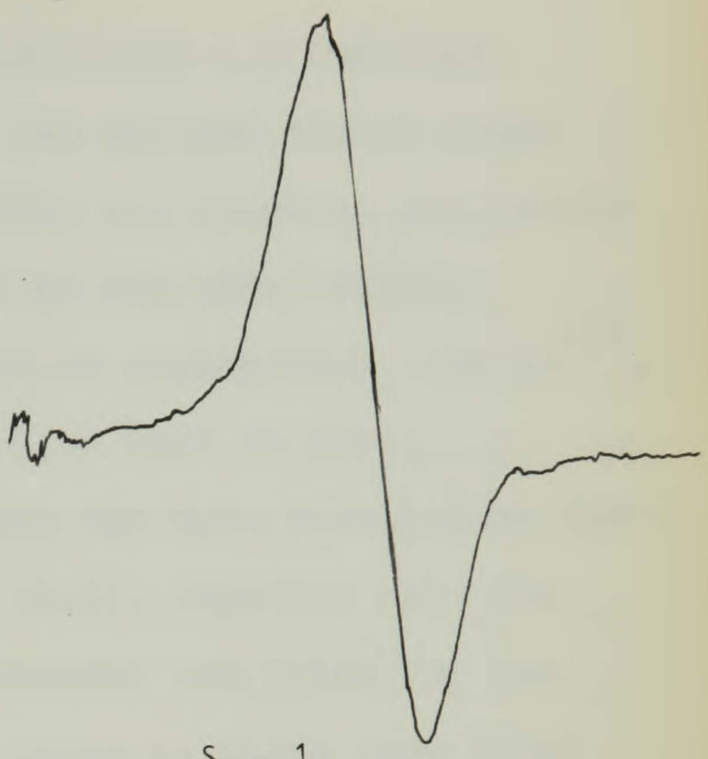

$S_z = \frac{1}{2}$

$\Delta I_z = \frac{1}{2} \leftrightarrow -\frac{1}{2}$

$S_z = -\frac{1}{2}$

$\Delta I_z = \frac{1}{2} \leftrightarrow -\frac{1}{2}$

$S_z = -\frac{1}{2}$

$\Delta I_z = \frac{3}{2} \leftrightarrow \frac{1}{2}$

Figure 4.5

The first three terms of this Hamiltonian are familiar. The last three represent some of the allowed higher order terms discussed in Chapter 2. Only the diagonal components of these terms have been included as the off-diagonal contributions to the energies will be negligible. For Yb^{171}, where $I = \frac{1}{2}$, the coefficients B, C, D must be zero.

The parameters required to fit the spin Hamiltonian for both isotopes are given in Table (4.2), together with the nuclear g-factor obtained by Olschewski and Otten for the free atom, expressed in the same units as those from ENDOR measurements. The weighted r.m.s. deviation between observed and calculated frequencies is 29 kc/s for Yb^{173} and 23 kc/s for Yb^{171}.

Nuclear g-factors: From Table (4.2) it can be seen that the effective nuclear g-factors of the Yb isotopes in CaF_2 are 64% larger than the free atom nuclear g-factor. This arises from the pseudo-nuclear g-factor discussed in Chapter 2. Using the crystal field states given in Table (4.1) and remembering that the ENDOR measurements were made with the magnetic field parallel to a cube axis of the crystal, it can be shown that the Zeeman interaction can only couple the Γ_7 doublet to two states of the Γ_8 quartet. From these results the energy separation of Γ_8 from Γ_7 can

TABLE 4.2

	Yb^{171}	Yb^{173}
g	3.443 ± 0.002	3.443 ± 0.002
A Mc/s	2638.66 ± 0.09	-727.234 ± 0.010
g'_n (Bohr magnetons)	$(-8.796 \pm 0.001) \times 10^{-4}$	$(2.409 \pm 0.002) \times 10^{-4}$
B c/s	-	47 ± 9
C kc/s	-	26.5 ± 3
D c/s	-	63 ± 6
g_n (Bohr magnetons)	-5.35816×10^{-4}	1.4761×10^{-4}

be shown to be 597 cm^{-1}, from the equations on page 2.17. In evaluating this energy a value for the hyperfine interaction has to be used. It is likely that crystal field interactions and higher order corrections will reduce this from the value quoted in Table (4.2) as the spin Hamiltonian parameter A. These will be considered in detail in the next section but the hyperfine interaction for a pure Γ_7 doublet is unlikely to differ from the spin Hamiltonian A value by more than 1%. It is thus reasonable that the energy separation between Γ_7 and Γ_8 in the ground manifold should be (597 ± 6) cm^{-1}.

Higher order terms

The general theory of these terms has been outlined in Chapter 2. For Yb^{171} the only possible terms of this sort should be of the form SIH^n where n is even. Terms of this type were found to be zero within experimental error and have not been included in the spin Hamiltonian.

For Yb^{173} several higher order terms are allowed within the general rules given in Chapter 2. As the electronic system Yb^{3+} in CaF_2 is simple and the positions of the excited terms are known from the crystal field parameters derived in Section 3 of this chapter, it should be possible to predict the magnitudes of these higher order terms. Ray (1964) has

published predicted values for these terms in this system, which do not fit the data given in Table (4.2). Her analysis is subject to two severe criticisms. Firstly she has used Low's (1962) excited state energies, which as discussed by Kirton and McLaughlan are based on an erroneous interpretation of the optical spectrum. Secondly, Ray appears to have omitted any contributions from the quadrupole interaction that can arise for Yb^{173}. Whilst there can be no quadrupole interaction in the ground state ($S = \frac{1}{2}$) of Yb^{3+} in the cubic crystal field of CaF_2, this interaction can produce important admixtures with the excited crystal field states. The pseudo-quadrupole interaction is zero for this system.

The higher order terms which are important for this system can be evaluated using second order perturbation theory between the Γ_7 doublet and the excited Γ_6 and Γ_8 states within the ground manifold. Admixture from the $J = 5/2$ manifold can be shown to be negligible. The eigenfunctions for the ground manifold states are given in Table (4.1), and the energies of these states are taken to be those predicted by the crystal field parameters deduced above. These give the energy of Γ_8, $E_8 = 597 \pm 6 cm^{-1}$, and that of Γ_6, $E_6 = 439 \pm 10\ cm^{-1}$, relative to Γ_7. There are several types of perturbation interaction to be considered.

(a) $$\frac{\langle \phi_1 | a\, J.I | \phi_2 \rangle \langle \phi_2 | a\, J.I | \phi_1 \rangle}{(E_1 - E_2)}$$

These terms are discussed in detail in Chapter 2, and for this system give rise only to one term $\frac{3a^2}{E_8}$

(b) $$\frac{\langle \phi_1 | a\, J.I | \phi_2 \rangle \langle \phi_2 | P | \phi_1 \rangle}{(E_1 - E_2)}$$

The operator P is the quadrupole interaction operator, which is written out fully in Chapter 2, section 2.

(c) $$\frac{\langle \phi_1 | \wedge \beta H_z J_z | \phi_2 \rangle \langle \phi_2 | P | \phi_1 \rangle}{(E_1 - E_2)}$$

Only matrix elements of the z components of the Zeeman interaction are necessary, as measurements were made only with the magnetic field parallel to a cube edge of the crystal

(d) $$\frac{\langle \phi_1 | P | \phi_2 \rangle \langle \phi_2 | P | \phi_1 \rangle}{(E_1 - E_2)}$$

These terms can connect both Γ_6 and Γ_8 to Γ_7. The overall effect of these terms for Yb^{3+} in CaF_2, is to introduce into the spin Hamiltonian terms of the form, for

Yb^{173},

$$\left(\frac{49.5}{E_8} + \frac{31.5}{E_6} \right) P^2 \left[35 I_z^4 - (30I(I+1)-25) I_z^2 \right]$$

$$+ 90 \left[\left(\frac{4}{E_8} + \frac{7}{E_6} \right) 8P^2 + \frac{aP}{E_8} \right] S_z I_z^3$$

$$- \frac{108 \wedge \beta P}{E_8} H_z S_z I_z^2$$

$$+ \left[\frac{3a^2}{E_8} - 18(9I(I+1)-4) \frac{aP}{E_8} - 288 [2I(I+1)-1] \frac{P^2}{E_8} \right.$$

$$\left. - 630 [4I(I+1)-1] \frac{P^2}{E_6} \right] S_z I_z$$

The first three terms have the same form as the terms B, C, D in the spin Hamiltonian. The final term has exactly the same form as the hyperfine interaction. Thus the coefficient of $\underline{A}\underline{S}.\underline{I}$ determined from the ENDOR data is the sum of the true hyperfine interaction together with the components of this interaction that derive from the perturbations discussed above. To evaluate the coefficients of these terms the quadrupole interaction has to be known. The value used for

a is $\frac{1}{3}$ of the spin Hamiltonian A factor. This should be corrected to give the true hyperfine interaction, but the error involved in taking the uncorrected value is small.

As the value that should be used for the quadrupole interaction in this system is not definitely known, it was decided to use the measured values of the higher order terms to deduce a value for P, which would then be used to provide the correction to the hyperfine interaction. Using the equations above, P was evaluated from the three equations to be - 4.9 ± 1 Mc/s from B, ± 3.5 ± 0.4 Mc/s from C, and - 5.9 ± 0.5 Mc/s from D. These have a mean value of - 4.7 ± 1.2 Mc/s. The values for P derived in this way give an indication of the validity of the perturbation description of these higher order terms. Other terms can provide contributions to these parameters but they are generally at least an order of magnitude smaller, and have thus been neglected. In view of the approximations made throughout these calculations the agreement between the values for P from the three equations is regarded as satisfactory.

Using the mean value for P of - 4.7 ± 1.2 Mc/s, the correction to the hyperfine interaction for Yb^{173} is - 121 ± 40 kc/s.

The quadrupole moment for Yb^{173} has been measured by

Ross and Hurakawa (1962) to be 2.8 ± 0.2 barns. The quadrupole interaction P for the free Yb^{3+} ion can be evaluated to be - 4.6 ± 0.4 Mc/s, assuming no shielding. This can only be regarded as an estimate of the interaction as no account has been taken of shielding or lattice effects. However, it is satisfactory that this value is close to that derived above, the agreement probably being fortuitous.

Magnetic Hyperfine Interaction

The values of A^{171} and A^{173} given in Table (4.1) are derived directly from the experimental data as spin Hamiltonian parameters. To find the interaction to be expected from a pure Γ_7 doublet a series of corrections would have to be applied to the experimental values for A. These are closely related to the corrections required for the electronic g-factor and, as discussed in Section 2, no thorough analysis can be made for Yb due to the lack of knowledge of the excited states. However, it is likely that the shift will be comparable or smaller than that calculated for Tm^{2+} by Bleaney, (1964), as the shift of the g-factor from the pure Γ_7 value is smaller. These corrections are all proportional to A as shown by Bleaney and thus do not affect the ratio of the A values for the two isotopes.

However, the correction term derived above is significant, reducing A^{173} to - 727.123 ± 0.06 Mc/s. The perturbation term (a) above can also arise for Yb^{171}, reducing the hyperfine interaction to 2638.53 ± 0.04 Mc/s.

The ratio of these interactions $\frac{A^{171}}{A^{173}} = -3.6288 \pm 0.0004$. The ratio of nuclear g-factors derived by Olschewski and Otten (1967) is $\frac{g_n^{171}}{g_n^{173}} = -3.6299 \pm 0.0005$. Thus a hyperfine structure anomaly of (- 0.03 ± 0.03)% for the Yb isotopes in CaF_2. This has to be compared with the value of the anomaly in the excited $^3P_1$ state of the Yb atom of - 0.376 ± 0.02%, derived by Budick and Snir (1967). The figure quoted in this reference is incorrect, the correction being reported by Unna (1967).

As outlined in Section 5 of Chapter 2, the hyperfine structure anomaly arises from s electrons, any contribution from $p_{\frac{1}{2}}$ electrons being regarded as negligible. If A(f) and A(s) represent the contributions to the hyperfine interaction from the f electrons and unpaired s electrons in the ion, we have the two equations $A_{exp} = A(f) + A(s)$, and $A_{exp} \triangle_{exp} = A(s) \triangle(s)$, where $\triangle(s)$ is the anomaly for a single s electron. In Budick and Snir's experiment the 6s6p state of Yb was used, and it is reasonable to assume that the anomaly arises from a single s electron. Any core

polarisation in the atom will be negligible compared with the 6_s electron contribution to the hyperfine interaction. From this we deduce that the ratio $\frac{A(s)}{A(f)}$ for the trivalent ion is $(8 \pm 8)\%$. This conflicts with the theory proposed by Bleaney (1964) for core polarisation in the rare-earths, which is discussed in section 3, Chapter 2, where the formula for core polarisation predicts $\frac{A(s)}{A(f)} = -(1.0 \pm 0.16)\%$.

The discrepancy may be due simply to some incompleteness in the treatment of the perturbation corrections to be applied to the system. The size of the anomaly is strongly dependent on these and whilst the treatment above appears to satisfy the data it must be treated with some caution. Further ENDOR measurements on this system at a different EPR frequency could provide a useful check upon these terms, particularly on the field dependent correction term. The importance of this is demonstrated in the next chapter with reference to Gd ENDOR.

However, in the light of the present work it appears that the assumptions underlying Bleaney's treatment of core polarisation should be re-examined. Previously no test of his extrapolation has been made, and this work should be regarded as a stimulus for further studies in this direction.

REFERENCES

Bessent, R.G., and Hayes, W., 1965. Proc. Roy. Soc. A285, 430.

Bierig, R.W., Weber, M.J. and Warshaw, S.I., 1964. Phys. Rev. 134, A1504.

Bleaney, B., 1963. Proc. Third Int. Conf. on Quantum Electronics, Dunod, Paris, 595.

Bleaney, B., 1964. Proc. Roy. Soc., A277, 289.

Budick B. and Snir, J., 1967. Phys. Letts. 24B, 276.

Dieke G.H. and Crosswhite, H.M., 1963. Appl. Optics, 2, 657.

Freeman, A.J. and Watson, R.E., 1962. Phys. Rev. 127, 2058.

Gossard, A.C., Jaccarino, V. and Wernick, J.H., 1964. Phys. Rev. 133, A881.

Inoue, M., 1963. Phys. Rev. Letts. 11, 196.

Jorgensen, C.K., 1956. Kgl. Dan. Videns. Selsk., Mat. fys. Medd. 30, No. 22.

Kirton, J. and McLaughlan, S.D., 1967. Phys. Rev. 155, 279.

Kiss, Z.J., 1962. Phys. Rev. 127, 718.

Lea, K.R., Leask, M.J.M. and Wolf, W.P., 1962. J. Phys. Chem. Solids, 23, 1381.

Low, W., 1962. J. Chem. Phys. 37, 30.

Olschewski, L. and Otten, E.-W. 1967. Zeits. für Phys., 200,224.

Ranon, U. and Hyde, J.S., 1966. Phys. Rev. 141, 259.

Ray. T., 1964. Proc. Roy. Soc. A277, 76.

Ross, J.S. and Murakawa, K., 1962. Phys. Rev. 128, 1159.

Twidell, J.W., 1963. D. Phil. Thesis, Oxford University.

Unna, I., 1967. Phys. Letts. 24B, 499.

Weber, M.J. and Bierig, R.W., 1964. Phys. Rev. 134, A1492.

Williams, F.I.B., 1961. D. Phil. Thesis, Oxford University.

CHAPTER 5

ENDOR MEASUREMENTS ON Gd ISOTOPES IN ThO_2 AND CeO_2

Naturally occurring gadolinium contains two isotopes with non-nuclear zero nuclear spin. These are 155, 14.8% abundant, and 157, 15.7% abundant, both of which have nuclear spin of $^3/_2$. ENDOR measurements on Gd^{157} in ThO_2 were reported by Hurrell (1965). The work reported here is, in part, a continuation of his experiments using higher magnetic fields, and a complementary series of measurements of both Gd^{157} and Gd^{155} in CeO_2.

EPR Properties:

Gadolinium enters substitutionally into crystals of ThO_2 and CeO_2 as the trivalent ion, replacing ions of Th^{4+} and Ce^{4+} respectively. The crystalline electric field at the Th^{4+} or Ce^{4+} ion site has cubic symmetry but the mismatch of ionic charge in the substitution process requires some sort of charge compensation. For crystals containing about 0.01% Gd^{3+}, only cubic crystal field EPR spectra are observed, indicating that the charge compensation is distant from the ion site. As the concentration of Gd^{3+} is increased

spectra of lower symmetries become observable (Abraham 1967, Bir and Vinokurov 1966).

Gd^{3+} has the ground state electronic configuration $4f^7$, $^8S_{7/2}$. It is thus an S state ion, isoelectronic with Eu^{2+} and Tb^{4+}. The ground state of the half filled shell cannot be split in first order by a crystal field acting alone regardless of its symmetry. However, it it well known from EPR studies that the ground state of the ion is split in zero magnetic field. The mechanisms responsible for these observed splittings are not understood at all well. A review of possible contributions to the zero field splitting is given by Abraham et. al.(1967), and Wybourne (1966) performs an extensive calculation of the splitting for Gd^{3+} in lanthanum ethyl-sulphate. He considers eight possible contributions to the splitting, taking his calculations to fifth order, but arrives at a splitting of twice the observed value and of the wrong sign. He concludes that a successful calculation of this quantity would have to include effects arising from overlap of the surrounding ligand orbitals with those of the central ion.

The EPR spectra of Gd^{3+} in ThO_2 and CeO_2 have been reported by several authors, particularly Low and Shaltiel (1958) and Abraham et. al. (1965, 1967). The spectra are

fitted to a spin Hamiltonian of the form, with effective spin $^7/_2$:

$$\mathcal{H} = g\beta \underline{H}.\underline{S} + B_4(O_4^0 + 5O_4^4) + B_6(O_6^0 - 21O_6^4).$$

The parameters g, B_4 and B_6 derived from these measurements are shown in Table (5.1) together with the lattice constants and EPR linewidth. The sign of the crystal field has been determined to be negative by observation of the intensity changes of the fine structure lines as a function of temperature. The EPR linewidths should be very narrow in these hosts as neither has ligands with any abundant isotopes of non-zero nuclear spin. This reduces inhomogeneous broadening of the EPR line. All the work reported in the published literature for ThO_2 shows linewidths between 0.5 and 1 gauss of ThO_2, and ~ 2 gauss for CeO_2. It is found generally that the EPR linewidth tends to increase as $|J_z|$ increases from $\frac{1}{2}$ to $^7/_2$. The increases reported in the references above are only small giving lines abouts 2 gauss wide for $\Delta S_z = {}^7/_2 \rightarrow \frac{5}{2}$. This increase in linewidth arises from the dependence of the energy for $|J_z| > \frac{1}{2}$ on crystal field gradients. Although the crystal field is cubic at the Gd^{3+} site, there will be residual strains in

TABLE 5.1

EPR PARAMETERS FOR Gd^{3+} in ThO_2 AND CeO_2

	ThO_2			CeO_2		
	a_o = 5.600 Å			a_o = 5.411 Å		
T^oK	g	c Mc/s	d Mc/s	g	c Mc/s	d Mc/s
297	1.9917±0.0002	-661.9±0.2	-4.7±0.15	1.9921±0.0007	-647.6±0.6	-4.5±1.0
77	1.9917±0.0002	-677.5±0.2	-4.85±0.15	1.9918±0.0005	-664.7±0.6	-4.2±1.0
20	1.9917±0.0002	-679.1±0.2	-4.94±0.2	1.9921±0.0005	-667.5±0.6	-4.6±1.0
4.2	1.9917±0.0002	-679.1±0.2	-502±0.2	1.9907±0.0005	-666.1±0.6	-4.5±1.0

Linewidth for 0.02 % Gd^{3+} 0.5 gauss 2 gauss

$c = 4b_4 = 240B_4$ $d = 4b_6 = 5040\ B_6$

From Abraham et. al. (1965, 1967).

the field experienced by the ion. These may be partially induced by the differences in ionic size between Gd^{3+} and the host ions, and partially by random strains formed in the crystal during growth. These latter strains may be reduced by annealing the crystal.

The properties of the crystals of Gd^{157} in ThO_2 that were used for the experiments to be described here were very similar to those listed in Table 5.1, from Abraham's data. Crystals of CeO_2 containing enriched Gd^{157} and enriched Gd^{155} isotopes obtained from Oak Ridge, were grown in this laboratory by Mrs. B. Wanklyn. She used a flux growth technique, using Pb F_2 flux. The CeO_2 and Pb F_2 powder was heated to 1280°C and held at this temperature for twelve hours. The melt was cooled at a rate of 1.5°C per hour. The crystals formed on the surface of the melt in the form of black regular cubes with sides of 1 to 2 mm. length. These crystals displayed the characteristic gadolinium cubic EPR spectra, consisting of seven fine structure groups of four hyperfine lines each. However, these hyperfine lines were much broader than those reported by Abraham et. al. For the best specimens the linewidth was about 2 gauss for the $\Delta J_z = \frac{1}{2} \rightarrow -\frac{1}{2}$ transition but increased as the transitions moved out to $|\Delta J_z| = |7/2| \rightarrow |5/2|$ transitions, where the

lines were $\sim$ 6 gauss in width. The separation of the hyperfine lines for a particular fine structure transition is about 5 gauss for Gd^{157} and 4 gauss for Gd^{155}. Thus, whilst the hyperfine structure was resolved on the central $\Delta J_z = \frac{1}{2} \rightarrow -\frac{1}{2}$ transition, it was only partially resolved on the outermost EPR transitions. The crystals were annealed without any improvement in the line-width. Other specimens were grown using different cooling rates and low concentrations of Gd without reduction of the linewidth, indicating that the lines were not broadened by spin-spin interactions. In Figure (5.1) typical EPR spectra from the $\Delta J_z = 7/2 \rightarrow 5/2$ transitions are shown for the specimens of Gd^{157} in ThO_2 and CeO_2, measured under identical conditions at 36 kMc/s. The difference in line-width is clear. The origin of the increased linewidth was probably in random crystal field strains, as discussed by Stoneham (1966).

ENDOR Experiments

The specimen of Gd^{157} in ThO_2 should be an ideal one for ENDOR experiments, as it fulfils most of the conditions outlined in Chapter 1 for a good ENDOR specimen. The well-resolved narrow EPR hyperfine lines will reduce cross-relaxation effects to a minimum in the specimen. The crystals

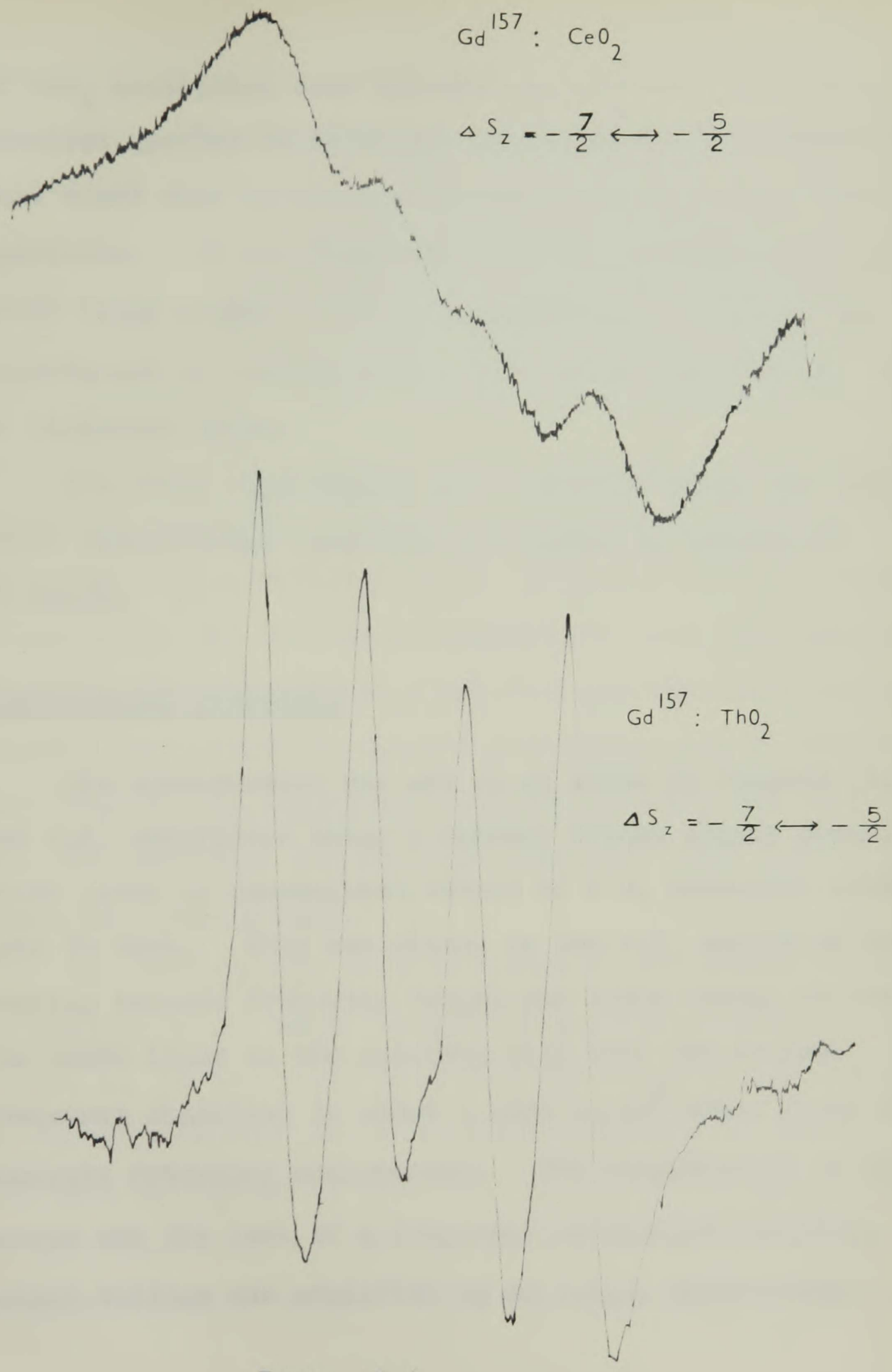
Gd^{157} : CeO_2
$\Delta S_z = -\frac{7}{2} \longleftrightarrow -\frac{5}{2}$
Gd^{157} : ThO_2
$\Delta S_z = -\frac{7}{2} \longleftrightarrow -\frac{5}{2}$

Figure 5.1

of CeO_2 containing each isotope did not show those well-resolved spectra as discussed above and one thus expects that there will be cross-relaxation arising within these specimens. It was found that the ThO_2 crystals gave good ENDOR lines whilst in CeO_2, considerable difficulty was experienced in finding many of the ENDOR transitions. This is discussed below.

The ENDOR experiments were performed using the Q-band ENDOR spectrometer described in Chapter 3, working at 36 kMc/s.

Experimental Procedure

The spectrometer was set up as shown in Diagram (3.1), the r.f. oscillator being a Marconi TF1414 signal generator which gives an unmodulated output of 2 v. peak-peak voltage into 70 ohms. This was chosen as the r.f. source as the overlap between frequency ranges was large enough to cover all the ENDOR lines in the spectrum with only one source. The frequency stability is about 1 part in 10^5 which leads to accurate frequency measurement. The disadvantage of this source was the lack of a frequency modulation facility. The output voltage was amplified by an I.F.I. distributed

amplifier, Model 500, which gives an output of 3 watts into 185 ohms. The amplifier was modified to permit amplitude modulation of the r.f. output, by connecting the output of a Schmidt trigger circuit to the grid of the last amplifier stage valve. This switched the valve off every alternate half-cycle, thus producing a 100% square wave amplitude modulated signal. Some preliminary investigations were carried out using a General Radio type 1211 B unit oscillator which was frequency modulated by applying an audio sine wave to a variable capacitance diode (Hughes HC 7002) connected in parallel with the tuning capacitor in the oscillator tank circuit. However, it was found that the amplitude modulated signals were easier to measure accurately, and of comparable magnitude to the frequency modulated signals, and thus all the measurements of the Gd ENDOR were made using the amplitude modulated ENDOR signal.

The measurements were performed in the manner outlined in Chapter 3, at pumped liquid hydrogen temperatures $\sim 14^{\circ}$ K. It was found desirable not to allow the hydrogen to solidify as the poor thermal conductivity of solid hydrogen was unable to keep the temperature of the cavity to the temperature of the bulk of the refrigerant. Investigations were made at 4.2° K but the electronic T_1 was so long

that very low microwave power was necessary to avoid saturating the EPR signals too strongly. The sensitivity of the 115 kc/s detection system is reduced at very low power level and thus the ENDOR sensitivity was reduced.

All ENDOR experiments were performed with the d.c. magnetic field aligned accurately parallel to a (100) edge of the crystal. This was achieved by rotation of the crystal mount about its horizontal axis and rotation of the magnetic field about a vertical axis. Alignment along a cube edge was detected by observing a turning point in the EPR spectrum, the $|\Delta J_z| = |7/2| \rightarrow |5/2|$ transitions moving to extreme fields at this alignment. Measurements were made 20 times on each ENDOR line, checking the alignment before each reading, and remounting the crystal every fourth reading to attempt to reduce systematic errors due to possible misalignment to a minimum.

ENDOR Results

Three separate systems were studied using the technique mentioned above, Gd^{157} in ThO_2, Gd^{157} in CeO_2, and Gd^{155} in CeO_2.

Gd^{157} in ThO_2 : This system had previously been studied by

Hurrell (1965) working at 9.4 kMc/s for his EPR frequency. As S = 7/2, I = 3/2 one expects to see 24 ENDOR transitions. All these transitions were observed by Hurrell, whose measurements are given in Appendix 5. He unfortunately gives no indication of the accuracy to which his measurements were made, except to indicate that those ENDOR frequencies arising from $S_z = \frac{1}{2}$ and $S_z = -\frac{1}{2}$ are probably ten times less accurate than all other ENDOR frequencies. I have measured the ENDOR spectra in the same crystal at 36 kMc/s and have measured all transitions except those from $S_z = -\frac{1}{2}$. Measurements of these transitions were difficult as the signal was only just greater than noise for a recording time constant of 10 secs, and in view of the large uncertainties in these measurements, they were not considered in the interpretation of the spectra. The measured frequencies are given in Appendix 5, together with the probable errors.

It was found, as reported by Hurrell (1963), that the intensities of the ENDOR lines decreased rapidly with decreasing $|J_z|$. Further it appears that for a particular EPR transition $\Delta J_z = |J_z| \rightarrow |J_z| - 1$, the intensities of all ENDOR lines arising from $|J_z| - 1$ are between one and two orders of magnitude smaller than those arising from $|J_z|$. Similar behaviour arose in the ENDOR on the Yb isotopes in

CaF_2 reported in Chapter 4, and in F^{19} ENDOR in the same system, reported by Ranon and Hyde (1966).

$\underline{Gd^{157} : CeO_2}$: The broadened EPR lines in the CeO_2 crystals suggested that the crystal field experienced by the Gd^{3+} ion was subject to random strains. Two serious consequences of this appeared in the ENDOR spectra from these crystals. Firstly the unresolved hyperfine EPR lines suggest that cross-relaxation will occur in these lines. Thus saturation of one hyperfine line involves saturation of the entire fine structure line. ENDOR signals from all nuclear transitions on this line should thus appear regardless of which portion of the EPR line is saturated. Secondly the nuclear $|m_I| = 3/2$ energy levels will be subject to the same mechanisms which broaden the electronic $|J_z| > \frac{1}{2}$ levels, and will thus be broadened. This will result in a broadening of the ENDOR frequencies from $\frac{1}{2} \rightarrow 3/2$ transitions. This was found to be the case for the CeO_2 crystals. Even in ThO_2 these transitions show a broadening over the $\frac{1}{2} \rightarrow -\frac{1}{2}$ transitions. A comparison of line width is shown in Table (5.2).

In Gd^{157} in CeO_2, all $\Delta J_z = \frac{1}{2} \rightarrow -\frac{1}{2}$ transitions were measured except for that from $S_z = -\frac{1}{2}$. The $\Delta I_z = |3/2| \rightarrow |\frac{1}{2}|$

TABLE 5.2

MEAN ENDOR LINEWIDTHS IN kc/s

	Gd^{157} ThO_2	Gd^{157} CeO_2	Gd^{155} CeO_2
$\Delta I_z = \frac{1}{2} \rightarrow -\frac{1}{2}$	50	70	40
$\Delta I_z = \left\|3/2\right\| \rightarrow \left\|\frac{1}{2}\right\|$	120	200	200

transitions were also measured but not to the same accuracy as the central lines, due to the increased linewidth and decreased intensity over $\frac{1}{2} \rightarrow -\frac{1}{2}$ transitions.

In Appendix 5, the mean measured frequencies and probable errors are tabulated.

$Gd^{155} : CeO_2$: The hyperfine interaction and nuclear moment of Gd^{155} is smaller than that of Gd^{157} and thus the resolution of the hyperfine EPR lines was rather worse than for Gd^{157}. Measurements of the $\Delta J_z = \frac{1}{2} \rightarrow -\frac{1}{2}$ transitions were made for all manifolds except $S_z = +\frac{1}{2}$ and $-\frac{1}{2}$. But the quadrupole broadening effect was rather more severe in this crystal, only the $\Delta J_z = |3/2| \rightarrow |\frac{1}{2}|$ transitions being observed for the $S_z = 7/2$. The frequencies measured are tabulated in Appendix 5.

In Table (5.3) a comparison is drawn between ENDOR lines observed in the three cases mentioned above, where it is clear that $Gd^{157} : ThO_2$ gives the most satisfactory ENDOR signals, traces of typical ENDOR lines are shown in Figures 5.2 and 5.3.

An interesting demonstration of the effect of cross-relaxation in these specimens was given by holding the ENDOR frequency constant at the value required for a resonance of the $S_z = 7/2$ $\Delta I_z = \frac{1}{2} \rightarrow -\frac{1}{2}$ line, and sweeping the

TABLE 5.3

TYPICAL ENDOR LINE SIGNAL/NOISE RATIOS

	$Gd^{157}ThO_2$	$Gd^{157}CeO_2$	$Gd^{155}CeO_2$
$S_z=7/2$ $\Delta I_z=\frac{1}{2} \rightarrow -\frac{1}{2}$			
$\tau =$ 0.1 sec.	100:1	20:1	20:1
$\Delta I_z=3/2 \rightarrow \frac{1}{2}$			
$\tau =$ 0.5 sec.	30:1	2:1	3:1
$S_z=\frac{1}{2}$ $\Delta I_z=\frac{1}{2} \rightarrow -\frac{1}{2}$	3:1	2:1	not observed
$\tau =$ 10 secs.			
$\Delta I_z=3/2 \rightarrow \frac{1}{2}$	2:1	< 2:1	not observed
$\tau =$ 10 secs.			

$Gd^{157}ThO_2$

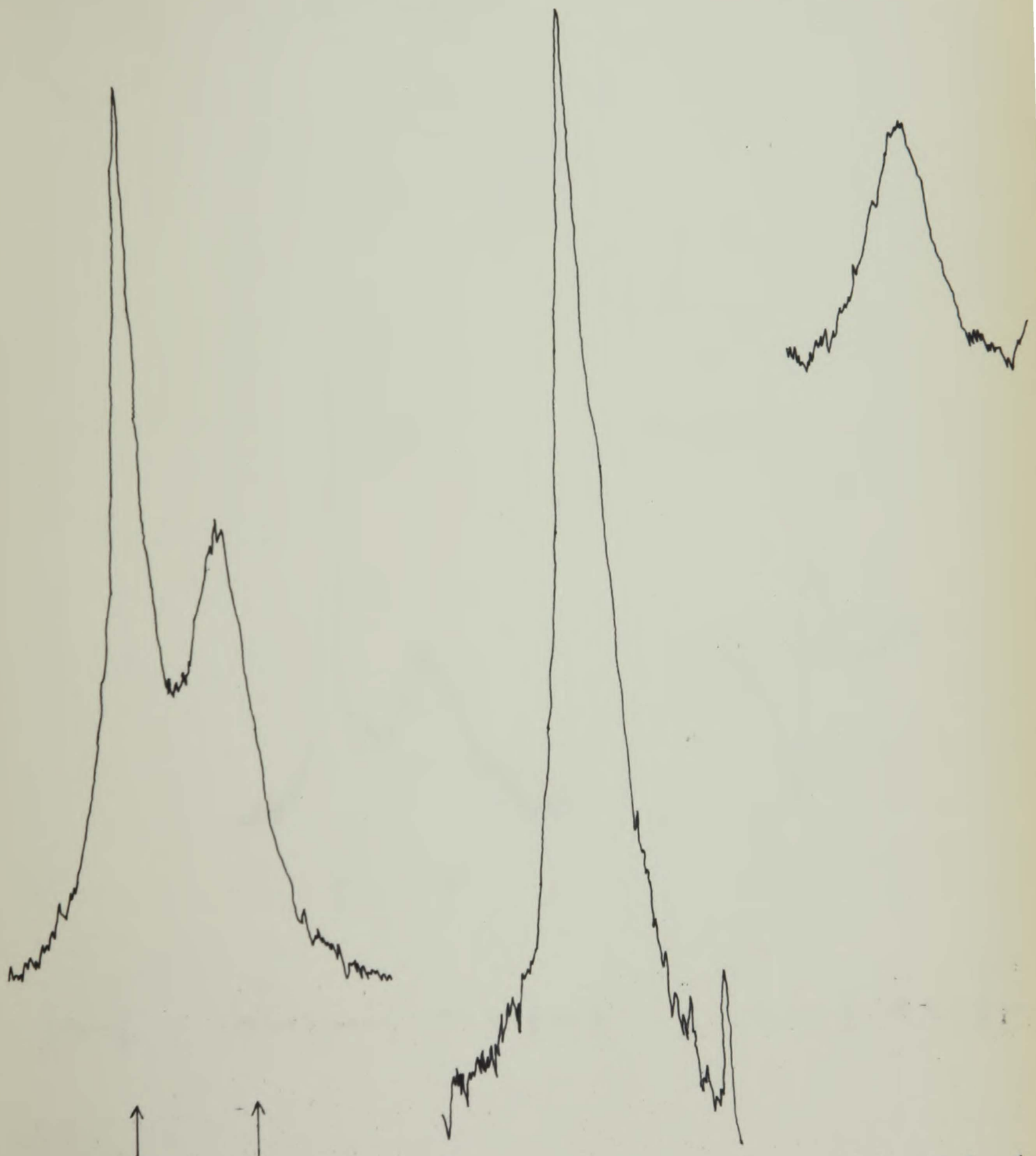

Figure 5. 2

$Gd^{155}\ CeO_2$

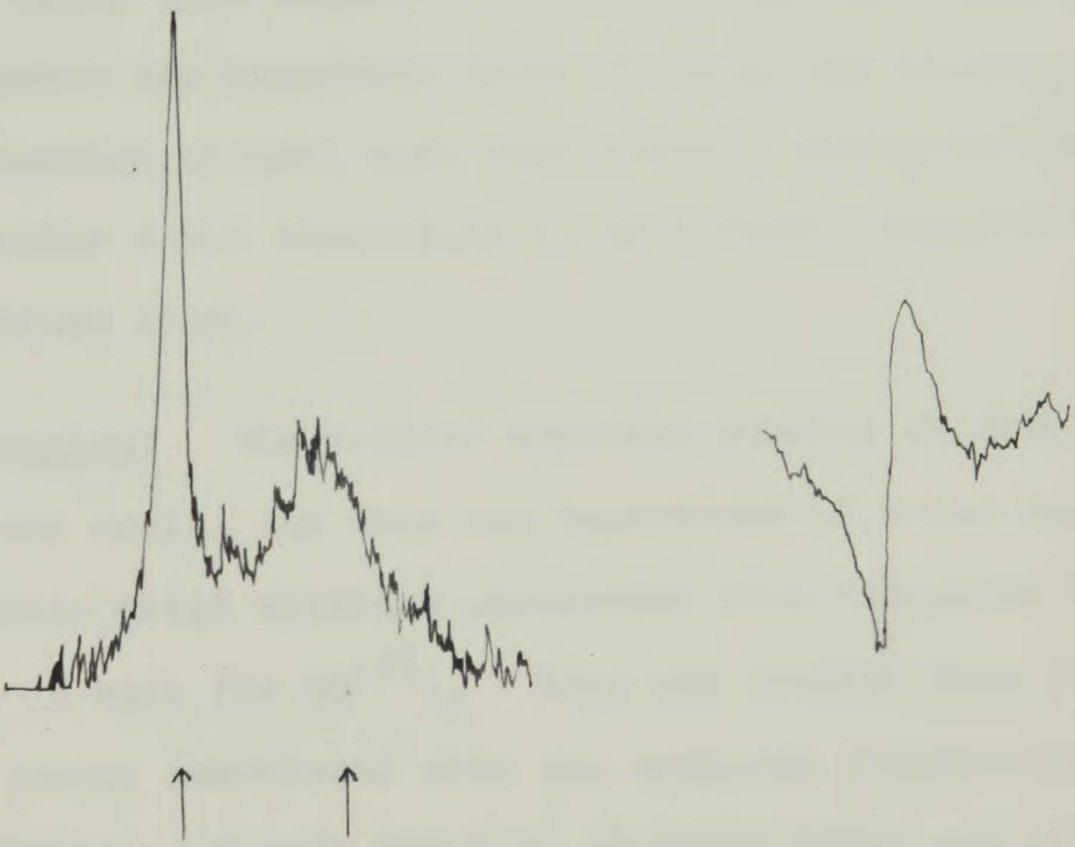

$S_z = -\frac{7}{2}$ $\quad \Delta I_z = \frac{1}{2} \leftrightarrow -\frac{1}{2}$ $\quad \Delta I_z = \frac{3}{2} \leftrightarrow \frac{1}{2}$ $\quad S_z = -\frac{3}{2}$ $\quad \Delta I_z = \frac{1}{2} \leftrightarrow -\frac{1}{2}$

Figure 5. 3

magnetic field through the $\Delta S_z = 7/2 \rightarrow 5/2$ EPR line. In Gd^{157} in CeO_2 a broad resonance was observed for the ENDOR output, whose width in gauss was close to that of the EPR line. Repeating the experiment on Gd^{157} in ThO_2, two narrow ENDOR lines were swept out, corresponding to the field positions of the $I_z = \pm \frac{1}{2}$ hyperfine lines. Very weak lines, $\sim$ 1% of the intensity of the main lines were observed when the $|I_z| = 3/2$ hyperfine lines were swept. Thus there was some weak interaction between the hyperfine lines in ThO_2, but in CeO_2 the cross-relaxation effects were sufficiently strong to enable any particular ENDOR transition to be induced within the EPR fine structure line.

Data Processing: The nuclear magnetic moments of both isotopes are small, and thus the dependence of ENDOR frequency upon magnetic field within a particular fine structure line was small ($\sim$ 3 kc/s for Gd^{157}). This was smaller than the probable errors associated with the measured frequencies which were typically $\sim$ 8 kc/s for $\frac{1}{2} \rightarrow -\frac{1}{2}$ ENDOR lines and 12 kc/s for $|3/2| \rightarrow |\frac{1}{2}|$ lines. To facilitate the data processing the ENDOR frequencies for a given fine structure EPR line were normalised to the mean central field position of that line. This could be done without using the quadratic field

reduction technique described by William (1961). Apart from this the approach to fitting the data to a spin Hamiltonian was identical with that described at length in his thesis. The spin Hamiltonian described in the next section was used to generate the 32 x 32 spin Hamiltonian matrix, which was exactly diagonalised for seven field positions for each isotope, corresponding to the fine structure EPR line positions. The spin Hamiltonian parameters were extracted using a weighted least squares method. Details of the programs used are given in Appendix 3.

Interpretation of Results:

The ENDOR measurements were fitted to a spin Hamiltonian which had the form:

$$\mathcal{H} = g\beta\underline{H}.\underline{S} + B_4(O_4^0 + 5O_4^4) + B_6(O_6^0 - 21O_6^4) + A\,\underline{S}.\underline{I}$$

$$+ g_n\beta\underline{H}.\underline{I} + \frac{B}{2I(2I-1)2S(2S-1)}\left[(3S_z^2 - S(S+1))(3I_z^2 - I(I+1)\right.$$

$$+ \tfrac{3}{2}(S_zS_+ + S_+S_z)(I_zI_- + I_-I_z) + \tfrac{3}{2}(S_zS_- + S_-S_z)(I_zI_+ + I_+I_z)$$

$$\left. + \tfrac{3}{2}(S_+^2I_-^2 + S_-^2I_+^2)\right]$$

$$A'\underline{S}^3\underline{I} + g[9]S_zI_zH_z^2 + g[10]S_z^3I_zH_z^2 .$$

The terms in this spin Hamiltonian are familiar, with

the possible exceptions of A', g[9], and g[10]. These arise from considering higher order interactions in the system as discussed in Chapter 2. The Hamiltonian differs from that given by Hurrell (1965) in the inclusion of the final two terms. It was found that these were necessary to bring his experimental data at low field, $\sim$ 3k gauss into agreement with mine at high field $\sim$ 12 k gauss. These both have the form permitted by the arguments given in Chapter 2. In Table (5.4), the spin Hamiltonian parameters derived from the experimental data are given for the three isotopes. It has been found necessary to modify Hurrell's published parameters to obtain a better fit to his measured data, using the smaller Hamiltonian that he used. The data for Gd^{157} and Gd^{155} in CeO_2 were analysed with these last two terms set to zero, as the field variation is not sufficient to show shifts arising from these terms.

Discussion of Results:

EPR Parameters: Abraham et. al. (1967) compare the EPR parameters for Gd^{3+} in ThO_2 and CeO_2. Their measurements are more accurate than any EPR measurements that could be performed on the crystals on which my ENDOR experiments were made, as their EPR line widths were considerably smaller, as

TABLE 5.4

SPIN HAMILTONIAN PARAMETERS FOR Gd^{3+} in ThO_2, CeO_2

	$Gd^{157} : ThO_2$	Gd^{157} CeO_2	Gd^{155} CeO_2
A Mc/s	15796.1 ± 0.5	15817.2 ± 0.7	12059.8 ± 0.5
g_n Bohr Magnetons	-1.224 ± 0.002 x 10^{-4}	-1.219 ± 0.002 x 10^{-4}	-0.932 ± 0.002 x 10^{-4}
A' kc/s	-3.05 ± 0.3	-0.85 ± 0.5	-1.26 ± 0.3
B kc/s	-687 ± 16	-806 ± 150	-2150 ± 300
g[9] c/s	-6.8 ± 0.5	-	-
g[10] c/s	0.60 ± 0.04	-	-

TABLE 5.5

The weighted root mean square deviations for the observed spectra from the calculated spectra using the spin Hamiltonian parameters given in Table 5.4 are given below, rejecting any reading whose deviation is greater than 4 x the r.m.s. value.

		$\Delta I_z = \frac{1}{2} \rightarrow -\frac{1}{2}$	$\Delta I_z = \lvert 3/2 \rvert \rightarrow \lvert \frac{1}{2} \rvert$
$Gd^{155}:CeO_2$		4 kc/s	58 kc/s
$Gd^{157}:CeO_2$		12 kc/s	126 kc/s
$Gd^{157}:ThO_2$	X band :	23 kc/s	38 kc/s
	Q band :	16 kc/s	18 kc/s
	Overall:	20 kc/s	29 kc/s

discussed earlier. However, they have restricted their spin Hamiltonian to the simple form given by the first three terms of the Hamiltonian given above. They were of course only measuring the EPR lines from the zero spin Gd isotopes, but they found the simple spin Hamiltonian to be incomplete as they were unable to fit their spectrum exactly. The divergences showed a systematic behaviour which was noted by those authors, who did not attempt to fit their spectrum by extending their Hamiltonian, as was done by Baker and Williams (1962) for Eu^{2+} in CaF_2. The quoted errors on the EPR parameters by Abraham et. al. were larger than the experimental errors, to account for the inexact description of their Hamiltonian. The interesting feature of the comparison made by them was that although the lattice constant for CeO_2 is about 3.5% smaller than ThO_2, the crystal field splitting in CeO_2 is smaller. In the alkaline earth fluorides the field splitting increased with decreasing lattice constant.

Marshall (1967) has made an EPR study of the crystal field effects in Gd^{3+} in ThO_2, where he measures the hyperfine structure lines very accurately for both isotopes in their natural abundances. He deduces from his data that the crystal field splitting parameters b_4 and b_6 are of different sizes for the two isotopes. The shifts he suggests arise

from the isotopes of different mass vibrating in an anharmonic potential. (Marshall et. al. 1964). He obtained a value of $\delta b_4 = 4.2 \times 10^{-3}$ % for the Gd isotopes 155 and 157 which he claims in just within his experimental accuracy. No shift in b_6 was detected. It is not clear from his paper whether he has accounted for the full effects of the hyperfine interaction spin-Hamiltonian, in particular it is difficult to see how he has taken the quadrupole interaction into account. A major criticism of this work is that from his measurements on some of the fine structure multiplets he deduced that the hyperfine interaction should have the opposite sign to that obtained by ENDOR. It would seem likely that his data has been misinterpreted and in the analysis of the data in this thesis, no isotopic-dependence of the crystal field interactions has been included.

Hyperfine Interaction

The magnetic hyperfine interaction can only arise from core-polarisation and relativistic effects as Gd^{3+} is an S-state ion. It is not possible to separate these effects for Gd^{3+} as insufficient data is available. One requires, as discussed in Chapter 2, a measurement of the hyperfine structure anomaly for both the ion and the atom in an S state.

From the data on Gd^{157} and Gd^{155} in CeO_2 given in Table (5.4) a hyperfine structure anomaly of + 0.27 ± 0.46% is derived, defined as $\frac{A^{157}}{A^{155}} \frac{g^{155}}{g^{157}} = 1 + \Delta$. The Nilsson states for both nuclei are identical (Mottelson and Nilsson 1958) which suggests that the nuclear magnetisation is distributed in a similar manner in each isotope. Thus one might expect the anomaly to be small, as the contribution from the distributed magnetisation is small. No data exists to date for the anomaly for Gd arising from an s electron. If one uses Bleaney's (1966) latest extrapolation for core polarisation in the rare-earths, a value for the contribution to the hyperfine interaction from core polarisation is + 18.4 ± 2 Mc/s.

Evans, Sandars and Woodgate (1965) have estimated the relativistic hyperfine interactions in Eu atom, using the theory developed by Sandars and Beck (1965). Using the relations developed for Eu, and assuming that the values of the double tensor operators are unchanged in passing from Eu to isoelectronic Gd^{3+}, the contributions to the hyperfine interactions can be evaluated to be A_{rel}^{157} = 0.12 Mc/s, B_{rel}^{157} = - 0.90 Mc/s for Gd^{157}, and A_{rel}^{155} = 0.09 Mc/s, B_{rel}^{155} = - 1.0 Mc/s. In this calculation the values of quadrupole moments given by Speck (1956) of Q^{157} = 1.0 barns and Q^{155} = 1.1 barns have been assumed. A further assumption

suggested by Bleaney (1966) that $\langle r^{-3} \rangle$ for relativistic effects is constant through the rare-earths has been made. Thus the overall hyperfine interaction for Gd^{157} is predicted, using these models, to be + 18.5 ± 2 Mc/s, with a quadrupole interaction predicted to be -0.9 Mc/s. These values are both of the right order of magnitude and signs but larger than the observed values. Evans et.al. state that they do not claim high accuracy for the quadrupole calculation, which for Eu, they underestimate by 18%. For Gd^{157} the extrapolation from Eu probably introduces a further uncertainty, and thus the agreement obtained is probably not unreasonable. For the magnetic hyperfine interaction the relativistic effects are only a small part of the overall effect, that of core polarisation being most important. To a certain extent this is fortuitous as the small effect arises from cancellation of two terms which are about 10 times larger than resulting effect. However, it does suggest that Bleaney's formula for the core polarisation contribution to A overestimates the size of the effect for Gd.

The agreement of the magnetic interaction for Gd^{155} is the same as for Gd^{157} as the contributions are all proportional to g_N, but for the quadrupole term, the measured value is

twice the size of the predicted value. This measured value however does originate from very poor experimental data as discussed above, and not too much reliance should be placed upon it.

High Order Hyperfine Interactions:

In order to fit the observed frequencies several higher order terms had to be included in the Hamiltonian as discussed earlier. The term in $A'\underline{S}^3.\underline{I}$ has the largest effect in the Hamiltonian and it is interesting that for the measurements made at Q-band the effect of this was largely countered by the term in $AS_z^3 I_z H_z^2$. If $A'\underline{S}^3.\underline{I}$ is expressed in traceless form a term of the type $\frac{1}{5}\underline{S}.\underline{I}\,(3S^2+3S-1)$ has to be included. This will transform exactly as the magnetic hyperfine interaction and thus the true value for this interaction is given by the difference between the value computed to fit the spin Hamiltonian given above, and a term 9.25 A'. In Gd^{157} in ThO_2, this correction to the magnetic hyperfine interaction is 28.2 ± 2.8 kc/s, giving a true hyperfine interaction of 15.7679 ± 0.0033 Mc/s. In the isotopes in CeO_2 the true interactions will be reduced to A^{157} = 15.8093 ± 0.0059 Mc/s and A^{155} = 12.0481 ± 0.0033 Mc/s, leading to a corrected value of Δ = 0.04 ± 0.6%. As the origin of the zero field

splitting in uncertain the origins of these higher order correction terms for an S state ion can only be suggested. The term $\underline{S}^3\underline{I}$ probably arises from some perturbation term involving the crystal field splitting and the hyperfine interaction, taken to one order higher than the perturbation determining the crystal field splitting. If this were the case, the ratio of these terms for the two isotopes should be equal to the ratio of the nuclear moments. In Eu^{2+} Baker and Williams (1962) showed that this is true to within experimental error. In Gd^{3+} it may be seen that just within the limits of experimental error this is true, but the mean values give a different value. However, the experimental errors on these terms are large compared with their magnitude. Assuming that these terms behave in CeO_2 as they do in ThO_2, if ENDOR spectra were to be measured at lower fields the contributions to these terms from the term S^3IH^2 would be reduced and a more accurate measure of these terms could be made.

The terms SIH^2 and S^3IH^2 only appear when ENDOR measurements are made in completely different magnetic fields as in Gd^{157} in ThO_2. These terms are probably proportional to $g_{\parallel}$ by similar arguments to those above and thus their neglect

in the analysis of the isotopes in CeO_2 is probably justified as any corrections that they would make to the magnetic hyperfine interaction will be proportional to that interaction. Thus the evaluation of the hyperfine structure anomaly will be unaffected. This work suggests very strongly that determination of hyperfine interactions by ENDOR techniques should be made in two widely different field regions, to enable these corrections terms to be evaluated accurately.

REFERENCES

Abraham, M.M., Boatner, L.A., Finch, C.B., Lee, E.J. and Weeks, R.A., 1967. J. Phys. Chem. Solids, 28, 81.

Abraham, M.M., Lee, E.J. and Weeks R.A., 1965. J. Phys. Chem. Solids, 26, 1249.

Baker, J.M. and Williams,F.I.B., 1962, Proc. Roy. Soc. A267, 283.

Bir, G.L. and Vinokurov, I.V., 1966, Sov. Phys. Solid State, 7, 2730.

Bleaney, B., 1966. La Structure Hyperfine Magnetique des Atomes Molecules No. 164. 13. Colloques Internationaux du Centre National de la Recherche Scientifique, Paris.

Evans, L., Sandars, P.G.H. and Woodgate, G.K., 1965. Proc. Roy. Soc. A289, 114.

Hurrell, J.P., 1963. D. Phil. Thesis, Oxford University.

Hurrell, J.P., 1965. Brit. J. Appl. Phys. 16, 755.

Low, W. and Shaltiel, D., 1958. J. Phys. Chem. Solids, 6, 315.

Marshall, S.A., 1967. Bull. Am. Phys. Soc. 12, 357, and to be published.

Marshall, S.A., Hodges, J.A. and Serway, R.A., 1964. Phys. Rev. 136, A1024.

Mottelson, B.R. and Nilsson S.G., 1958. Mat. Fys. Skr. Dan. Vid. Selsk, 1. No.8.

Ranon, U. and Hyde, J.S., 1966. Phys. Rev. 141, 259.

Sandars, P.G.H. and Beck, J., 1965. Proc. Roy. Soc. A289, 97.

Speck, D.R., 1956. Phys. Rev. 101, 1725.

Stoneham, A.M., 1966. Proc. Phys. Soc. 89, 909.

Wybourne, B.G., 1966. Phys. Rev. 148, 317.

CHAPTER 6

EXPERIMENTS ON TERBIUM

The hyperfine interaction and nuclear moment of Tb^{159} in Tb^{4+} in ThO_2 have been measured using ENDOR techniques by Baker et. al. (1965). The value of the nuclear moment of $1.994\beta_N$ which they obtained differs by 5% from that estimated by Bleaney (1964). This estimate was based on the value of A for Tb^{3+} measured by Baker and Bleaney (1958), after allowing for a core polarisation correction and assuming a value of $\langle r^{-3} \rangle$ determined by interpolation between Nd^{3+} and Er^{3+} for which $\langle r^{-3} \rangle$ values were calculated from the nuclear moments determined from atomic beam measurements and hyperfine interactions measured in the ions.

An ENDOR experiment on Tb^{3+} could provide useful information on the theory of hyperfine interactions. Firstly Tb^{4+} is an S-state ion and thus the nuclear g-value which was measured for this ion should be very close to the real nuclear g-value, as the first excited crystal field state is at too high an energy to introduce any appreciable pseudo-nuclear g-factor. A measurement of the effective nuclear g-factor in the trivalent ion, coupled with a knowledge of the

positions of the excited states for this ion should permit a check on the Baker and Bleaney theory of the pseudo-nuclear g-factor. Secondly, a measurement of the magnetic hyperfine interaction together with the nuclear moment would give an accurate value for $\langle r^{-3} \rangle$ for Tb^{3+}. Thirdly, ENDOR measurements would permit the evaluation of the quadrupole interaction for Tb^{159} in Tb^{3+}.

ENDOR experiments were performed on Tb^{3+} in two separate hosts, yttrium ethylsulphate (YES) and calcium tungstate ($CaWO_4$).

Tb^{3+} in YES

The free ion electronic configuration for Tb^{3+} in $4f^8$, $^7F_6$, with Landé splitting factor = $\frac{3}{2}$. When substituted into YES, the ion replaces an yttrium ion, experiencing a crystalline electric field of symmetry C_{3h} as discussed by Elliott and Stevens (1952, 1953, a,b).

The crystal field potential may be written using Stevens' operator equivalents, in the form :

$$A_2^0 \langle r^2 \rangle \alpha O_2^0 + A_4^0 \langle r^4 \rangle \beta O_4^0 + A_6^0 \langle r^6 \rangle \gamma O_6^0 + A_6^6 \langle r^6 \rangle \gamma O_6^6 \qquad (6.1)$$

Hüfner (1962) has considered the data existing on crystal

field levels in several rare-earth ions in ethylsulphates, and by extrapolation between the data for Sm^{3+} and Dy^{3+}, has reached values for the parameters in equation (6.1). These are, in cm^{-1} :

$$A_2^0 \langle r^2 \rangle = 110 \qquad A_4^0 \langle r^4 \rangle = -75 \qquad A_6^0 \langle r^6 \rangle = -34$$

$$A_6^6 \langle r^6 \rangle = 465$$

Using these parameters to find the positions of the crystal field levels, he predicts a ground doublet split by 0.4 cm^{-1}, and excited states at 100.9 cm^{-1}, 111.2 cm^{-1}, and higher energies. Kahle and Kalbfleish (1962) who studied the absorption spectrum of Tb^{3+} in YES, found a level at 111.0 cm^{-1}, which agrees very well with the predicted second excited state.

Hüfner's parameters differ considerably from those suggested by Baker and Bleaney (1958), who deduced the parameters from observation of the ground doublet zero field splitting by EPR and extrapolation from Nd^{3+}. In calculating the ground doublet splitting they considered only contributions from J=6 and J=5 excited states. However, contributions from other values of J are important, being of the same order of magnitude as those from J=5. A calculation

of these effects using the methods outlined in Appendix 1, gives reasonably good agreement with Häfner's values, which predict the position of one excited state accurately.

The crystal field theory predicts a ground doublet, with wave-functions

$$\frac{1}{\sqrt{2}}\left(|6\rangle - |-6\rangle\right) \quad \text{and} \quad \left[\sin\theta\,|0\rangle + \frac{\cos\theta}{\sqrt{2}}\left(|6\rangle + |-6\rangle\right)\right]$$

$\frac{1}{\sqrt{2}}(|6\rangle - |-6\rangle) = |6a\rangle$ $\qquad$ $\frac{1}{\sqrt{2}}(|6\rangle + |-6\rangle) = |6s\rangle$

separated by a zero field splitting of 0.4 cm^{-1}, with $\sin\theta = 0.05$, using Hüfner's parameters. This leads to a crystal field spin Hamiltonian with $S = \frac{1}{2}$, for the ground doublet of $\mathcal{H} = g_z\beta H_z S_z + g_x\beta H_x S_x + g_y\beta H_y S_y + \Delta_x S_x + \Delta_y S_y$ where the terms $\Delta_x S_x + \Delta_y S_y$ account for the zero field splitting. Tb^{159} has a nuclear spin of $\frac{3}{2}$ and thus hyperfine interaction terms should be added into the spin Hamiltonian to give:

$$\mathcal{H} = g_z\beta H_z S_z + g_x\beta H_x S_x + g_y\beta H_y S_y + \Delta_x S_x + \Delta_y S_y + AS_zI_z + B(S_xI_x + S_yI_y) + P\left(I_z^2 - \tfrac{1}{3}I(I+1)\right) - g_n'\beta\underline{H}.\underline{I} \qquad (6.2)$$

It is clear from the crystal field wavefunctions of the ground doublet that transitions of the type $\Delta M = \pm 1$ which are normally observed for EPR by applying an r.f. field perpendicular

to the D.C. magnetic field are not allowed in this system. However EPR can be observed by applying the r.f. field parallel to the D.C. magnetic field through $\Delta M = 0$ transitions. These are allowed through the admixtures of excited states into the ground state. For Tb^{3+} in YES, Baker and Bleaney (1958) give the following parameters:

$g_z = 17.72 \quad g_x = g_y < 0.1 \quad A = 6270 \pm 60$ Mc/s

$$\Delta = \sqrt{(\Delta_x^2 + \Delta_y^2)} = 11610 \pm 30 \text{ Mc/s.}$$
$$= 0.387 \text{ cm}^{-1}$$

Effective Nuclear g-factor

As discussed in Chapter 2 the nuclear g-factor observed in ENDOR experiments on the rare-earths differs from the true g-factor by a second order correction term. To evaluate this we make use of Hüfner's crystal field parameters to evaluate the wave-function of the state at 111 cm^{-1}, $\cos\theta\,|0\rangle - \sin\theta\,|6s\rangle$ which is the only state within the J=6 manifold which is admixed into the ground doublet. However, appreciable admixtures can be shown to occur into the ground doublet from excited J manifolds J=5, 4, 3, 2, 1, 0, using the methods in Appendix 1. The overall effect of the admixtures is to

produce a value for the effective nuclear g-factor of $g_n' = -1.224 \times 10^{-3}$ Bohr magnetons.

Estimate of Quadrupole Interaction

Tb^{159} has a nuclear spin of $\frac{3}{2}$, confirmed by the observation of four hyperfine lines in the EPR spectrum. An ENDOR experiment which observes nuclear $\Delta m_I = \pm 1$ transitions will enable the quadrupole interaction to be measured. To reduce the region of search for ENDOR in this system it is essential that a reasonable estimate of the quadrupole interaction P be made initially

$$P = -\frac{3e^2Q}{4I(2I-1)} \left\langle \frac{1}{r^3} \right\rangle \langle J \| \alpha \| J \rangle \left\langle \phi_i \left| J_z^2 - \frac{1}{3} J(J+1) \right| \phi_j \right\rangle \qquad (6.3)$$

Elliott and Stevens (1953,a)

Shielding and polarisation corrections modify the quadrupole interaction considerably from the expression given above. Also pseudo-quadrupole terms (Baker and Bleaney 1958) will arise and should be included in the overall quadrupole interaction. The various contributions to the quadrupole interaction may be written as:

$$P_{lat} = -\frac{3Q}{I(2I-1)} (1 - \gamma_\infty) A_2^0$$

$$P_{4f} = - \frac{3e^2Q}{4I(2I-1)} (1-R_Q) \langle r^{-3} \rangle_{4f} \langle J \| \alpha \| J \rangle \langle + | 3J_z^2 - J(J+1) | + \rangle \quad (6.4)$$

Blok and Shirley (1966) estimate γ = - 80 for trivalent lanthanide ions. Bleaney and Hill (1961) show that a value for the quadrupole interaction of P = 420 Mc/s gives the best fit to specific heat data in ferromagnetic terbium metal. The Sternheimer atomic shielding factor R_Q is of the order of 0.1 (Sternheimer 1966). These parameters lead to values for the major components of the quadrupole interaction of P_{lat} = - 45 (± 9) Mc/s, P_{4f} = + 420 (± 84) Mc/s giving the overall quadrupole interaction to be 375 ± 95 Mc/s. The lattice contribution to the quadrupole interaction is thus small compared with the ionic contribution. The pseudo-quadrupole correction is only of the order of 2 Mc/s.

Since this work was completed, the N.M.R. of Tb^{159} in the ferromagnetic metal has been measured using a spin echo technique by Kobayashi, Sano and Itoh (1967). They observed three lines centred on 3108 ± 3 Mc/s, with a separation of the quadrupole transitions of 668 Mc/s, corresponding to a value of P_{4f} of 334 Mc/s. This is some 20% lower than the value deduced from specific heat data, which shows that the overall quadrupole interaction predicted above is too high, the lower predicted error found being close to the real value.

The ENDOR frequencies predicted using the estimates based on the earlier data were those used in the investigations and are shown on Fig. 6.1. The error in the quadrupole interaction did not affect the position of the $\Delta m_I = \frac{1}{2} \rightarrow -\frac{1}{2}$ transition, which was in fact, the only one for which searches were made for ENDOR. The cumulative effect of the uncertainties in the estimate of the quadrupole interaction made the frequency region in which the $\frac{3}{2} \rightarrow \frac{1}{2}$ nuclear transitions might be found very wide.

Relaxation Times in Tb^{3+} : YES

It is very useful for ENDOR studies to know the electronic and nuclear relaxation rates of the system, to enable a reasonable choice of saturation and modulation conditions to be made. The electronic spin-lattice relaxation rate for this system has been studied by Larson and Jeffries (1966) who find the empirical expression $T_{1e}^{-1} = 59\ T + 0.92 \times 10^{-2}\ T^7$ giving a value of $T_{1e} = 2.5$ msecs. at $4.2^{\circ}K$.

The nuclei of Tb^{159} in Tb^{3+} probably relax very slowly compared with the electrons. From the spin-Hamiltonian for this system the only coupling between the electrons and nuclei arises from the AS_zI_z term representing the scalar hyperfine interaction. This term cannot induce transitions between

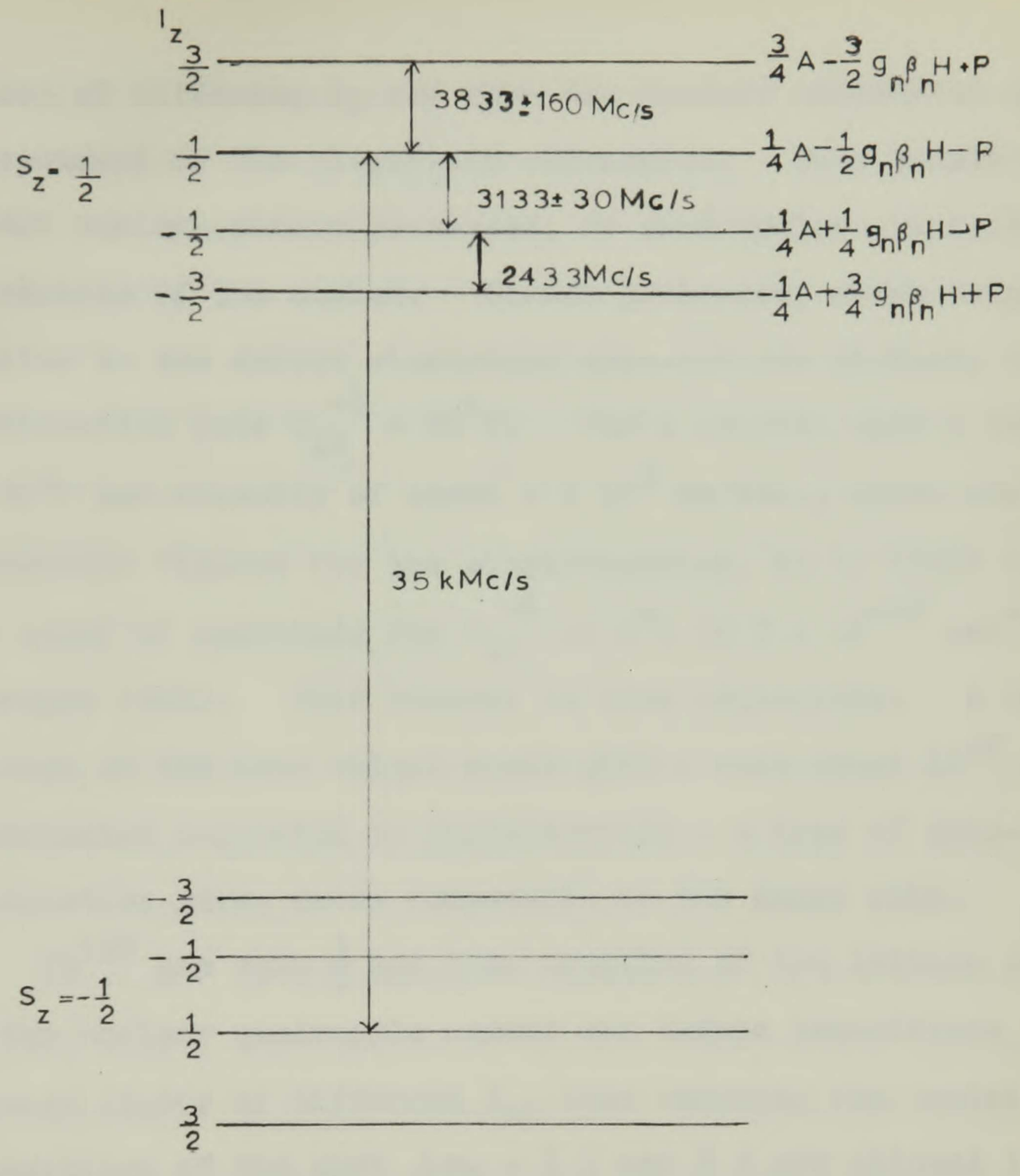

HYPERFINE LEVELS OF Tb^{3+} IN YES SHOWING PREDICTED ENDOR FREQUENCIES

Figure 6. 1

states of differing I_z and thus the nuclear relaxation is independent of the electronic relaxation. This leaves only direct nucleus-phonon processes, or quadrupolar processes for relaxation of the nuclei. Direct processes, whose origin is similar to the direct electronic spin-lattice process, have a relaxation rate $T_{1N}^{-1} = CH^2T$. For a crystal with a Debye θ of 60^oK and velocity of sound 2×10^5 cm/sec., which are reasonable figures for the ethylsulphates, it is found that the order of magnitude for T_{1N}^{-1} at 4^oK is 3×10^{-18} sec^{-1} (Abragam 1961). This process is thus negligible. A Raman process of the same origin would give a rate about 10^{-8} $secs^{-1}$. A mechanism suggested by Khutshishvili - a type of spin-orbit interaction gives rates comparable to the Raman rate.

Tb^{159} has spin $\frac{3}{2}$ and thus coupling of the lattice phonons to the nuclear quadrupole moment can induce transitions between states of different I_z, thus relaxing the nuclei. Transitions of the sort $\Delta m_I = \pm 1$ and ± 2 are allowed in this relaxation process, and although there are no matrix elements of this interaction that exist between $I_z = +\frac{1}{2}$ and $I_z = -\frac{1}{2}$ the nuclei can be relaxed between these states indirectly by a $\Delta I_z = 2$ transition. The dominant process in quadrupolar relaxation is a Raman process. A first order Raman process was described in detail by van Kranandonk (1954). The

relaxation perturbation is taken to be $\mathcal{H} = \frac{e^2 Q \gamma \epsilon}{r^3}$, Q = quadrupole moment, $\frac{e^2}{r^3}$ is the ionic field gradient, γ a shielding factor to account for the modification of the ionic field gradient as seen by the nucleus by core polarisation, covalency, and optical phonon modes. ϵ is a thermal lattice strain, introduced phenomenologically. For a direct process a rate of $T_{1N}^{-1} \simeq 10^{-10}\ T\ \text{sec}^{-1}$ is predicted for the ethylsulphates, which is negligible compared with the Raman process

$$(T_{1N}^{-1}) \simeq \frac{9 \times 6!}{4\rho^2 \pi^3 v^{10}} \left(\frac{k}{h}\right)^7 T^7 \left(\frac{e^2 Q \gamma}{r^3}\right)^2 \qquad (6.5)$$

for temperatures $T \ll \Theta$. This leads to a relaxation rate $10^{-9} \times T^7$ for the ethylsulphate lattice, giving at $4^\circ K$, $T_{1N} \simeq 7 \times 10^4$ secs. Van Kranandonk and Walker (1967) discuss the importance of anharmonic terms in the phonon spectrum, showing that a combination of direct spin-lattice relaxation and anharmonic lattice forces gives a second order Raman process with the same temperature and isotopic dependence of relaxation time as the first order process, but is roughly two orders of magnitude faster. The expression that they derive applies to cubic alkali halide crystals, but the order of magnitude of the effect should be the same for the ethylsulphate lattice. Thus we would expect this process to be

dominant for relaxation of Tb^{159} nuclei in Tb^{3+} : YES, giving a relaxation time of the order of 100 secs.

Tb^{3+} in $CaWO_4$

$CaWO_4$ has a scheelite structure with the Ca^{2+} sites having a tetragonal symmetry, point group S_4. There is good evidence that trivalent rare-earth ions substitute for Ca^{2+} ions, the charge compensation being effected by addition of Na^+ ions to the flux from which the crystal is grown. (Nassau et. al. 1963). The EPR spectrum of Tb^{3+} in $CaWO_4$ has been investigated by Forrester and Hempstead (1962), whose measurements can be fitted to the same spin Hamiltonian as was used for Tb^{3+} in YES, equation (6.2), with the parameters:

$$g_z = 17.772 \qquad g_x = g_y = 0 \qquad A = 6284 \pm 5 \text{ Mc/s}$$

$$B = 0 \qquad \Delta = 8161 \pm 6 \text{ Mc/s}$$

showing that the ground doublet must be closely symmetric and anti-symmetric combinations of $J_z = |\pm 6\rangle$, as in YES, separated by a zero field splitting of 0.271 cm^{-1}.

The crystalline electric field produced at the Ca^{2+} site in $CaWO_4$ which has S_4 symmetry, has been studied by Pappalardo

and Wood (1963) and Shekun (1965, 1967), who show that it may be represented in terms of operator equivalents as :

$$A_2^0 \langle r^2 \rangle \; \alpha O_2^0 + A_4^0 \langle r^4 \rangle \; \beta O_4^0 + A_4^0 \langle r^4 \rangle \; \beta O_4^4$$

$$+ A_6^0 \langle r^6 \rangle \; O_6^0 + A_6^4 \langle r^6 \rangle \; O_6^4 \; .$$

Shekun gives values for these crystal field parameters in both of his papers which differ, those published in 1967 being claimed to give better agreement with experiment. These are, expressed in cm^{-1}:

	$A_2^0\langle r^2\rangle$	$A_4^0\langle r^4\rangle$	$A_6^0\langle r^6\rangle$	$A_4^4\langle r^4\rangle$	$A_6^4\langle r^6\rangle$
1965	260	-75	0	-800	-380
1967	260	-83	-10	-750	-500

Little indication is given in either of his papers as to the evidence from which his parameters were deduced, but they are claimed to describe the overall behaviour of several different rare-earth ions in the Ca^{2+} site in the scheelite structures. A test of the predicted energy levels from both sets of parameters could be made using the zero field splitting observed in the EPR of Tb^{3+} in $CaWO_4$ of 0.271 cm^{-1} and the

position of an excited state in this material at 56 cm^{-1}. This excited state position was determined by electronic spin lattice relaxation time measurements, to be discussed later, which showed an Orbach process to a state at 55 cm^{-1}. Also a brief spectroscopic study of the same specimen was made by Maxwell (1966) who observed a weak absorption line at 56 ± 3 cm^{-1} which he attributed to Tb^{3+}.

Exact diagonalisation of the crystal field spin Hamiltonian matrix generated using both sets of Shekun's parameters was performed. As in the work of Tb^{3+} in YES described earlier, the effect of excited J manifolds on the positions of the ground doublet levels was important, this being evaluated as outlined in Appendix 1. The results of the calculations are shown in Table 6.1, together with the experimental values mentioned above. The calculations of the effects of the admixtures is probably only accurate to 20% as the wavefunctions and positions of the excited states are not known to any better accuracy. From the results shown in Table 6.1 it is clear that neither set of parameters predicts the excited state positions well, but the first set gives a better overall fit than the second.

No attempt has been made to estimate the quadrupole interaction or effective nuclear g-factor due to lack of

TABLE 6.1

Tb^{3+} in $CaWO_4$. Crystal Field States Using Shekun's Parameters

State	Energy without admixtures from excited states cm^{-1}	Energy with admixtures cm^{-1}
1965		
$(0.998 \|6s\rangle + 0.07 \|2s\rangle)$	0	0.36
$(0.999 \|6a\rangle + 0.03 \|2a\rangle)$	0.24	0
$(\pm 0.367 \|5\rangle \pm 0.853 \|1\rangle \pm 0.364 \|-3\rangle)$	162	140
1967		
$(0.9997 \|6s\rangle + 0.023 \|2s\rangle)$	0	1.13
$(0.9999 \|6a\rangle + 0.0104 \|2a\rangle)$	0.02	0
$(0.35 \|5\rangle + 0.81 \|1\rangle \pm 0.48 \|-3\rangle)$	170	153

Observed energies are : 0, 0.271, 55 cm^{-1}.

The energies are all quoted relative to zero defined for the lowest energy in each case.

precise wave functions for this system but it is expected that the quadrupole interaction should be close to that for the ethylsulphate, where it was shown that the ionic contribution was much greater than the lattice contribution.

Spin Lattice Relaxation Time

The electronic spin lattice relaxation time of $Tb^{3+}:CaWO_4$ was measured to give some indication of the conditions required for saturation of the EPR lines. The measurements were made on the line arising from $m_I = +\frac{1}{2}$, at X band (9.4 kMc/s), using a pulse saturation recovery method, on the apparatus described by Breen (1966).

The system used was a superheterodyne X band spectrometer, with an English Electric K350 klystron used to provide the saturating pulses of $\sim$ 1 watt. The saturating pulse of microwave power was derived by pulsing the reflector voltage of the klystron rather than by use of wave-guide switches. Full details of the apparatus and pulsing equipment are given in Breen's thesis. The EPR signal recovering after saturation was monitored using a low power CV 2304 klystron, and the signal was displayed on a Tektronix 581A oscilloscope and photographed. A base line was recorded by triggering the oscilloscope in the interval between pulses and after spin

temperature equilibrium had been reached. Using the pulse saturation recovery method care must be taken to eliminate the effects of spin diffusion and cross relaxation, to avoid confusion between this faster energy sharing process and the true relaxation of the spins to the lattice. To facilitate this the pulse length was increased until the recovery signal was exponential with a time constant that was unchanged for longer pulse durations. In practice this was only true for the tail of the observed trace, and thus only the tail of the recovery traces was used. When this condition is fulfilled it is reasonably certain that any other spins in thermal contact with those being monitored have also been saturated, giving only a single overall decay rate.

The photographs of the recovery traces were measured and the amplitude of the recovery signal plotted on semi-log graph paper as a function of time. This enabled any non-exponential recoveries, or recoveries with more than one time constant to be eliminated. The relaxation times were taken from these graphs and plotted as a function of temperature as giving the points shown in Fig. 6.2.

Tb^{3+} is a non-Kramers ion and thus the spin lattice relaxation rate should be a function of temperature of the form:

$$T_1^{-1} = AT + BT^7 + Ce^{-\Delta/T}$$

Orbach (1961)

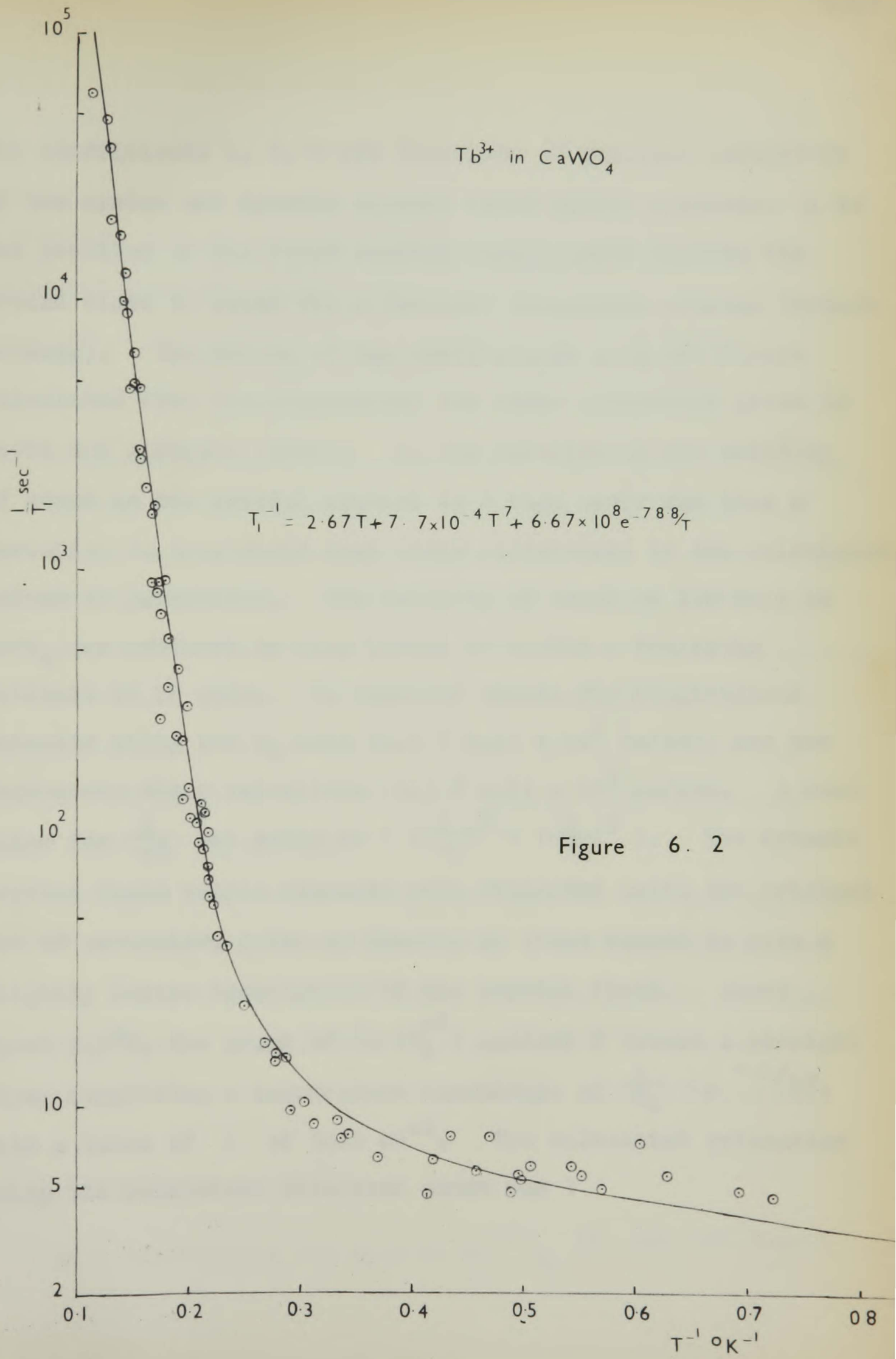
Tb^{3+} in $CaWO_4$
$T_1^{-1} = 2{\cdot}67T + 7{\cdot}7\times10^{-4}T^7 + 6{\cdot}67\times10^8 e^{-788/T}$
T_1^{-1} sec^{-1}
10^5
10^4
10^3
10^2
10
5
2
0·1
0·2
0·3
0·4
0·5
0·6
0·7
0·8
T^{-1} °K^{-1}

Figure 6. 2

The coefficients A, B, C are functions of physical parameters of the system and dynamic crystal field matrix elements. Δ is the position of the first excited state, which enables the ground state to relax via a resonant two-phonon process (Orbach process). The values of the coefficients A, B and C were calculated from the expressions for these parameters given in Scott and Jeffries (1962). In the calculation the velocity of sound in the crystal appears to a high power and thus a variation in this could make large differences in the calculated values of parameters. The velocity of sound at 100 Mc/s in $CaWO_4$ was measured by King (1966) to enable a realistic estimate to be made. He obtained values for longitudinal velocity along the C_4 axis $(4.6 \pm 0.1) \times 10^5$ cm/sec. and two degenerate shear velocities $(2.3 \pm 0.1) \times 10^5$ cm/sec. A mean value for $\frac{1}{v^5}$ was taken as $\left(\left(\frac{1}{v_l}\right)^5 + \left(\frac{2}{v_s}\right)^5 \right)$. The dynamic crystal field matrix elements were evaluated using the original set of parameters given by Shekun, as these seemed to give a slightly better description of the crystal field. Above about $5.5^{\circ}K$, the graph of $\ln (T_1^{-1})$ against T showed a straight line, suggesting a temperature dependence of $\frac{1}{T_1} \propto e^{-\Delta/kT}$, with a value of Δ of $54.6\ cm^{-1}$. The calculated relaxation using the parameters discussed above was :

$$T_1^{-1} = 1.4T + 2.6 \times 10^{-3}T^7 + 6 \times 10^7 e^{-78.7/T}.$$

A computed fit of the measured data using a curve fitting procedure gave the parameters:

$$T_1^{-1} = 2.67T + 7.7 \times 10^{-4}T^7 + 6.65 \times 10^8 e^{-78.7/T}.$$

The programme is given in Appendix 2. This curve is plotted on Fig. 6.2 as the solid line. The agreement between the calculated and measured temperature dependence is surprisingly good for the direct and Raman processes, and the difference of one order of magnitude for the Orbach rate is not surprising in view of the approximations that are inherent in the phenomenological theory which is used, and the differences between the computed and observed crystal field splittings using Shekun's parameters.

A single measurement of T_2 was made for the same specimen of $Tb^{3+} : CaWO_4$ at 4^oK by Breen using a spin echo technique. He found a value of 3×10^{-7} secs, which in view of the slow T_1 represented a remarkably fast T_2. This is of great importance in the discussion of predicted ENDOR linewidths.

ENDOR Experiments on Tb^{3+}

In a non-Kramers ion such as Tb^{3+} g_1 is zero and thus B

is zero. This means that there are no operators of the form $S_{\pm}I_{\mp}$ to couple states S_z, I_z to states $S_{z\pm1}, I_{z\mp1}$. If a nuclear r.f. field is applied perpendicular to H_0 and H_1, the only operator that can induce transitions between the hyperfine levels arises from $g_N\beta_N\underline{H}.\underline{I}$. For any system where $B \neq 0$, there are also terms of the type BS_+I_- to couple these states, leading to an enhancement of the ENDOR transition moment as discussed by Whiffen (1966). It should be noted that rotation of the crystal axis relative to the D.C. magnetic field will not produce any operators of the required form (Bleaney 1951). In view of the fact that only the nuclear Zeeman term can contribute to the nuclear transition, it is worth considering the advantages that an ENDOR study of this system would hold over a conventional NMR study. This is best performed by reference to an idealised energy level diagram, considering initially a simple case of $S = \frac{1}{2}$, $I = \frac{1}{2}$, as in Fig. 6.3. The states are labelled by wavefunctions $\pm$ corresponding to S_z or $I_z = \pm \frac{1}{2}$. These states are, to second order, pure states as there is no off-diagonal term in the hyperfine interaction to admix them.

ENDOR is performed by saturation of an allowed EPR transitions, AB or CD. Consider the transition AB. A second r.f. field is then swept through the nuclear resonance

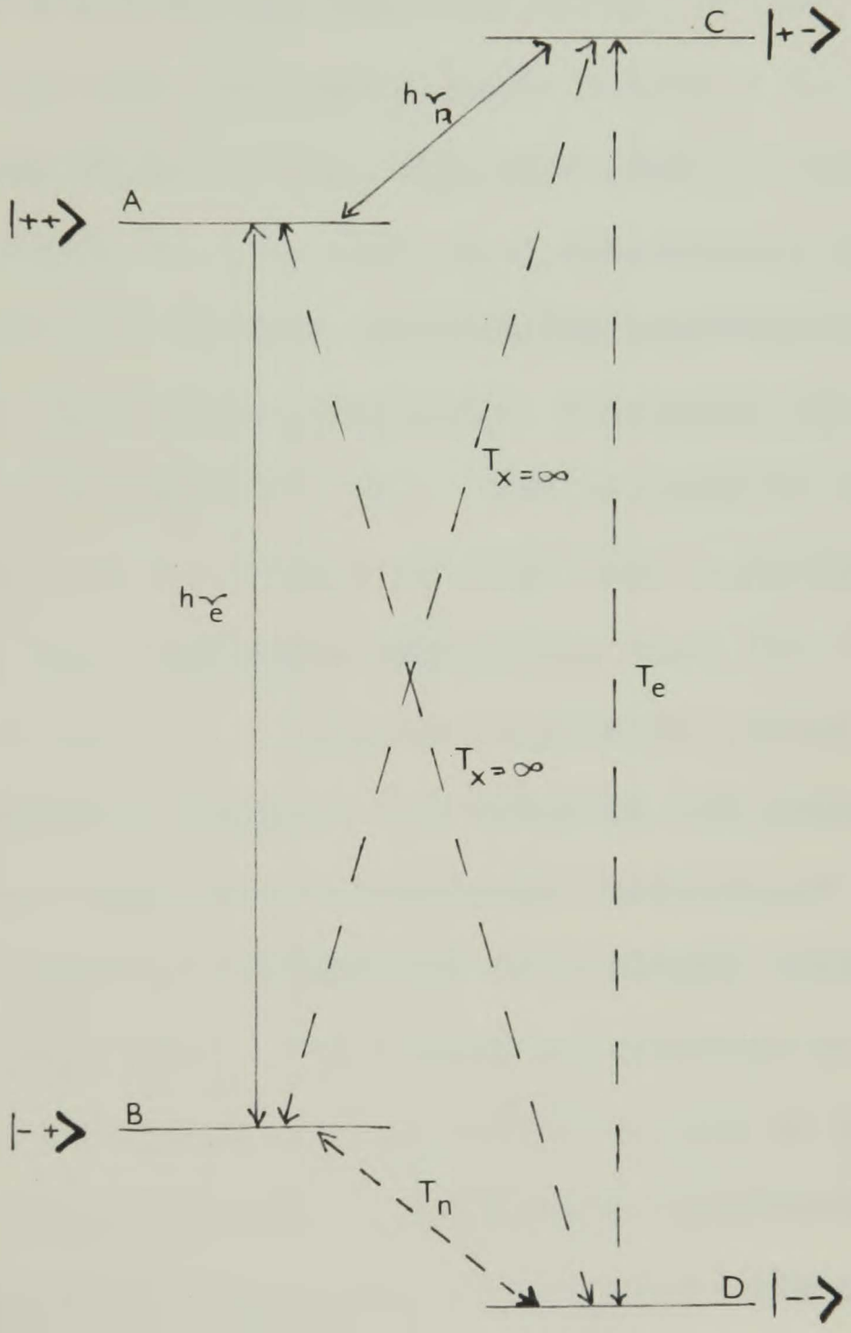
C
|+->
h ν n
A
|++>
T x = ∞
h ν e
T e
T x = ∞
B
|- +>
T n
D
|-->
IDEALISED ENDOR SYSTEM WITH B(S x I x + S y I y) = 0

Figure 6.3

frequency to either saturate or perform fast passage on the transition AC or BD. This field will induce transitions between A and C and change the populations of both levels. If one considers the relaxation paths possible in the system shown as dotted lines in Fig. 6.3, the paths AD and CA are strictly forbidden as B is zero in a non-Kramers salt. Thus if one disturbs the thermal equilibrium populations of A and C by applying the nuclear frequency, electrons can be relaxed to B only via the paths CD, DB. The process CD is an allowed EPR transition and will occur rapidly with a characteristic time given by the electronic relaxation time for the ion. The path DB however is a nuclear relaxation process estimated to have a relaxation time of the order of 100 secs. This slow relaxation path will effectively "bottleneck" the ENDOR process, reducing the probability of a steady state ENDOR signal being observed. The signal is observed by monitoring the change of EPR signal caused by the change of population in A by the nuclear signal. Elementary consideration of Boltzmann statistics shows that one expects this change of population to be proportional to $g_z\beta H/kT$. Thus use of the EPR signal to detect the change in nuclear polarisation leads to a signal that is proportional to the electronic Zeeman splitting. If the nuclear resonance were to be observed

directly the signal would be proportional to the hyperfine splitting, which for Tb^{3+} is an order of magnitude smaller than the electronic splitting as shown by Abragam (1961).

If the nuclear frequency is amplitude modulated at a rate which is slow compared with T_{1N} we should arrive at the following situation. With the r.f. switched on the relaxation path between the levels A and C is effectively short-circuited, and spins are transferred from level A to level C. This transfer of spins changes the equilibrium population difference between A and B and causes a change in the EPR absorption signal. The spins relax rapidly to level D by an electronic T_1 process. However, the process relaxing the spins to level B is slow, of the order of 100 secs. This causes a bottleneck in the relaxation path for the spins. The population of level D increases rapidly as the electrons are being relaxed to this level. This causes a build-up of electrons in C as the ratio of populations between C and D is constant. This reduces the number of electrons being transferred from B, hence reducing the change in EPR signal. The nuclear T_1 is of the order of 100 secs. and thus the overall change in EPR signal when the nuclear signal is switched on is very small after an initial transient. At the end of the amplitude modulation cycle the system will relax with a time-constant

T_{1N}. To observe any signal on the next cycle, the time interval between cycles would have to be $\geq T_{1N}$. This means that the efficiency of square wave amplitude modulated nuclear frequency for ENDOR observation is very low in this case, a useful signal being produced as a transient at the beginning of a pulse and not being repeated until after a time $\sim$ 100 secs. later. Frequency modulation will not improve the position as time must be given for the system to relax before the nuclear transition is swept again. Probably the most satisfactory method of detection would be to sweep the nuclear frequency through the region in a time that is fast compared to T_{1N}. This would produce a transient signal as the nuclear resonance is induced, and would remove the driving frequency from the nuclear resonance quickly, enabling the saturation of the nuclear resonance to relax immediately after the transient. If a nuclear frequency were swept sufficiently far to become resonant with the transition DB this would short circuit that relaxation path and produce a second change in the EPR level, also enhancing the relaxation of the level C. This technique has also been suggested by McIrvine et. al. (1964).

Another possibility for relieving the relaxation bottleneck in this system would be the simultaneous application of

two nuclear radio frequency fields, one inducing the nuclear transition A - C, the other inducing the transition D - B. This would short circuit the slow T_{1N} times in the system and produce a situation in which ENDOR signals could be observed continuously. The frequency separation between these transitions is simply $g'_N\beta_N H$. Thus if two nuclear frequency signals separated by $\sim$ 5 Mc/s were applied to the specimen simultaneously the relaxation bottleneck should be relieved and the probability of observing ENDOR would be greatly enhanced. One possible method of performing this experiment was tried, the two frequencies being produced by square wave amplitude modulation of the S band klystron output, using a wave-guide switch. If the microwave power is switched at 2.5 Mc/s, sidebands of microwave power should be produced at a separation of 5 Mc/s. However, the amount of power expected in these sidebands is small, thus reducing the r.f. field available for inducing the nuclear transitions. The amplitude modulation frequency had to be adjusted over a range of 500 kc/s to cover the possible errors in the estimate of the frequency separation between the two transitions. No ENDOR was seen using this technique.

An extensive search for ENDOR of Tb^{3+} in YES and $CaWO_4$ was made using both the Q and J band apparatus described in

Chapter 3. Let us first consider the work at Q band. The EPR was easily observed and saturated at 4.2°K. The linewidth was narrower for $CaWO_4$, being about 2 gauss whilst the YES lines were about 15 gauss wide. Thus it looked as though the $CaWO_4$ specimen should be the easier to study, and despite the lack of information available for this crystal it was investigated more thoroughly than the YES. It was hoped to observe the Tb^{159} $\frac{1}{2} \rightarrow -\frac{1}{2}$ transitions in this specimen and to use these for optimising the apparatus sensitivity before searching for the lines in YES.

The hyperfine interaction is determined to $\pm$ 5 Mc/s and thus the region in which the ENDOR search need be conducted is limited to $\pm$ 2.5 Mc/s for the $\frac{1}{2} \rightarrow -\frac{1}{2}$ transition. This region was searched intensively under different conditions without any reproducible effects being observed. The nuclear frequency was frequency modulated at 140 c/s, 30 c/s and 2 c/s to varying depths by applying small voltages to the klystron reflector voltage. The frequency was also amplitude modulated using a wave-guide switch and Schmidt trigger producing 100% square wave modulation at frequencies down to 0.5 c/s. The nuclear frequency was also swept whilst unmodulated to attempt to see the transient EPR response to a nuclear transition. These various modes of nuclear frequency were applied

under different conditions of EPR saturation and different depths of 115 kc/s modulation. A similar but rather less extensive search was conducted on the Tb^{3+} : YES crystal, also with no reproducible effects at 4.2°K.

One possible explanation for the lack of response was a lack of r.f. field at the nuclear frequency, and thus the J band apparatus was designed to give a much larger r.f. field at the specimen. A similar series of investigations was started on this system, the frequency range in which the ENDOR was to have been expected being changed as the experiment was being conducted in low field. The EPR frequency of 15 kMc/s is only slightly larger than the zero field splitting of the EPR levels, and the separation between the hyperfine structure levels is not linear in magnetic field. An exact diagonalisation of the spin Hamiltonian was performed on substitution of the approximate spin Hamiltonian parameters, showing that the ENDOR spectrum should be centred on 2802 Mc/s for $CaWO_4$ and 2292 Mc/s for YES. Shortly after starting the search for ENDOR at the appropriate frequency it was realised that there was another more serious consequence of working at low field in this system. The dependence of ENDOR frequency upon magnetic field can be found by differentiation of the eigenvalues with respect to magnetic field. For the case of YES,

where the EPR line is inhomogeneously broadened to 15 gauss by the surrounding protons, this leads to a variation in the ENDOR frequency of about 20 Mc/s depending upon which part of the EPR line is being saturated. In practice it appears that there is a fast spin diffusion process in these lines which would spread the saturation through the entire ENDOR linewidth as in Tm^{2+} and Yb^{3+} in CaF_2(Chapter 4). This would give an ENDOR linewidth of the order of 20 Mc/s. The case in $CaWO_4$ should be rather better suggesting a linewidth of 3 Mc/s. The detection of lines of these widths is likely to be very difficult. The search for ENDOR of Tb^{159} was abandoned after no evidence for the effect was found. It would appear that any search for ENDOR in a system where the energy levels are a higher order function of field than linear should be carefully examined for the possibility of very wide lines in the light of the above results.

Despite extensive searches for ENDOR using several different techniques, no reproducible effect was found for either host. In describing the experiments I have outlined the possible difficulties and reasons for lack of success in the search. It would appear that the absence of terms of the form BS_+I_- in non-Kramers ions is the principal source of difficulty in performing stationary ENDOR experiments.

whilst the high nuclear frequency with its associated problems makes transient ENDOR signals difficult to observe. Transient effects are the most likely to give an ENDOR response in non-Kramers rare-earth systems and the design of an experiment in the light of the above investigations should render ENDOR of Tb^{3+} observable. The apparatus with which this work was performed was designed principally to perform slow frequency sweeps to observe ENDOR in the more conventional stationary mode.

REFERENCES

Abragam, A., 1961. The Principles of Nuclear Magnetism, Clarendon Press.

Baker, J.M. and Bleaney, B., 1958. Proc. Roy. Soc. A245, 156.

Baker, J.M., Chadwick, J.R., Garton, G. and Hurrell, J.P., 1965. Proc. Roy. Soc. A286, 352.

Bleaney, B., 1951. Phil. Mag. 42, 441.

Bleaney, B., 1964. Proc. Int. Conf. on Quantum Electronics, 3, 595.

Bleaney, B. and Hill, R.W., 1961. Proc. Phys. Soc. 78, 313.

Blok, J. and Shirley, D.A., 1966. Phys. Rev. 143, 278.

Breen, D.P., 1966. D. Phil. Thesis. Oxford University.

Elliott, R.J. and Stevens, K.W.H., 1952. Proc. Roy. Soc. A215, 437.

Elliott, R.J. and Stevens, K.W.H., 1953a. Proc. Roy. Soc. A218, 553.

Elliott, R.J. and Stevens, K.W.H., 1953b. Proc. Roy. Soc. A219, 387.

Forrester, P.A. and Hempstead, C.F., 1962. Phys. Rev. 126, 923.

Häffner, S., 1962. Zeits. für Phys. 169, 417.

Kahle, H.G. and Kalbfleisch, H., 1962. Zeits für Phys. 166, 184.

King, P.J., 1966. Private Communication.

Kobayashi, S., Sano, N. and Itoh, J., 1967. J. Phys. Soc. Japan, 22, 676.

Larson, G.H. and Jeffries, C.D., 1966. Phys. Rev. 141, 461.

McIrvine, E.C., Lambe, J. and Laurence, N., 1964. Phys. Rev. 136, A467.

Maxwell, K., Private communication.

Nassan, K., Loiacono, G.M., 1963. J. Phys. Chem. Solids, 24, 1503

Orbach, R., 1961. Proc. Roy. Soc. A264, 458.

Pappalardo, R. and Wood, D.L., 1963. J. Mol. Spectroscopy, 10, 81.

Scott, P.L. and Jeffries, C.D., 1962. Phys. Rev. 127, 32.

Shekun, L. Ya., 1965. JETP. Letts, 2, 437.

Shekun, L. Ya., 1967. Sov. Phys. Solid State, 8, 2340.

Sternheimer, R.M., 1966. Phys. Rev. 146, 140.

Van Kranendonk, 1954. Physica, 20, 781.

Van Kranendonk, and Walker, M.B., 1967. Phys. Rev. Letts. 18, 701.

Whiffen, D.H., 1966. Mol. Phys. 10, 595.

APPENDIX 1

CALCULATION OF ADMIXTURES FROM EXCITED STATES INTO GROUND STATE

The crystalline electric field at the Ca^{2+} site in $CaWO_4$ given by Shekun (1965) has the form :

$$B_2^0 V_2^0 + B_4^0 V_4^0 + B_6^0 V_6^0 + B_4^4 V_4^4 + B_6^4 V_6^4 .$$

In Stevens' operator equivalent formulation the field may be written:

$$V = A_2^0 \langle r^2 \rangle \alpha O_2^0 + A_4^0 \langle r^4 \rangle \beta O_4^0 + A_4^4 \langle r^4 \rangle \beta O_4^4 + A_6^0 \langle r^6 \rangle \gamma O_6^0 + A_6^4 \langle r^6 \rangle \gamma O_6^4 , \quad \text{(A1.1)}$$

where β, β, γ are numerical factors tabulated for the ground manifold in Elliott and Stevens (1953). Using the treatment of Hutchings (1964) the crystal field can be expressed in tesseral harmonics :

$$V = \langle r^2 \rangle \gamma_{20} Y_2^0 + \langle r^4 \rangle [\gamma_{40} Y_4^0 + \frac{\gamma_{44}^c}{\sqrt{2}} (Y_4^4 + Y_4^{-4})] + r^6 [\gamma_{60} Y_6^0 + \frac{\gamma_{64}^c}{\sqrt{2}} (Y_6^4 + Y_6^{-4})] \quad \text{(A1.2)}$$

Where Y_n^m are spherical harmonics,

$$\Upsilon_{na}^{c} = \sum_{j=1}^{n} \left(\frac{4\pi}{2n+1}\right) e_j \frac{Z_{na}^{c}(\theta_j,\phi_j)}{R_j^{n+1}} \qquad \text{(A1.3)}$$

$$Z_{no} = Y_n^o \qquad Z_{nm}^{c} = \frac{1}{\sqrt{2}} \left[Y_n^{-m} + (-1)^m Y_n^m\right] \qquad \text{(A1.4)}$$

This method of writing the potential avoids the use of imaginary quantities. When the Z_{na} are expressed in Cartesian co-ordinates there is an immediate correspondence between them and Stevens' Operator equivalent, the difference being some numerical factor. The more commonly occurring Z_{na}'s are tabulated in Hutchings (1964). From this we find the relationships :

$$A_2^0 = \Upsilon_{20} \frac{1}{4}\left(\frac{5}{\pi}\right)^{\frac{1}{2}} \qquad A_6^0 = \Upsilon_{60} \frac{1}{32}\left(\frac{13}{\pi}\right)^{\frac{1}{2}} \qquad A_6^4 = \Upsilon_{64}^{c} \frac{21}{32}\left(\frac{13}{7\pi}\right)^{\frac{1}{2}}$$

$$A_4^0 = \Upsilon_{40} \frac{3}{16}\left(\frac{1}{\pi}\right)^{\frac{1}{2}} \qquad A_4^4 = \Upsilon_{44}^{c} \frac{3}{16}\left(\frac{35}{\pi}\right)^{\frac{1}{2}} \qquad \text{(a1.5)}$$

The advantage of expressing the crystal field in this is that spherical harmonics can be directly related to tensor operators through the relation:

$$C_q^{(k)} = \left(\frac{4\pi}{2k+1}\right)^{\frac{1}{2}} Y_{kq}(\theta,\phi) \qquad \text{(A1.6)}$$

whereas it is not immediately obvious how to relate operator equivalents to tensor operators. The evaluation of γ_{nc} for a particular symmetry, is a lengthy but fortunately, unnecessary calculation for the particular application being considered here. We are interested in the admixture of states from the J manifolds into the ground states, and thus need to evaluate matrix elements of the form

$$\langle LSJM_J \mid \mathcal{H}_c \mid LSJ'M'_J \rangle$$

in the crystal field interaction Hamiltonian, from (A1.2)

$$\mathcal{H}_c = \langle r^2 \rangle \gamma_{20} \left(\frac{5}{4\pi}\right)^{\frac{1}{2}} C_0^{(2)} + \langle r^4 \rangle \left(\frac{9}{4\pi}\right)^{\frac{1}{2}} \left[\gamma_{40} C_0^{(4)} + \frac{\gamma^c_{44}}{\sqrt{2}} \left(C_4^{(4)} + C_{-4}^{(4)}\right)\right]$$

$$+ \langle r^6 \rangle \left(\frac{13}{4\pi}\right)^{\frac{1}{2}} \left[\gamma_{60} C_0^{(6)} + \frac{\gamma^c_{64}}{\sqrt{2}} \left(C_4^{(6)} + C_{-4}^{(6)}\right)\right] \qquad (A1.7)$$

Let us consider a general term in $\mathcal{H}_c$ of $\lambda C_m^{(n)}$

The matrix element becomes :

$$\lambda \langle LSJM_J \mid C_m^{(n)} \mid LSJ'M'_J \rangle$$

Now using the theory outlined in Judd (1963) we can reduce this matrix element making use of the Wigner-Eckart theorem:

$$\langle LSJM \left| C^{(n)}_m \right| LSJ'M'_J \rangle = (-1)^{J-M_J} \begin{pmatrix} J & n & J' \\ -M_J & m & M'_J \end{pmatrix} \langle LSJ \| C^{(n)} \| LSJ' \rangle$$

$$= (-1)^{L+S+J+J'-M_J+n} [(2J+1)(2J'+1)]^{\frac{1}{2}}$$

$$\begin{Bmatrix} J & n & J' \\ L & S & L \end{Bmatrix} \begin{pmatrix} J & n & J' \\ -M_J & m & M'_J \end{pmatrix} \langle L \| C^{(n)} \| L \rangle . \qquad \text{(A1.8)}$$

This has effectively uncoupled the vectors L and S, leaving three quantities to be evaluated. $\begin{Bmatrix} J & n & J' \\ L & S & L \end{Bmatrix}$ is a 6-j symbol and $\begin{pmatrix} J & n & J' \\ -M_J & m & M'_J \end{pmatrix}$ is a 3-j symbol. These are tabulated for all half integral angular momenta from 0 to 8 by Rotenberg et, al. (1959). The reduced matrix element $\langle L \| C^{(n)} \| L \rangle$ is independent of the particular J values of the manifold under consideration and is a property of the atom and order of the tensor operator only. For a simple one or two electron atom this quantity can be evaluated easily in an explicit form. For Tb^{3+} with 8 electrons, or 6 holes, in the 4f shell, the evaluation of this is more complicated and thus we shall treat it as a parameter to be evaluated, together with γ_{nq}.

These parameters always occur as a product and can be lumped together as a single parameter, whose value can be determined by use of equation (A1.8) above, within the ground

manifold, i.e., for Tb^{3+}, $L = S = 3$, $J = J' + 6$. This can be evaluated, for any particular component of the crystal field e.g.,

$$V_4^4 = \left(\frac{2}{8\pi}\right)^{\frac{1}{2}} \gamma_{44}^c \left(C_4^{(4)} + C_{-4}^{(4)}\right) = \lambda \left(C_4^{(4)} + C_{-4}^{(4)}\right)$$

$$\lambda \left\langle 3366 \left| C_4^{(4)} \right| 3362 \right\rangle = \lambda \begin{pmatrix} 6 & 4 & 6 \\ -6 & 4 & 2 \end{pmatrix} \begin{Bmatrix} 6 & 4 & 6 \\ 3 & 3 & 3 \end{Bmatrix} \sqrt{13 \cdot 13} \left\langle L \| C^4 \| L \right\rangle$$

$$= \frac{\lambda}{33} \left\langle 3 \| C^4 \| 3 \right\rangle \qquad \text{(A1.9)}$$

But as we are interested solely in the ground manifold at this stage, we could equally well apply Stevens' operator equivalent methods to determine the same matrix element. Using this approach we have :

$$\left\langle 3366 \left| A_4^4 \beta O_4^4 \right| 3362 \right\rangle = A_4^4 \beta \left\langle 6 \left| O_4^4 \right| 2 \right\rangle$$

$$= A_4^4 \beta \; 36 \sqrt{55} \qquad \text{(A1.10)}$$

as $A_4^4 = \gamma_{44} \frac{3}{16} \left(\frac{35}{\pi}\right)^{\frac{1}{2}}$ we have, equating both approaches:

$$\left\langle 3 \| C^4 \| 3 \right\rangle = \sqrt{\frac{14}{11}}$$

This reduced matrix element may now be used to evaluate matrix elements of the crystal field between states of different J. Similarly the elements $\langle 3 \| C^2 \| 3 \rangle$ and $\langle 3 \| C^6 \| 3 \rangle$ may be evaluated.

Having evaluated the matrix elements between states of different J, perturbation theory may be used to find the effects of admixtures from excited states into any states in the ground manifold.

REFERENCES

Elliott, J.J. and Stevens, K.W.H., 1953. Proc. Roy. Soc. A218, 553.

Hutchings, M.T., 1964. Solid State Phys. 16, 227.

Judd, B.R., 1963. Operator Techniques in Atomic Spectroscopy, McGraw-Hill Book Company.

Rotenberg, M., Bivins, R., Wooten, J.K. and Metropolis, N., The 3-j and 6-j symbols, Technology Press, M.I.T.

Shekun, L. Ya., 1965. JETP Letts. 2.

APPENDIX 2

LEAST SQUARES TREATMENT OF T_1 AS A FUNCTION OF TEMPERATURE in Tb^{3+} : $CaWO_4$.

In order to fit the measured spin lattice relaxation times to an analytical function of temperature, it was assumed that the system would obey the function:

$$\frac{1}{T_1} = AT + BT^7 + C \exp\left(-\frac{\Delta}{T}\right)$$

The parameters A, B, C, Δ are regarded as unknowns. Initially the behaviour for $T > 5^{\circ}K$ was used to find a value for Δ. This was fitted by hand to give $\Delta = 78.7^{\circ}K$. In order for the least squares procedure MINOG not to cause a real overflow on the computer, reasonably accurate values of the coefficients A, B and C are required as starting values. These parameters were initially extracted by hand calculation to within two orders of magnitude of the final values. These values were then fed as starting values for the least squares fitting program FAREAllAPU. The program was written in KDF9 ALGOL language and compiled using the Whetstone compiler, as it was found that only two runs

lasting about 12 mins. each were necessary to find the least squares result.

The data required for this program are in Table (A.1). The value of Δ is written into the program, at the position; delta = 78.7. The program is printed out in full in Figure (A.1) as the procedure MINOG is no longer available in the computing laboratory program library. The program finds new values of the parameters A, B and C by stepping A initially by the quantity "pas" read in from the data, and evaluating the r.m.s. deviation between the data and the new values for $\frac{1}{T_1}$. New values of the parameters are produced and the process repeated, until the r.m.s. deviation does not change by more than the quantity "eps" read in from the data. After each iteration the new values of the parameters and the r.m.s. deviation are printed. When the program finds a minimum it prints each parameter in the format [d.dddddd$_{10}$+nd] and then evaluates $\frac{1}{T_1} = AT + BT^7 + C \exp - \frac{\Delta}{T}$ between 1° and 10° K in steps of 0.2°K. This final output is shown in Table (A.2), being the data used to plot the solid curve in Figure (6.2).

Figure (A .1)

```
FAREA11APU
COPLAND LEAST SQUARES→

begin library A0,A6,A12;
      real eps,pas,delta,t;
      integer f1,k,i,n;
      real array xmin,x[1:3],P,V[1:72];
    real procedure func(x); array x;
    begin real sum; integer m;
    sum:=0;
    for m:=1,2,3 do write(30,format([3s+d.dddd10+nd]),x[m]);

    for m:= 1 step 1 until 72 do
    sum:= sum+(ln(P[m])-ln(x[1]xV[m]+x[2]x
            V[m]↑7+x[3]xexp(-delta/V[m])))↑2;
    func:= sum;
    write(30,format([3s+d.dddd10+ndc]),sum);
    end;

procedure minog(function,n,x1,eps,step)result:(xmin);
  value n,x1,eps,step;
  real procedure function; integer n; array x1,xmin;
  real eps,step;
comment
--> Not using gradients.  See Powell, Comp.J. 7(1964)155;

begin array pp[1:n,0:n],p[0:n],x,y[1:n];
real delta,f1,f2,f3,fx,fy;
  integer m,j,r,cycle,count;

  procedure switch(x,fx,rx,y,fy,ry);
    real fx,rx,fy,ry; array x,y;
  begin real z; integer j;
    for j:=1 step 1 until n do
    begin z:=x[j]; x[j]:=y[j]; y[j]:=z;
    end;
    z:=fx; fx:=fy; fy:=z;
    z:=rx; rx:=ry; ry:=z;
  end switch;
```

```
  procedure locmin(fx,x,q,fy,y); value fx,x;
    real fx,fy; array x,q,y;
  begin array p,z1,z2,z3,z4[1:n]; integer j;
    real p0,w1,w2,w3,w4,r1,r2,r3,r4,det;
    for j:=1 step 1 until n do
    begin z1[j]:=x[j]; p[j]:=q[j];
      z2[j]:=x[j]+p[j]
    end; p0:=q[0]; w1:=fx; r1:=0; r2:=1; w2:=function(z2);
    count:=count+1;
L1:  if w1<w2 then switch(z1,w1,r1,z2,w2,r2);
    r3:=2xr2-r1;
    for j:=1 step 1 until n do
    z3[j]:=x[j]+r3xp[j]; w3:=function(z3); count:=count+1;
    if w3<w2 then
    begin switch(z3,w3,r3,z2,w2,r2); goto L1
    end;
L2:  det:=(r2-r3)xw1+(r3-r1)xw2+(r1-r2)xw3;
    r4:=((r2↑2-r3↑2)xw1+(r3↑2-r1↑2)xw2+(r1↑2-r2↑2)xw3)/det/2;
    for j:=1 step 1 until n do z4[j]:=x[j]+r4xp[j];
    w4:=function(z4); count:=count+1;
    if w4≤w2 and w4≤fx then goto exit;
    if(r4-r2)x(r3-r1)>0 then
    begin if w4>w2 then switch(z3,w3,r3,z4,w4,r4) else
      begin switch (z2,w2,r2,z1,w1,r1);
        switch(z4,w4,r4,z2,w2,r2)
      end; goto L2
    end else
    begin if w4>w1 and r1=0 then
      begin switch(z2,w2,r2,z4,w4,r4); goto L1
      end else
      if w4>w2 then switch(z1,w1,r1,z4,w4,r4) else
      begin switch(z2,w2,r2,z3,w3,r3);
        switch(z4,w4,r4,z2,w2,r2);
      end; goto L2
    end;
exit:  for j:=1 step 1 until n do y[j]:=z4[j]; fy:=w4;
    for j:=0 step 1 until n do q[j]:=q[j]xr4;
  end locmin;
```

```
count:=0;
 for r:=1 step 1 until n do
 begin pp[r,0]:=step;
   for j:=1 step 1 until n do
   pp[r,j]:=if r=j then step else 0
 end;
 for j:=1 step 1 until n do x[j]:=x1[j];
 for cycle :=1 step 1 until n-1,n,cycle+1 while delta>eps do
 begin delta:=-1; f1:=fx:=function(x1); count:=count+1;
   for r:=1 step 1 until n do
   begin for j:=0 step 1 until n do
     p[j]:=pp[r,j];
     locmin(fx,x,p,fy,x);
     if p[0]≠0 and p[0]<stepxn then
     for j:=0 step 1 until n do pp[r,j]:=p[j];
     if fx-fy≥delta then
     begin delta:=fx-fy;
       m:=r
     end; fx:=fy;
   end; f2:=fx;
   for j:=1 step 1 until n do
   y[j]:=2xx[j]-x1[j]; f3:=function(y); count:=count+1;
   if f3<f1 then
   begin if (f1-2xf2+f3)x(f1-f2-delta)↑2<delta/2x(f1-f3)↑2 then
     begin for r:=m+1 step 1 until n-1 do
       for j:=0 step 1 until n do
       pp[r,j]:=pp[r+1,j]; p[0]:=0;
       for j:=1 step 1 until n do
       begin p[j]:=pp[n,j]:=x[j]-x1[j];
         p[0]:=p[0]+abs(p[j]);
       end; pp[n,0]:=p[0];
       locmin(fx,x,p,fx,x);
     end
   end;

   delta:=0;
   for j:=1 step 1 until n do
   begin delta:=delta+abs(x1[j]-x[j]);
     x1[j]:=x[j]
   end
 end; for j:=1 step 1 until n do xmin[j]:=x[j]
end minimize;
```

```
    f1:= format([ss+d.dddddd₁₀+nd]);
    open(20); open(30);
    for i:= 1,2,3 do x[i]:= read(20);
    eps:= read(20); pas:= read(20); n:= 3;

    for k:= 1 step 1 until 72 do
begin   P[k]:= read(20);
    V[k]:= read(20);
end;

        delta:=78.700;
         minog(func,n,x,eps,pas,xmin);
         for i:=1,2,3 do write(30,f1,xmin[i]);
         newline(30,2);
         for i:=13step 2 until 90do
begin    t:=0.1xi;
         write(30,format([ss+d.dss]),t);
      write(30,f1,xmin[1]xt+xmin[2]xt↑7+xmin[3]xexp(-delta/t));
end;
      close(20); close(30);
end→
```

Table (A.1)

2.5; 1.0₁₀-3; 3.2₁₀8; A; B; C;
₁₀-4; 5₁₀-4; eps; pas;

T_1^{-1} secs^{-1}	T °K	T_1^{-1} secs^{-1}	T °K
8.74;	3;	2.02₁₀3;	6.17;
9.01₁₀3;	6.92;	4.16₁₀2;	5.5;
2.44₁₀2;	5.28;	1.5₁₀1;	3.59;
1.01₁₀1;	3.29;	7.81;	2.96;
6.31;	2.7;	5.44;	2.41;
1.6₁₀1;	3.61;	1.58₁₀1;	3.52;
1.59₁₀1;	3.47;	3.71₁₀1;	4.2;
4.84₁₀3;	6.7;	1₁₀4;	7.08;
5.24₁₀1;	4.42;	3.97₁₀1;	4.22;
2.38₁₀1;	3.99;	1.71₁₀1;	3.72;
9.56;	3.44;	8.4;	3.22;
7.88;	2.94;	1.22₁₀4;	6.9;
1.76₁₀4;	7.2;	2.29₁₀1;	3.9;
6.1₁₀4;	8.7;	4.64₁₀4;	7.8;
1.97₁₀4;	7.65;	1.21₁₀2;	5.15;
2.40₁₀2;	5.28;	1.63₁₀3;	6.17;
5.49;	2.01;	3.68₁₀2;	5.5;
3.69₁₀2;	5.55;	1.13₁₀2;	4.8;
6.94₁₀2;	5.75;	2.62₁₀3;	6.45;
6₁₀1;	4.58;	1.04₁₀2;	4.6;
3.1₁₀2;	5.04;	4.31₁₀2;	5.26;
8.34₁₀2;	5.61;	1.76₁₀3;	5.9;
4.85₁₀3;	6.4;	6.45₁₀3;	6.65;
4.95₁₀3;	6.6;	1.03₁₀3;	5.7;
3.16₁₀2;	5;	4.5₁₀2;	5.3;
1.25₁₀2;	4.7;	8.4₁₀2;	5.87;
2.36₁₀2;	5.15;	9.35₁₀1;	4.78;
1.28₁₀2;	4.93;	7.81₁₀1;	4.63;
5.65₁₀1;	4.52;	5.99;	1.97;
7.81;	2.13;	7.64;	2.29;
5.81;	1.84;	5.18;	1.76;
4.59;	1.38;	5.4;	1.59;
5.79;	2.17;	4.61;	2.08;
5.41;	1.81;	4.87;	1.76;
4.79;	1.44;	6.21;	2.38;
5.26;	2.29;	5.55;	2.01;

→

Table (A.2)

FINAL FAREA11APU OUTPUT:

A= +2.667532$_{10}$+0 B = +7.702281$_{10}$-4 C= +6.652903$_{10}$+8

T°K	T secs	T°K	T secs
1.3	3.47262$_{10}$+0	1.5	4.01445$_{10}$+0
1.7	4.56641$_{10}$+0	1.9	5.13716$_{10}$+0
2.1	5.74054$_{10}$+0	2.3	6.39757$_{10}$+0
2.5	7.13895$_{10}$+0	2.7	8.00817$_{10}$+0
2.9	9.06557$_{10}$+0	3.1	1.03947$_{10}$+1
3.3	1.21147$_{10}$+1	3.5	1.44061$_{10}$+1
3.7	1.75668$_{10}$+1	3.9	2.21193$_{10}$+1
4.1	2.90041$_{10}$+1	4.3	3.98954$_{10}$+1
4.5	5.76771$_{10}$+1	4.7	8.71130$_{10}$+1
4.9	1.35732$_{10}$+2	5.1	2.14932$_{10}$+2
5.3	3.41290$_{10}$+2	5.5	5.38051$_{10}$+2
5.7	8.36741$_{10}$+2	5.9	1.27885$_{10}$+3
6.1	1.91754$_{10}$+3	6.3	2.81926$_{10}$+3
6.5	4.06527$_{10}$+3	6.7	5.75300$_{10}$+3
6.9	7.99714$_{10}$+3	7.1	1.09305$_{10}$+4
7.3	1.47048$_{10}$+4	7.5	1.94904$_{10}$+4
7.7	2.54772$_{10}$+4	7.9	3.28734$_{10}$+4
8.1	4.19058$_{10}$+4	8.3	5.28186$_{10}$+4
8.5	6.58723$_{10}$+4	8.7	8.13429$_{10}$+4
8.9	9.95203$_{10}$+4		

APPENDIX 3

MATRIX DIAGONALISATION PROGRAM

The evaluation of the spin Hamiltonian parameters from the ENDOR data on Gd and Yb isotopes was performed in a manner similar to that described by Williams [D.Phil. Thesis, Oxford University 1961]. However no quadratic field reduction processes were required. In the Gd isotopes the dependence of ENDOR frequency upon field is small (~ 100 c/s for 1 gauss) so that the variation of frequency involved by correcting all ENDOR frequencies for a particular S_z manifold to a single field was less than the random experimental errors. For Yb isotopes where this would have been important, the magnetic field variation for different measurements on the same ENDOR transition was only ~ 5 gauss, and thus small compared with the probable errors on those lines.

A computer program was written in ALGOL to set up the spin Hamiltonian matrix for the following spin Hamiltonian :

$$\mathcal{H} = g''.\beta H \cos\theta\, S_z + \tfrac{1}{2}g^{\perp}\beta H \sin\theta (S_+ + S_-) + B_4(O_4^0 + 5O_4^4)$$

$$+ B_6(O_6^0 - 21O_6^4) + A\,\underline{S}.\underline{I} + g''\beta H \cos\theta I_z + g_1^{\perp}\beta H \sin\theta (I_+ I_-)$$

$$+ b\,[\;[3S_z^2 - S(S+1)]\;[3I_z^2 - I(I+1)]$$

$$+ \frac{3}{2}(S_zS_+ + S_+S_z)(I_zI_- + I_-I_z) + \frac{3}{2}(S_zS_- + S_-S_z)(I_zI_+ + I_+I_z)$$

$$+ \frac{3}{2}(S_+^2I_-^2 + S_-^2I_+^2)\;] + g^3\beta\underline{H}.\underline{S}^3 + g^5\beta H_zS_z^5 + A'\underline{S}^3.\underline{I}$$

$$+ B H_zS_zI_z^2 + g_I'\beta H_zS_z^2I_z + CS_zI_z^3 + E S_zI_zH_z^2$$

$$+ F S_z^3I_zH_z^2 + DI_z^2.$$

This is the spin Hamiltonian used by Hurrell, with additional high order terms.

Having generated the matrix, the computer program (FAREA8120KPU) then diagonalised it using magnetic fields and Hamiltonian parameters provided as data. The diagonalisation procedure used was the Householder diagonalisation procedure, from the Computing laboratory library procedure DIAGR. The program printed out all matrix elements that were generated, the eigenvalues and predicted ENDOR frequencies for each S_z manifold for each magnetic field at which diagonalisation was required. This program, when translated with the Kidsgrove compiler would diagonatise the Gd 32 x 32 matrix in 63 seconds. A weighted least squares program

written by Hurrell (D.Phil. Thesis, Oxford University 1963) was transliterated from its original Mercury Autocode language into KDF9 autocode, and used to analyse the Gd ENDOR results as discussed in his thesis.

A print out of the matrix generation and diagonalisation program is given in Figure A2. For ease of understanding the symbols used in the program, the equivalence between the above spin Hamiltonian parameters and the symbols used in the program is given :

$g''\beta$ = G[1]

$\frac{1}{2}g'\beta$ = G[2]

B_4, B_6 = bigb [4], bigb [6].

A	= biga [1]	B	= G [7]
$g'_I\beta$	= G [3]	g'_I	= G [8]
$g''_I\beta$	= G [4]	C	= biga [4]
b	= biga [3]	D	= biga [5]
g^3	= G [5]	E	= G [9]
g^5	= G [6]	F	= G [10]
A'	= biga [2]		

The details of the procedures HOUSEHOLDER, TRIDIAGONALISATION, TRIDIBISECTION, and DIAGR have been omitted as these are readily available from the Computing Laboratory procedure

The data tape for this program has the form :

t : = number of magnetic fields at which diagonalisation is required.

bigb [4]; bigb [6];

G [1]; G [2]; G [3]; G [4]; G [5]; G[6]; G [7];

G [8]; G [9]; G [10];

A [1]; A [2]; A [3]; A [4]; A [5];

I ; S; theta ;

t values of magnetic field.

• ; • ; •; •; •;

A call and data tape print-out for Gd^{157} in CeO_2 is shown after the program print out.

The output from the program takes the form :

MAGNETIC FIELD : - prints magnetic field at which diagonalisation is performed.

MATRIX ELEMENTS : Prints all non zero matrix elements for that field putting the diagonal elements first.

ENDOR MANIFOLD : Prints S_z value of ENDOR manifold

EIGENVALUES : Prints (2I+1) eigenvalues for all I_z levels to this S_z value.

ENDOR FREQS : Prints modulus of the 2I differences between successive eigenvalues on that manifold.

These are repeated (2S+1) times for all values of S_z from $S_z = S$ to $S_z = -S$.

These are all repeated for each field at which diagonalisation occurs.

A Note on Units. Several of the g-values used in this program have to include the value of the Bohr magneton as the program sets up e.g.,

$$g \beta H = G[1] \times H.$$

Also it is often useful to include the proton resonance frequency for 1 kgauss in these g-factors to enable magnetic fields measured in terms of proton resonance frequencies to be substituted directly into the program without previous conversion into gauss.

One other point to be noted is that the term $D I_z^2$ is represented by biga [5] which in the program is evaluated

as biga [5] x m^2 x $(bigm)^2$. Thus a pseudo-quadrupole term of this sort will be multiplied by S_z^2 by the program.

FAREA8120 KPU→

```
begin library A6,A30;
      real bigi,bigs,bigm,m,bigk,bigl,theta,sn,cs,a,b,c,d,i,j,
      k,l,n,p,q;
      integer r,t,y,z,f1,f2,f3,f4,f5;
      begin real array bigb[4:6],G[1:10],biga[1:5];

      open(20);
      open(30);
      t:=read(20);
      for i:=4,6 do bigb[i]:=read(20);
      for j:=1 step 1 until 10 do
      begin G[j]:=read(20);
      end;
      for i:=1,2,3,4,5 do biga[i]:=read(20);
      bigi:=read(20);
      bigs:=read(20);
      theta:=read(20);
      bigk:=bigs↑2+bigs;
      bigl:=bigi↑2+bigi;
      sn:=sin(thetax3.1415926/180);
      cs:=cos(thetax3.1415926/180);
      n:=(2xbigs+1)x(2xbigi+1);
      f1:=format([ss+d.ddddd10+ndc]);
      f2:=format([3s+d.ddddddddd10+nd]);
      f3:=format([3s+d.ddddddddd10+ndcc]);
      f4:=format([ss+dd.ddc]);
      f5:=format([ss+d.ddddd10+nd]);
      write(30,f4,n);
      write(30,f4,t);
      write(30,f4,theta);
      begin real array bigd[-bigi+0.5:bigi+0.5],matrix[1:n,1:n],
      F[-bigs+0.5:bigs+0.5],endor[1:n],
      X[-bigs+0.5:bigs+0.5,-bigs+0.5:bigs+0.5,-bigi+0.5:
      bigi+0.5,-bigi+0.5:bigi+0.5],roots[1:n],H[1:t];
procedure householder tridiagonalisation (n,a,c,b);

procedure tridibisection 1 (c,b,n,gu,go,t,gamma,w,norm,m1);

procedure diagr(a,n,roots);
```

```
for j:=1 step 1 until t do H[j]:=read(20);
      close(20);
      for bigm:=bigs-1 step -1 until -bigs do
      begin     k:=bigm+0.5;
                F[k]:=bigk-bigm↑2-bigm;
      end;
      for m:=bigi-1 step -1 until -bigi do
      begin  l:=m+0.5;
             bigd[l]:=bigl-m↑2-m;
      end;
      for a:=bigs+0.5 step -1 until -bigs+0.5 do
      begin for b:=bigs+0.5 step -1 until -bigs+0.5 do
      begin for c:=bigi+0.5 step -1 until -bigi+0.5 do
      begin for d:=bigi+0.5 step -1 until -bigi+0.5 do
      begin X[a,b,c,d]:=0;
      end;
      end;
      end;
      end;

      for i:=1 step 1 until t do
      begin  write text (30,[[2c]MAGNETIC*FIELD[2s]]);
      write(30,f1,H[i]);
      write text (30,[MATRIX*ELEMENTS[2c]]);

      for bigm:=bigs step -1 until -bigs do
      begin for m:=bigi step -1 until -bigi do
      begin k:=bigm+0.5;
            l:=m+0.5;
      X[k,k,l,l]:=bigb[4]x(35xbigm↑4-30xbigkxbigm↑2+
      25xbigm↑2-6xbigk+3xbigk↑2)+bigb[6]x(231xbigm↑6-
      105x(3xbigk-7)xbigm↑4+(105xbigk↑2-525xbigk+294)x
      bigm↑2-5xbigk↑3+40xbigk↑2-60xbigk)-3xbiga[3]x
      biglxbigm↑2-3xbiga[3]xbigkxm↑2+biga[1]xbigmxm+
      H[i]x(G[1]xbigm+G[3]xm+G[5]xbigm↑3+G[6]xbigm↑5+
      G[7]xbigmxm↑2+G[8]xmxbigm↑2)xcs+(9xbiga[3]+
      biga[5])x(bigm↑2)x(m↑2)+biga[3]xbigkxbigl+biga[2]
      xmxbigm↑3+biga[4]xbigmxm↑3+G[9]xbigmxmxH[i]↑2+
      G[10]xbigm↑3xmxH[i]↑2;

      write(30,if m=-bigi then f1 else f5, X[k,k,l,l]);
      end;
      end;
      for bigm:=bigs step-1until -bigs do
      begin for m:=bigi-1 step-1until -bigi do
      begin     k:=bigm+0.5;
                l:=m+0.5;
```

```
X[k,k,l+1,1]:=0.5xG[4]xH[i]xsnxsqrt(bigd[1]);
write(30,if m=-bigi then f1 else f5, X[k,k,l+1,1]);
X[k,k,1,l+1]:= X[k,k,l+1,1];
end;
end;
for m:=bigi step -1 until -bigi do
begin for bigm:=bigs-1 step -1 until -bigs do
begin k:=bigm+0.5;
      l:=m+0.5;
X[k+1,k,1,1]:=0.5xG[2]xH[i]xsnxsqrt(F[k]);
write(30, if bigm=-bigs then f1 else f5,X[k+1,k,1,1]);
X[k,k+1,1,1]:= X[k+1,k,1,1];
end;
end;

for bigm:= bigs-2 step -1 until -bigs do
begin for m:=bigi step -1 until -bigi+2 do
begin k:=bigm+0.5;
      l:=m+0.5;
X[k+2,k,1-2,1]:=1.5xbiga[3]xsqrt(F[k]xF[k+1]x
bigd[1-1]xbigd[1-2]);
write(30, if m=-bigi+2 then f1 else f5,X[k+2,k,1-2,1]);
X[k,k+2,1,1-2]:= X[k+2,k,1-2,1];
end;
end;

for bigm:=bigs-3 step -1 until -bigs do
begin for m:=bigi-1 step -1 until -bigi do
begin  k:=bigm+0.5;
       l:=m+0.5;
X[k+3,k,1+1,1]:=0.125xbiga[2]xsqrt(F[k]xF[k+1]xF[k+2]x
                bigd[1]);
write(30, if m=-bigi then f1 else f5, X[k+3,k,1+1,1]);
X[k,k+3,1,1+1]:= X[k+3,k,1+1,1];
end;
end;
for m:= bigi step -1 until -bigi do
begin forbigm:=bigs-4 step -1 until -bigs do
begin  k:=bigm+0.5;
       l:=m+0.5;
X[k+4,k,1,1]:=(2.5xbigb[4]-10.5xbigb[6]x(11xbigm↑2+44
          xbigm+50-bigk))xsqrt(F[k]xF[k+1]xF[k+2]xF[k+3]);
write(30, if bigm= -bigs then f1 else f5, X[k+4,k,1,1]);
X[k,k+4,1,1]:= X[k+4,k,1,1];
end;
end;
```

```
for bigm:= bigs-1 step -1 until -bigs do
begin for m:= bigi step -1 until -bigi+1  do
begin  k:=bigm+0.5;
       l:=m+0.5;
X[k+1,k,l-1,l]:=((0.5xbiga[1])+((0.375xbigk-0.25)-0.375x
bigmx(bigm+1))xbiga[2]+((0.375xbigl-0.25)-0.375x
mx(m-1))xbiga[4]+1.5xbiga[3]x(4xmxbigm-3xbigm+2xm-1))
x sqrt(F[k]xbigd[l-1]);
write(30,if m=-bigi+1 then f1 else f5,X[k+1,k,l-1,l]);
X[k,k+1,l,l-1]:= X[k+1,k,l-1,l];
end;
end;
for bigm := bigs-1 step -1 until - bigs do
begin for m :=bigi-3 step -1 until - bigi do
begin k:=bigm+0.5;
      l:=m+0.5;
X[k+1,k,l+3,l]:=0.125xbiga[4]x sqrt(F[k]xbigd[l]x
          bigd[l+1]xbigd[l+2]);
write(30,if m=-bigi then f1 else f5, X[k+1,k,l+3,l]);
X[k,k+1,l,l+3]:= X[k+1,k,l+3,l];
end;
end;

p:=0;
for a:=bigs+0.5 step -1 until -bigs+0.5 do
begin for c:=bigi+0.5 step -1 until -bigi+0.5 do
begin p:=p+1;
          q:=0;
for b:=bigs+0.5 step -1 until -bigs+0.5 do
begin for d:=bigi+0.5 step -1 until -bigi+0.5 do
begin q:=q+1;
matrix[p,q]:=X[a,b,c,d];
end;
end;
end;
end;

diagr(matrix,n,roots);
```

```
r:=0;
for y:=0 step 1 until 2 xbigs  do
beginwrite text(30,[[2c]ENDOR*MANIFOLD[2c]]);
write(30,f4,bigs-y);
writetext(30,[[2c]EIGENVALUES********ENDOR*FREQ*IN*MC/S[2c]]);
for z:=1 step 1 until (2xbigi+1) do
      begin r:=r+1;
write(30,f2,roots[r]);
if z<2xbigi+1 then endor[r]:=abs(roots[r]- roots[r+1])x10^4;
write(30,f1,endor[r]);
end;
end;
end;
end;
close(30);
end;
end
→
```

Data for diagonalisation of Gd157 in CeO2.

```
K
FAREA8120 KPU;
PROGAREA 3500;
IN8.
OUTL.→
7;
-2.7795;  -0.000992;
654.54;  654.54  0.04002;  0.04002;  0;0;0;0;0;0;
15.818;  -0.0007517  -0.0033;  0;0;
1.5;  3.5;  0;
59.7720;  52.1328;  51.6705;  54.6965;
57.6967;  57.2740;  49.6461;→
```

APPENDIX 4

In this appendix the mean values for the observed ENDOR frequencies are tabulated for the Yb isotopes. Each transition is labelled by S_z and ΔI_z. The probable error on the readings is quoted and the mean magnetic field in units of proton resonance frequency Mc/s is quoted for each hyperfine line. The final column contains the ENDOR frequency computed from the parameters quoted in Chapter 4.

Yb173 in CaF2

Sz	ΔIz	Observed Mc/s	Error kc/s	Field	Computed Mc/s
1/2	5/2→3/2	378.313	160	33.3274	378.282
-1/2	5/2→3/2	375.704	30	33.3274	375.722
1/2	3/2→1/2	371.183	50	32.6578	371.200
-1/2	5/2→3/2	375.880	30	32.6578	375.891
-1/2	3/2→1/2	368.777	60	32.6578	368.776
1/2	3/2→1/2	371.494	30	31.9998	371.472
1/2	1/2→-1/2	364.159	25	31.9998	364.123
-1/2	3/2→1/2	368.791	40	31.9998	368.781
-1/2	1/2→-1/2	361.927	30	31.9998	361.932
1/2	1/2→-1/2	364.223	40	31.3608	364.223
1/2	-1/2→-3/2	357.115	20	31.3608	357.103
-1/2	1/2→-1/2	361.775	10	31.3608	361.784
-1/2	-1/2→-3/2	355.127	30	31.3608	355.132
1/2	-1/2→-3/2	357.082	50	30.7272	357.045
1/2	-3/2→-5/2	350.240	40	30.7272	350.198
-1/2	-1/2→-3/2	354.806	20	30.7272	354.818
-1/2	-3/2→-5/2	348.246	40	30.7272	348.314
-1/2	-3/2→-5/2	347.767	120	30.1138	347.896

Yb 171 in CaF2

Sz	ΔIz	Observed Mc/s	Error kc/s	Field Mc/s	Computed Mc/s
-1/2	1/2→-1/2	1375.520	32	32.8602	1375.557
-1/2	1/2→-1/2	1378.458	22	30.5228	1378.472
1/2	1/2→-1/2	1260.208	35	30.5228	1260.216

APPENDIX 5

In this appendix the mean values for the observed ENDOR frequencies at Q band for the Gd isotopes are tabulated. Each transition is labelled by the S_z value of the level from which the line originated and the I_z values involved in the transition. The probable error calculated from the standard deviations of the readings is listed, together with the mean magnetic field for the particular S_z manifold in units of proton resonance frequency. In the last column the ENDOR frequency computed by exact diagonalisation of the spin Hamiltonian matrix is tabulated, using the final values of the parameters quoted in Chapter 5.

Gd157 in ThO2

Sz	ΔIz	Observed Mc/s	Error kc/s	Field Mc/s	Computed Mc/s
7/2	3/2→1/2	57.1913	20.0	59.6730	57.1704
7/2	1/2→-1/2	57.5632	25.4	59.6730	57.5562
7/2	-1/2→-3/2	57.9519	14.2	59.6730	57.9430
5/2	3/2→1/2	41.4053	8.6	51.9759	41.4139
5/2	1/2→-1/2	41.4705	4.7	51.9759	41.4777
5/2	-1/2→-3/2	41.5585	10.7	51.9759	41.5415
3/2	3/2→1/2	25.8008	5.8	51.5019	25.8325
3/2	1/2→-1/2	25.6671	2.4	51.5019	25.6865
3/2	-1/2→-3/2	25.5497	11.0	51.5019	25.5400
1/2	3/2→1/2	10.2511	19.0	54.5390	10.2870
1/2	1/2→-1/2	10.0371	5.6	54.5390	10.0343
1/2	-1/2→-3/2	9.8030	16.4	54.5390	9.7811
-3/2	3/2→1/2	21.2304	14.7	57.5697	21.2082
-3/2	1/2→-1/2	21.3820	9.2	57.5697	21.3732
-3/2	-1/2→-3/2	21.5291	10.3	57.5697	21.5386
-5/2	3/2→1/2	37.1672	17.7	57.1256	37.1689
-5/2	1/2→-1/2	37.1718	11.5	57.1256	37.1368
-5/2	-1/2→-3/2	37.1032	7.1	57.1256	37.1044
-7/2	3/2→1/2	53.5151	8.0	49.5120	53.5084
-7/2	1/2→-1/2	53.1825	6.6	49.5120	53.1704
-7/2	-1/2→-3/2	52.8318	7.6	49.5120	52.8315

Gd157 in ThO2

Hurrell's X-band data, no errors given in his thesis from which this table is compiled. The computed frequencies come from the parameters in Table (5.4).

Sz	ΔIz	Observed Mc/s	Field Mc/s	Computed Mc/s
7/2	3/2→1/2	55.396	18.9930	55.386
7/2	1/2→-1/2	55.849	18.9930	55.841
7/2	-1/2→-3/2	56.278	18.9930	56.301
5/2	3/2→1/2	39.517	11.1151	39.567
5/2	1/2→-1/2	39.547	11.1151	39.548
5/2	-1/2→-3/2	39.489	11.1151	39.523
3/2	3/2→1/2	23.828	10.6660	23.850
3/2	1/2→-1/2	23.723	10.6660	23.724
3/2	-1/2→-3/2	23.602	10.6660	23.597
1/2	3/2→1/2	8.400	13.7240	8.419
1/2	1/2→-1/2	8.225	13.7240	8.210
1/2	-1/2→-3/2	8.050	13.7240	7.999
-1/2	3/2→1/2	7.350	13.7240	7.327
-1/2	1/2→-1/2	7.600	13.7240	7.538
-1/2	-1/2→-3/2	7.850	13.7240	7.751
-3/2	3/2→1/2	22.897	16.8508	22.919
-3/2	1/2→-1/2	23.120	16.8508	23.116
-3/2	-1/2→-3/2	23.254	16.8508	23.316
-5/2	3/2→1/2	38.673	16.4250	38.759
-5/2	1/2→-1/2	38.815	16.4250	38.808
-5/2	-1/2→-3/2	38.863	16.4250	38.855
-7/2	3/2→1/2	54.989	8.6590	54.999
-7/2	1/2→-1/2	54.743	8.6590	54.733
-7/2	-1/2→-3/2	54.480	8.6590	54.465

Gd157 in CeO2

Sz	△Iz	Observed Mc/s	Error kc/s	Field Mc/s	Computed Mc/s
7/2	3/2→1/2	57.4390	75.0	59.7720	57.2684
7/2	1/2→-1/2	57.7018	4.7	59.7720	57.7076
7/2	-1/2→-3/2	58.1278	39.4	59.7720	58.1479
5/2	3/2→1/2	41.2941	100.7	52.1328	41.5058
5/2	1/2→-1/2	41.5933	15.2	52.1328	41.5773
5/2	-1/2→-3/2	41.8432	116.8	52.1328	41.6987
3/2	1/2→-1/2	25.7494	4.3	51.6703	25.7376
1/2	1/2→-1/2	10.2385	200.0	54.6965	10.0426
-3/2	1/2→-1/2	21.4509	6.5	57.6967	21.4563
-3/2	-1/2→-3/2	21.8072	238.0	57.6967	21.6446
-5/2	3/2→1/2	37.4488	108.0	57.2740	37.3066
-5/2	1/2→-1/2	37.2642	2.4	57.2740	37.2667
-7/2	3/2→1/2	53.7806	59.0	49.6461	53.7446
-7/2	1/2→-1/2	53.3618	3.3	49.6461	53.3531
-7/2	-1/2→-3/2	53.0352	98.2	49.6461	52.9606

Gd155 in CeO2

Sz	ΔIz	Observed Mc/s	Error kc/s	Field Mc/s	Computed Mc/s
7/2	3/2→1/2	43.5529	185.0	59.8337	43.5675
7/2	1/2→-1/2	43.9742	1.8	59.8337	43.9741
7/2	-1/2→-3/2	44.3000	130.0	59.8337	44.3814
5/2	1/2→-1/2	31.7065	2.9	52.2791	31.7052
3/2	1/2→-1/2	19.6373	3.7	51.7002	19.6382
-3/2	1/2→-1/2	16.3340	6.7	57.7334	16.3353
-5/2	1/2→-1/2	28.3859	5.0	57.2902	28.3821
-7/2	1/2→-1/2	40.6309	2.0	49.6659	40.6276